THE INFRARED SPECTRA DUE TO H^- IONS IN THE ALKALI HALIDES

THE INFRARED SPECTRA DUE TO H^- IONS IN THE ALKALI HALIDES

By

RONALD WILLIAM MACPHERSON, B.Sc.,M.Sc.

A Thesis

Submitted to the Faculty of Graduate Studies

in Partial Fulfilment of the Requirements

for the Degree

Doctor of Philosophy

McMaster University

May 1970

DOCTOR OF PHILOSOPHY (1970) McMASTER UNIVERSITY
(Physics) Hamilton, Ontario.

TITLE: The Infrared Spectra Due to H^- Ions in the Alkali Halides

AUTHOR: Ronald William MacPherson, B.Sc., (U.B.C.), M.Sc., (U.B.C.)

SUPERVISOR: Dr. Thomas Timusk

NUMBER OF PAGES: viii, 110

SCOPE AND CONTENTS:

Measurements of the infrared absorption spectra of potassium and sodium halide crystals with substitutional H^- ion impurities are presented and compared with calculations which use rigid ion and ordinary shell models for the defect along with phonon data obtained from inelastic neutron scattering measurements. It is shown that the shell model is necessary to give a satisfactory account of the observed anharmonic side band absorption in the sodium halide crystals and that it improves the rigid ion results for the potassium halide crystals. The same model also satisfactorily describes the impurity induced far-infrared absorption in these materials. Some Van Hove singularities observed in the far infrared measurements occur at frequencies predicted from phonon densities of states calculated from neutron scattering data while others occur at slightly different frequencies.

ACKNOWLEDGEMENTS

It is with pleasure that I thank my supervisor, Dr. T. Timusk, who has been a great source of encouragement and help throughout the course of this work. Dr. J. P. Carbotte and Dr. J. B. Page, Jr. have been very helpful with the understanding of the theoretical aspects. I also thank the faculty and staff of the computing centre for their assistance.

This research was partially funded by the National Research Council of Canada to whom I am also grateful for the award of a scholarship.

Finally, I thank Mrs. H. M. Kennelly for typing the final draft of the manuscript.

TABLE OF CONTENTS

LIST OF FIGURES

LIST OF TABLES

CHAPTER I

INTRODUCTION

The infrared absorption spectra of substitutional H^- ions in the alkali halides has been of great interest for the past several years because its study presents an excellent opportunity to investigate the perturbed vibrations in a lattice containing impurities. The details of these vibrations reveal a large amount of information about the nature of the defect and the surrounding lattice. The first infrared measurements of the absorption due to the H^- ion in the alkali halides were made by Schäfer (1960). This absorption was theoretically shown to be due to an infrared active, high frequency, localized mode (Rosenstock and Klick, 1960; Wallis and Maradudin, 1960). The high frequency is a consequence of the small mass of the hydrogen compared with the mass of the host anion mass.

Theoretical calculations of the local mode frequency require a knowledge of the dynamics of the unperturbed crystal. The early calculations used first and second nearest neighbours force constant models for the lattice. When the long range electrostatic forces were taken into account, it was found by Jaswal and Montgomery (1964) using the rigid ion and deformation dipole

models, by Fieschi et al. (1965) using the shell model, and by Page and Strauch (1967) using the breathing shell model that a decrease of typically 50% in the force constants connecting the H^- ion to its nearest neighbours was necessary to obtain agreement with the observed values of the local mode frequency.

Schäfer (1960) also observed that the main H^- ion absorption was accompanied by side bands. These were examined in more detail in NaCl, NaBr, KCl, KBr, KI, RbCl and RbBr by Fritz et al. (1965) and were shown to correspond to the annihilation or creation of a band mode phonon along with the creation of the local mode phonon. These side bands have also been studied by several others (Mitra and Brada, 1964; Dötsch et al. 1965; Timusk and Klein, 1966; Bäuerle and Fritz, 1967; and Dötsch, 1969). Their existence is attributed to anharmonic coupling of the local mode to the other modes of the crystal (Fritz, 1965; Elliot et al. 1965; Timusk and Klein, 1966; Xinh, 1966; Bilz et al. 1966). The possibility of coupling by means of second order dipole moment interactions was considered in detail by Xinh (1966 and 1967) and by Page and Dick (1967) and they concluded that the dominant coupling is anharmonic.

The very detailed measurements of the absorption in KBr by Timusk and Klein (1966) and their theoretical calculations showed that the side band line shape is dependent

only on the perturbed vibrational spectrum of the ions near the H^- ion defect. The calculations were based on a rigid ion model for the defect and used unperturbed phonon data derived from the shell model for KBr (Woods et al. 1963). The model of the defect was extended by Gethins et al. (1967) who obtained improved results in KBr and KI. Page and Strauch (1968) used a breathing shell model for the defect and phonons from the breathing shell model (Nüsslein and Schröder 1967 and Schröder 1966) to calculate the side band absorption in KCl, KBr and KI.

In addition to the absorption associated with the local mode, there is some induced absorption below the reststrahlen frequency in crystals containing hydrogen. This absorption is a consequence of the lack of translational symmetry in crystals with a random distribution of impurities and was observed in KI containing hydrogen by Seivers (1965) and in KBr and KI by Timusk et al. (1968). A theoretical explanation in terms of the extended rigid ion defect model of Gethins et al. (1967) was given by Woll et al. (1968).

Any theoretical model of the defect should be tested in a variety of systems and in particular in those systems in which the dynamics of the perfect lattice are well known. Recently inelastic neutron scattering measurements have been completed for almost all of the common alkali halides. In the work of this thesis new detailed measurements of the

infrared absorption due to substitutional H^- ions in NaF, NaCl, NaBr, KCl, and KI are presented. The observed spectra are compared with the results of calculations based on the extended rigid ion model and on an ordinary shell model of the defect. The calculations use unperturbed phonon data interpolated from neutron scattering results by the shell model for the alkali halides. It is shown that the rigid ion model of the defect satisfactorily explains the side band in the potassium halides but not in all the sodium halides. The use of an ordinary shell model for the defect improves the quantitative agreement with the observed positions of resonances in the side bands in KBr and KI without adversely affecting the results for KCl. The model also satisfactorily describes the far-infrared absorption which is attributed to the presence of H^- ions.

Chapter II discusses the sample preparation and the experimental measurements of the side band and induced far infrared absorption at liquid helium temperature. The notation and background theory used in the calculations of the absorption is reviewed in Chapter III and the calculations themselves are discussed in Chapter IV. Chapter V compares the calculated results with the experimental measurements.

CHAPTER II

EXPERIMENTS

A. SAMPLE PREPARATION

Single crystals of the alkali halides were used throughout the experiments. These were obtained from various sources. The KCl, NaF and some of the NaBr crystals were purchased from the Harshaw Company, Cleveland, Ohio and the NaI, NaCl and the rest of the NaBr crystals were grown from the melt by the Kryopoulos-Czochralski technique in a specially constructed Vycor glass chamber that allowed the crystals to be grown in various atmospheres or under vacuum. The metal parts in contact with the boules were made of Inconel and the remainder were made of stainless steel. Melt materials for the crystals consisted mainly of reagent grade chemicals from Fisher Scientific, from British Drug Houses, or from McArther Chemicals Ltd. An attempt was made to produce some very pure NaBr by reacting reagent grade sodium bicarbonate with reagent hydrobromic acid. The impurity concentrations in these reagent materials are much lower than in reagent grade NaBr. The salt was obtained from the solution by evaporation and then dried at 150°C in an oven. The NaBr was then heated to melting and

gaseous bromine was bubbled through it to remove OH^- and CO_3^{--} radicals. Optran Grade NaBr and NaI was obtained from British Drug Houses for some of the crystals. The Optran Grade material is an especially pure grade which is claimed to be suitable for growing crystals of optical quality.

To obtain the crystals the melt materials were heated to melting temperatures under vacuum. During growing visibility was aided by a flow of ultra high purity argon gas (from Matheson of Canada, Ltd.) which reduced condensation of evaporated alkali halide on the walls of the glass chamber. Boules weighing 100 gm to 150 gm and measuring 25 mm in diameter and 25 mm to 50 mm in length could be obtained within 4 or 5 hours after seeding. The crystals were grown in a variety of containers but most were done in glazed porcelain #3 Coors crucibles. Serious problems with impurities were encountered only with NaBr and NaI and these were not helped by the use of nickel or graphite crucibles. The impurities did not seem to be related to the source of the crystals as even the NaBr crystals obtained from Harshaw exhibited the same impurity bands as the laboratory grown crystals.

The introduction of the hydrogen impurity to the alkali halides or "colouring" of the crystals was accomplished in several ways. The basic methods were (1) a two

step process in which F centres (negative ion vacancies occupied by an electron) were first produced and then hydrogen was diffused into the crystal under high pressure in the second step; and (2), a single step process in which the H^- ions were formed by the simultaneous introduction of F centres and diffused hydrogen.

The formation of the F centres for the two step process was done by various techniques. The highest concentrations were obtained in the potassium halides by additive colouration and in the sodium halides by electrolytic formation. In the additive colouration method, the alkali halide crystals were heated for several hours at about 50°C below their melting points in alkali metal vapour. They were then removed from the furnace and cooled rapidly to prevent coagulation of the F centres and the formation of colloids. The concentration of the F centres was controlled by the pressure of the alkali metal vapour during heating. In the electrolytic method of F centre formation, the crystals were also heated to about 50°C below their melting points. Electrodes passed currents of the order of a few milliamperes per cm^2 of crystal crossection at 100 to 200 volts through the samples. The positive electrode consisted of a flat nickel plate in contact with the surface of one end of the crystal. The negative electrode was a sharp stainless steel needle point which was pressed into the other end of the

crystal. During the colouring process the F centres formed at the negative point and diffused towards the positive electrode throughout the volume of the specimen.

After the F centres were obtained they were then converted to H^- ion centres by heating the crystals at 200°C to 300°C below their melting points in hydrogen at a pressure of 50 to 100 atmospheres. The diffusion of the hydrogen took up to 24 hours for a 1 cm thick crystal containing 10^{18} to 10^{19} F centres per cc. The rate depended upon the concentration of the F centres and on the temperature of the crystal. Care was taken not to let the crystals become too hot since at high temperatures the F centres tended to coalesce and form colloids before they could be converted to H^- ion centres.

In the single step process for forming H^- ion centres the crystals were heated in a mixture of alkali metal vapour and high pressure hydrogen or were electrically treated in hydrogen at high pressure for several hours. Temperatures were about 50°C below the melting points of the samples.

The colouring methods used by other workers have also included growing crystals from the melt with alkali hydride added as impurity and the X-ray irradiation of crystals containing OH^- radicals as impurity to break the O-H bond and produce H^- ions (e.g. Dötsch et al., 1965).

The method which is used depends largely on the particular material to be doped with H^- ions and on the

available equipment. Each of the alkali halides that was investigated required somewhat different treatments and these are outlined below.

1. Potassium Halide Salts

Potassium bromide was successfully doped in high concentrations by Timusk and Klein (1966) by means of the two step process using additive colouration. Potassium chloride and potassium iodide were successfully treated in a similar manner. The most highly concentrated samples were obtained in KCl by sealing the crystals with triply distilled potassium metal into evacuated Vycor glass tubes. The sealed tubes were heated in an open copper tube at 680°C for two hours after which time they were removed from the furnace and rapidly cooled with the blast from an air gun. The resulting crystals were deep purple to black in appearance and sections of about 0.5 mm thickness were opaque to visible light. Small crystal chips had a vivid purple colour. These samples were reheated in hydrogen at 1200 to 1800 psig and 450°C for 24 to 48 hours. The crystals were removed from the furnace for inspection once or twice during this latter process. Hydrogenated portions of the crystals were transparent while the unconverted portions remained as deep purple 'clouds' in the centre of the crystals. The boundary between the converted and unconverted regions was quite sharp and measurements of the penetration rate of the hydrogen could be

made to estimate the length of time required to just complete the hydrogenation process. It was found that crystals could be removed just as the last vestiges of the F centre cloud disappeared from the centre of the samples . Such crystals had concentrations of H^- ion of the order of 10^{19} per cc. Concentrations were estimated from the strength of the infrared local mode absorption of thin samples at room temperature. The strength is related to the concentration by a Smakula type of formula such as given by Klein (1968).

2. Sodium Halide Salts

The stability of the F centres in the sodium salts is such that high concentrations of H^- ions could not be obtained by the two step process which is so successful with the potassium salts. The F centres were lost before any appreciable number of them could be converted to H^- ion centres. The simultaneous hydrogenation with electrolytic or additive colouration methods worked about equally well to produce useable concentrations of H^- centres in the sodium halides. The electrolytic process produced slightly lower concentrations than the additive method but distributed the hydrogen more uniformly throughout the volume of the crystal. The additive process produced higher concentrations but these were confined to within a millimeter or so of the surface of the crystals.

The NaF samples were coloured by the additive method since the concentrations obtained from the electrolytic method were too small to see the side bands. Difficulties were experienced with impurities in the NaBr and NaI crystals. The spectra contained unwanted impurity bands which were independent of the colouring process. The main impurity in NaBr was OH^- and in NaI a strong band due to unknown impurities appeared near 480 cm^{-1} and completely masked the H^- ion local mode. No useable crystals of NaI could be obtained by any of the colouring methods described here.

The best results for NaCl and NaBr were obtained by the electrolytic process in high pressure hydrogen. A special stainless steel high pressure bomb was constructed for this purpose. The details are shown in Figure 1. The bomb was placed vertically into a two inch diameter temperature controlled furnace and connected via the Swagelok fitting on the cap through a system of valves to a mechanical vacuum pump and a cylinder of high purity hydrogen obtained from The Matheson Company. The air was replaced with the hydrogen by successively pumping out the bomb and refilling with hydrogen four times before pressurizing to about 750 psig. During heating the pressure rose to around 1350 psig. A current limiting power supply (HP Model 6209B) set to 200 volts and 10 ma. was connected between the cap and the positive electrode wire. The voltage dropped to 20 to 30 volts when the crystals reached colouring temperature. Temperatures were

FIGURE 1

High pressure electrolytic colouring bomb. The labelled parts are: (1) "O"-ring seal, (2) nickel bushings to prevent parts from sliding along the rods, (3) welded joints, (4) steel retaining spring, (5) quartz tube liner, (6) stainless steel needle electrode, (7) positive electrical connection fed through a glass insulator and sealed with epoxy, the negative connection is made to the metal body of the cap, (8) peripholite insulating spacers, (9) nickel positive electrode,(10) crystal to be coloured and (11) stainless steel rods with left hand threads on one end to facilitate assembly. The drawing is full scale and the bomb has an overall length of 24". In operation the bottom half is inserted vertically into a tube furnace so that the crystal is centred in the hottest part. Hydrogen gas admitted through the Swagelok fitting in the top.

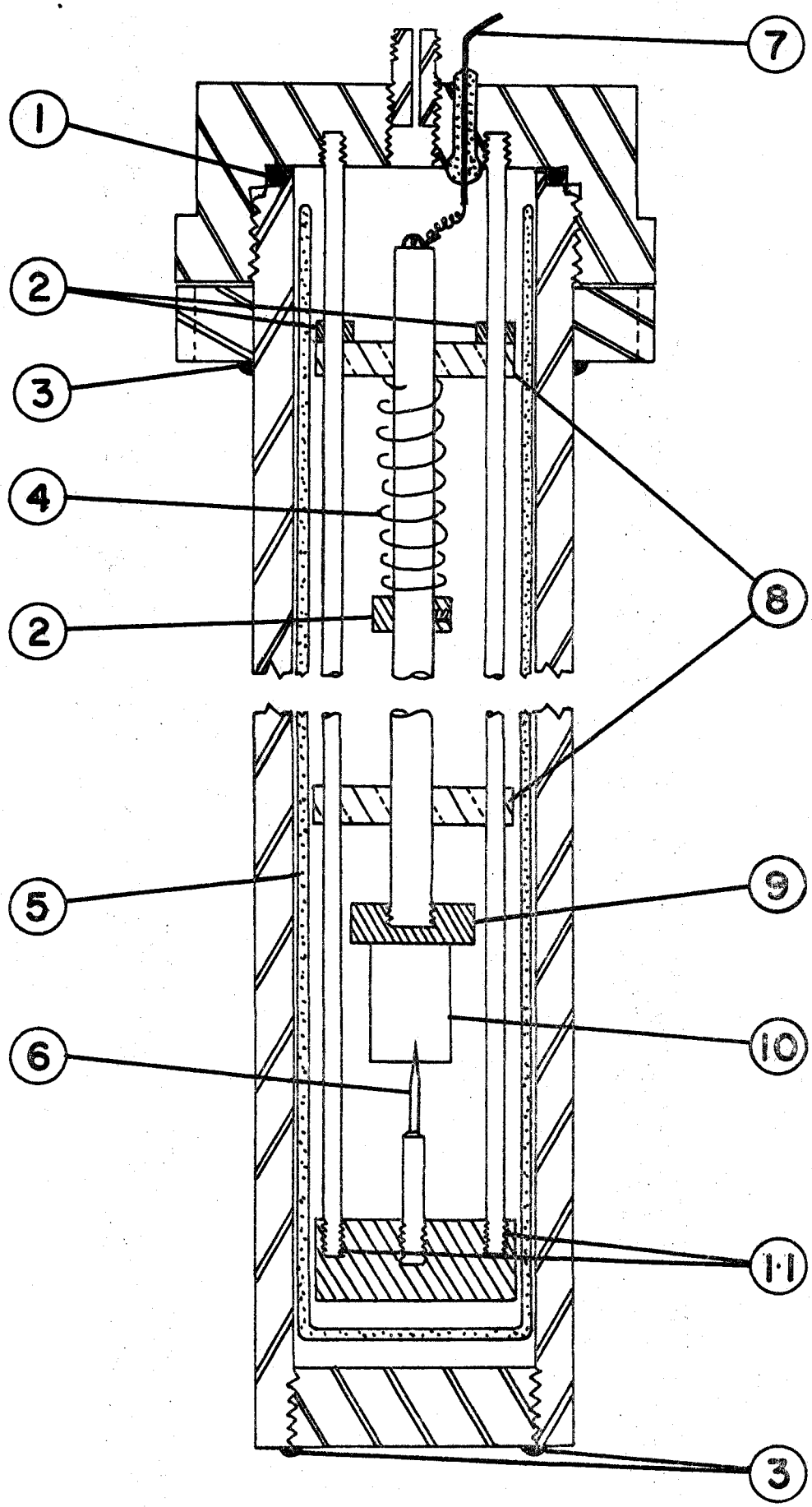
7
1
2
3
4
2
8
5
9
6
10
11
3

700°C for NaBr and 750°C for NaCl. The bomb required about an hour to reach operating temperature. The colouring process was continued for an additional two hours and then the furnace was turned off. The power supply was turned off after the apparatus had cooled to room temperature so that the hydrogen could be safely vented from the bomb. The treated crystals were removed and stored in a dry box until they were mounted in the dewars for taking the spectra.

B. MEASUREMENTS

The side band absorption measurements were carried out at liquid helium temperatures in a cryostat with potassium iodide or polyethylene windows. A specially constructed sample mount held two crystals side by side so that both samples could be examined in one experimental run by means of a small lateral translation of the dewar. One of the crystals was a pure sample and the other contained the H^- ions. Both crystals were cleaved to within a few percent of the same thickness so that they were identical in all respects except for the H^- ion doping. The absorption spectrum was calculated by taking the ratio of the recorder tracings of both crystals. In this way any background absorption not due to the hydrogen was eliminated. The spectra were taken on a Beckman IR-12 infra-red spectrophotometer.Measurements were made in the double beam mode with a beam condenser in

the sample beam. The instrument was flushed with dry nitrogen obtained by boiling off liquid nitrogen from a storage dewar with a small heater. Slit widths were 1.0 or 1.5 times the standard slit program widths of the instrument. These corresponded to spectral widths of 1.0 to 2.0 cm^{-1}. Temperature measurements were made with an 0.2 At.% Fe-Au vs. copper differential thermocouple between the liquid helium container and the crystals. The temperature sensing junction was electrically insulated from the sample holder by means of a sandwich of alkali halide crystals. Thermal contact was achieved by means of thin layers of indium foil between the sample holder, crystals and thermocouple. The temperatures were determined to be 7°K and were conservatively estimated to be in error by about ±2°. Temperature measurements were made primarily to make sure the crystals were below about 10°K and were not made to measure the temperature accurately, since the observed spectra are essentially temperature independent below 15°K or 20°K for all the alkali halides.

The far-infrared spectra were measured with an RIIC FS-720 Fourier Spectrophotometer using a liquid helium cooled germanium bolometer developed by Tumber (1968). This instrument was capable of 0.11 cm^{-1} resolution but most of the spectra were obtained adequately using a resolution of 0.61 cm^{-1}. The experimental arrangement was essentially the same as that

used by Timusk and Ward (1969). Four samples consisting of two doped specimens and two undoped crystals were mounted in a rotatable turret inside an evacuated copper container which was immersed in liquid helium. The light pipe entered from above and the turret could be turned from the outside to bring each crystal in turn into the light beam. Crystal temperatures were not measured but were probably around 10°K since the turret was not too well thermally anchored to the container.

CHAPTER III

THEORY

In a discussion of the infrared spectra due to the presence of impurities in the lattice it is important to know the dynamics of the unperturbed crystal. The lattice dynamics of the alklai halides are well described by the shell model (Cowley et al., 1963). The best parameters for this model are determined from the results of inelastic neutron scattering experiments. Results are now available for LiF (Dolling et al., 1968), NaF (Buyers, 1967), NaCl (Almqvist et al., 1968, Raunio et al., 1969, and Raunio and Rolandson 1970), NaBr (Reid et al. 1970), KCl (Copley et al., 1969, Raunio and Almqvist, 1969, and Raunio and Rolandson, 1970), KBr and NaI (Woods et al., 1963 and Cowley et al., 1963), KI (Dolling et al., 1966), RbCl and RbF (Raunio and Rolandson, 1970). The details of the shell model as applied to the alkali halides and the notation are reviewed in Appendix A. The pertinent results required from the shell model for calculations of the perturbed modes are the eigenfrequencies and polarization vectors evaluated at numerous points on a suitable grid in the Brillouin zone of the crystal.

In addition to using realistic unperturbed phonon data for understanding the defect spectra, it is important to have

a realistic model for the defect. The H^- ion is known to substitute for the halide ion in the alkali halides (Hilsch and Pohl, 1938). The ionic radius of the H^- ion is generally smaller than the ion it replaces so that a different overlap of the ions and some relaxation of the lattice around the defect is expected. Changes in the forces surrounding the defect are presumably due mainly to short range overlap force differences which result from the interaction between different ions and from the equilibrium positions being altered by relaxation. Changes in the long range Coulomb forces make the usual Green's function formalism (Lifshits, 1956) impractical. However, the Coulomb forces do not have as strong a spatial dependence as the repulsive forces so Coulomb changes due to relaxation are expected to be small. Charge changes have a greater effect on the electrostatic interactions and these may be treated by an extended Lifshits formalism as discussed in detail by Strauch (1967). Charge changes may be neglected for the H^- ion in the alkali halides because the effect on the local mode frequency is slight (Page and Strauch, 1967 and 1968) and the even parity side band modes are independent of charge changes because of symmetry (Strauch and Page, 1968). A reasonable model of the H^- ion centre would therefore include a change in mass at the defect site and changed force constants between the H^- ion and its nearest neighbours and, because of relaxation, a change in the force constants be-

tween the first and fourth nearest neighbours.

Such a model in which the H^- ion was treated as a rigid ion has been discussed by Gethins et al. (1967) for the side bands and by Woll et al. (1968) for the far-infrared absorption in KBr and KI. A breathing shell model of the defect which improved the results was described for the hydrogen side bands in KCl, KBr and KI by Page and Strauch (1968). The defect model used in this work is based on the ordinary shell model for the alkali halides. The ions are represented by a charged core made up of the nucleus and inner shell electrons, connected with a rigid shell of valence electrons by means of an isotropic force constant. The effects of deformations of the shell such as in the breathing shell model (Nüsslein and Schröder,1967 and Schröder, 1966) are very small and so are neglected. (See Appendix B for a further discussion on this point.)

The lattice perturbed by an impurity defect may be described by the equation

$$(\underset{\sim}{\Phi} + \underset{\sim}{\Gamma} - \omega^2 \underset{\sim}{I})\underset{\sim}{\chi} = 0 \qquad \text{(III-1)}$$

which is similar to Equation [A-3] given in the Appendix for the perfect lattice. The $\underset{\sim}{\Gamma}$ matrix contains all the changes in the dynamical matrix assumed to be due to introducing the impurity. The unperturbed and perturbed Green's function matrices $\underset{\sim}{G}$ and $\underset{\sim}{\bar{G}}$ respectively are defined by

$$(\underset{\sim}{\phi} - \omega^2\underset{\sim}{I})\underset{\sim}{G}(\omega^2) = \underset{\sim}{I} \qquad \text{(III-2)}$$

$$(\underset{\sim}{\phi} + \underset{\sim}{\Gamma} - \omega^2\underset{\sim}{I})\underset{\sim}{\bar{G}}(\omega^2) = \underset{\sim}{I} \qquad \text{(III-3)}$$

By multiplying equation (III-3) on the left by $\underset{\sim}{G}$, the perturbed Green's function $\underset{\sim}{\bar{G}}$ can be expressed as

$$\underset{\sim}{\bar{G}} = (\underset{\sim}{I} + \underset{\sim}{G}\underset{\sim}{\Gamma})^{-1}\underset{\sim}{G} \qquad \text{(III-4)}$$

or by rearranging the terms

$$\underset{\sim}{\bar{G}} = \underset{\sim}{G} - \underset{\sim}{G}\underset{\sim}{T}\underset{\sim}{G} \qquad \text{(III-5)}$$

where

$$\underset{\sim}{T} = \underset{\sim}{\Gamma}(\underset{\sim}{I} + \underset{\sim}{G}\underset{\sim}{\Gamma})^{-1}. \qquad \text{(III-6)}$$

The non-zero space of $\underset{\sim}{\Gamma}$ is called the defect space. The $\underset{\sim}{T}$ matrix is also non-zero only in this space. When the defect space is of small dimensions expressions (III-4) and (III-5) are particularly useful for determining $\underset{\sim}{\bar{G}}$ from a knowledge of $\underset{\sim}{G}$. Expression (III-4) is useful when elements of $\underset{\sim}{\bar{G}}$ corresponding to coordinates in the vicinity of the impurity are required and (III-5) is convenient when the other elements are required.

In the shell model used here, the H^- is a substitutional defect and is assumed to consist of a changed mass and isotropic core-shell force constant at the site, changed longitudinal force constants to the nearest neighbours and changed longitudinal force constants between the shells of the first and fourth nearest neighbours. These changes are denoted by Δm, Δk, Δf, and Δg respectively and are shown in

FIGURE 2

"Defect molecule" showing ions affected by changes introduced by the insertion of the impurity. The H^- ion is at the centre with Δm representing the change in mass at the defect site. Nearest neighbours are alkali metal ions located $\pm r_o \hat{\alpha}$ and the fourth neighbours are halide ions at $\pm 2\ r_o \hat{\alpha}$, $\alpha = x,y,z$. The force constant changes Δf and Δk are restricted by the local mode frequency and the position of the incipient E_g resonance in the anharmonic side band. The Δg force constant is obtained from the positions of resonances in the side band as explained in Chapter V.

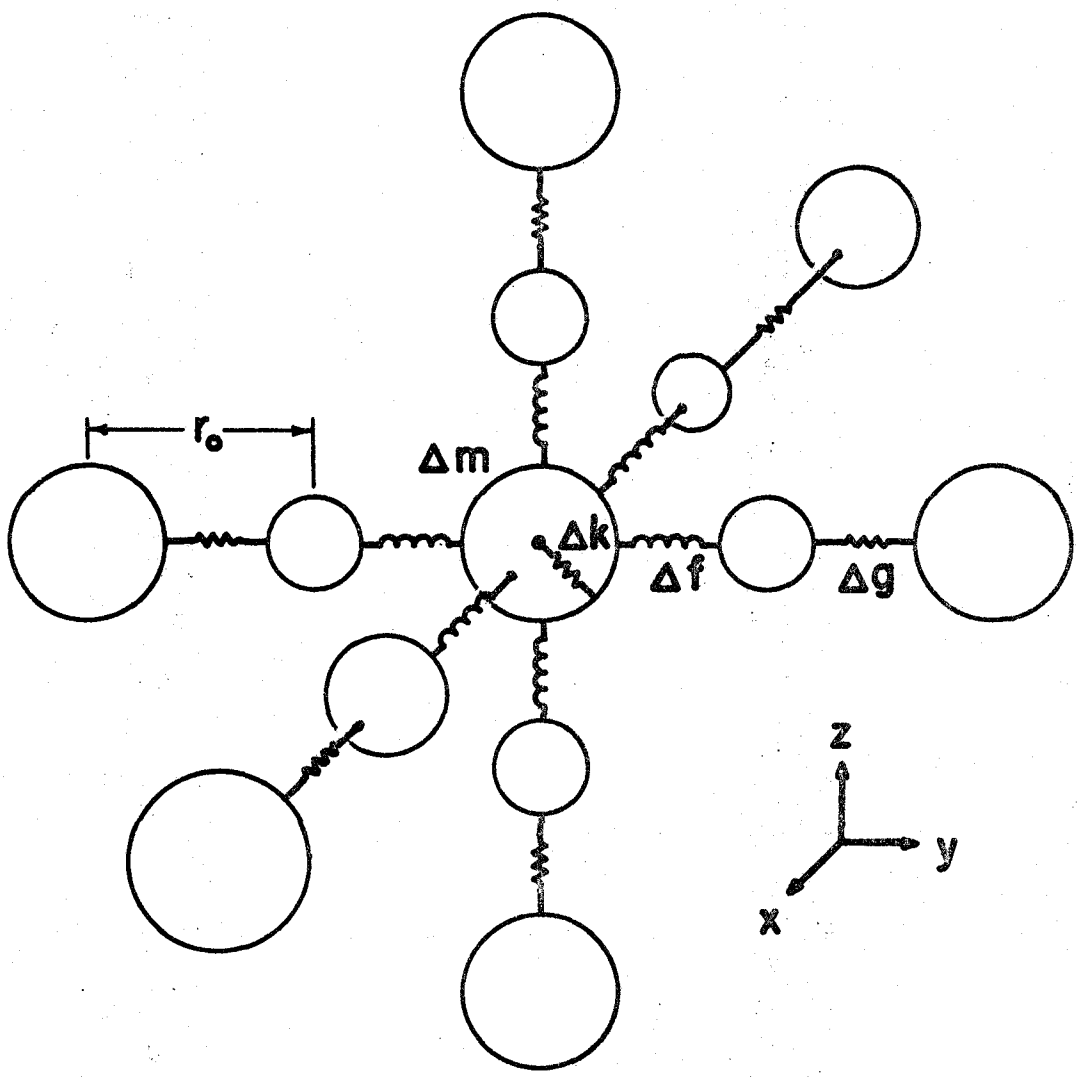
r_o
Δm
Δk
Δf
Δg
z
y
x

Figure 2. The associated matrix is zero everywhere except for an 18-dimensional submatrix γ. In the representation labelled by L, the unit cell index, $\kappa = \pm$, the ion index, and α, the Cartesian component of displacement, the γ matrix is diagonal in three 6-dimensional blocks $\gamma_{\alpha\alpha}$; $\alpha = x,y,z$ where

$$\gamma_{\alpha\alpha} = \begin{bmatrix} \frac{\Delta g}{M} & \frac{-\Delta g}{M} & 0 & 0 & 0 & 0 \\ \frac{-\Delta g}{M} & \frac{\Delta f+\Delta g}{M_+} & 0 & \frac{-\Delta f}{M} & 0 & 0 \\ 0 & 0 & \frac{\Delta k-\Delta m\omega^2}{M_-} & \frac{-\Delta k}{M} & 0 & 0 \\ 0 & \frac{-\Delta f}{M} & \frac{-\Delta k}{M_-} & \frac{\Delta k+2\Delta f}{M_-} & \frac{\Delta f}{M} & 0 \\ 0 & 0 & 0 & \frac{\Delta f}{M} & \frac{\Delta f+\Delta g}{M_+} & \frac{-\Delta g}{M} \\ 0 & 0 & 0 & 0 & \frac{-\Delta g}{M} & \frac{\Delta g}{M_-} \end{bmatrix} \quad \text{(III-7)}$$

with $M_\pm$ being the masses of the ions and $M = \sqrt{M_+ M_-}$. If, for example, the displacement in the $\hat{\alpha}$ direction of the shell at the ion position $r_o\hat{\alpha}$ is called $S_\alpha(r_o\hat{\alpha})$ and the displacement of the defect core at the origin is called $U_\alpha(0)$, then the rows and columns of $\gamma_{\alpha\alpha}$ refer to the displacements. $S_\alpha(-2r_o\hat{\alpha})$, $S_\alpha(-r_o\hat{\alpha})$, $U_\alpha(0)$, $S_\alpha(0)$, $S_\alpha(r_o\hat{\alpha})$, $S_\alpha(+2r_o\hat{\alpha})$ in that order. This perturbation matrix retains the full point symmetry of the cubic lattice. The $\underset{\sim}{\gamma}$ matrix and both $\underset{\sim}{G}$ and $\underset{\sim}{\bar{G}}$ are block diagonalized by transforming to coordinates which form an irreducible basis for the O_h group.

The basis coordinates in the symmetrized defect space are

$$
\begin{aligned}
S(A_{1g};r) &= 1/\sqrt{3}(S_x(g;r)+S_y(g;r)+S_z(g;r)) \\
S(E_g;r) &= 1/\sqrt{2}(S_x(g;r)-S_y(g;r)) \\
S(E'_g;r) &= 1/\sqrt{6}(2S_z(g;r)-S_x(g;r)-S_y(g;r)) \qquad \text{(III-8)} \\
S_\alpha(T_{1u};r\hat{\alpha}) &= S_\alpha(u;r\hat{\alpha}) \\
U_\alpha(T_{1u};0) &= U_\alpha(0)
\end{aligned}
$$

where $S_\alpha(g;r) = 1/\sqrt{2}(S_\alpha(-r\hat{\alpha})-S_\alpha(+r\hat{\alpha}))$

$S_\alpha(u;r) = 1/\sqrt{2}(S_\alpha(-r\hat{\alpha})+S_\alpha(+r\hat{\alpha}))$

$S_\alpha(u;0) = S_\alpha(0)$

for $r = r_o, 2r_o$ and $\alpha = x,y,z$.

When expressed in terms of this basis, the γ matrix has the form

$$
\gamma = \begin{vmatrix}
\gamma(E_g) & & & & & & \\
& \gamma(E'_g) & & & & & \\
& & \gamma(A_{1g}) & & & & \\
& & & \gamma(T_{1ux}) & & & \\
& & & & \gamma(T_{1uy}) & & \\
& & & & & \gamma(T_{1uz}) &
\end{vmatrix} \qquad \text{(III-9)}
$$

where

$$
\gamma(E_g) = \gamma(E'_g) = \gamma(A_{1g}) = \begin{pmatrix} \frac{\Delta f+\Delta g}{M_+} & \frac{-\Delta g}{M} \\ \frac{-\Delta g}{M} & \frac{\Delta g}{M_-} \end{pmatrix} \qquad \text{(III-10)}
$$

and

$$\underset{\sim}{\gamma}(T_{1u\alpha}) = \begin{bmatrix} \frac{\Delta k - \Delta m\omega^2}{M} & \frac{-\Delta k}{M} & 0 & 0 \\ \frac{-\Delta k}{M} & \frac{2\Delta f + \Delta k}{M_-} & \frac{-\sqrt{2}\Delta f}{M} & \\ 0 & \frac{-\sqrt{2}\Delta f}{M} & \frac{\Delta f + \Delta g}{M_+} & \frac{-\Delta g}{M} \\ 0 & 0 & \frac{-\Delta g}{M} & \frac{\Delta g}{M} \end{bmatrix} \qquad \text{(III-11)}$$

Note that as a consequence of the particular form of the defect model, $\underset{\sim}{\gamma}$ has no parts of T_{2g} symmetry. The rows and columns of $\underset{\sim}{\gamma}(A_{1g})$ refer to the coordinates $S(A_{1g};r_o)$ and $S(A_{1g};2r_o)$ and similarly for $\underset{\sim}{\gamma}(E_g)$ and $\underset{\sim}{\gamma}(E_g')$. The corresponding row and column indices for $\underset{\sim}{\gamma}(T_{1u\alpha})$ are $(T_{1u};0)$, $S_\alpha(T_{1u};0)$, $S_\alpha(T_{1u};r_o)$ and $S_\alpha(T_{1u};2r_o)$. The results for the rigid ion defect model are similar except that ion coordinates replace the shell coordinates in the even parity parts of γ. The T_{1u} part is different and has the form

$$\underset{\sim}{\gamma}(T_{1u\alpha}) = \begin{bmatrix} \frac{2\Delta f - \Delta m\omega^2}{M_-} & \frac{-\sqrt{2}\Delta f}{M} & 0 \\ \frac{-\sqrt{2}\Delta f}{M} & \frac{\Delta f + \Delta g}{M_+} & \frac{-\Delta g}{M} \\ 0 & \frac{-\Delta g}{M} & \frac{\Delta g}{M_-} \end{bmatrix} \qquad \text{(III-12)}$$

with the corresponding row and column indices $U_\alpha(T_{1u};0)$, $U_\alpha(T_{1u},r_o)$, $U_\alpha(T_{1u},2r_o)$.

The local mode resonance occurs if a solution exists outside the eigenfrequencies of the perfect lattice to the equation (Klein 1963)

$$\det\left|\underset{\sim}{I} + \underset{\sim}{G}\underset{\sim}{\Gamma}\right| = 0. \qquad \text{(III-13)}$$

Since $\underset{\sim}{\Gamma}$ and $\underset{\sim}{G}$ are block diagonal in the representation defined in equation (III-8), $\underset{\sim}{I} + \underset{\sim}{G}\underset{\sim}{\Gamma}$ is also block diagonal and the determinant in (III-13) reduces to a product of the determinants of each of the blocks. It can be seen from (III-8) that the H^- ion moves only in the T_{1u} modes so the triply degenerate local mode frequency of the substitutional ion is given by

$$\det\left|(\underset{\sim}{I} + \underset{\sim}{g}(\Omega^2)\underset{\sim}{\gamma}(\Omega^2)\right|_{T_{1u}} = 0 \qquad \text{(III-14)}$$

where $\underset{\sim}{g}(\Omega^2)$ is the submatrix of $\underset{\sim}{G}(\Omega^2)$ in the defect space. In the case of the H^- ion in the alkali halides, the local mode frequency Ω is much larger than the maximum frequency of the unperturbed lattice so to a good approximation only the motion of the ion and its nearest neighbours need to be considered. This amounts to assuming Δg is zero in $\underset{\sim}{\gamma}(T_{1u\alpha})$ of equation (III-14). As Ω is known from experiment, this leads to a dependence relation between Δf and Δk which is independent of Δg (Page and Strauch, 1967). The Green's function matrix is real at the local mode frequency and the required elements in the defect space can be calculated as described in Appendix A.

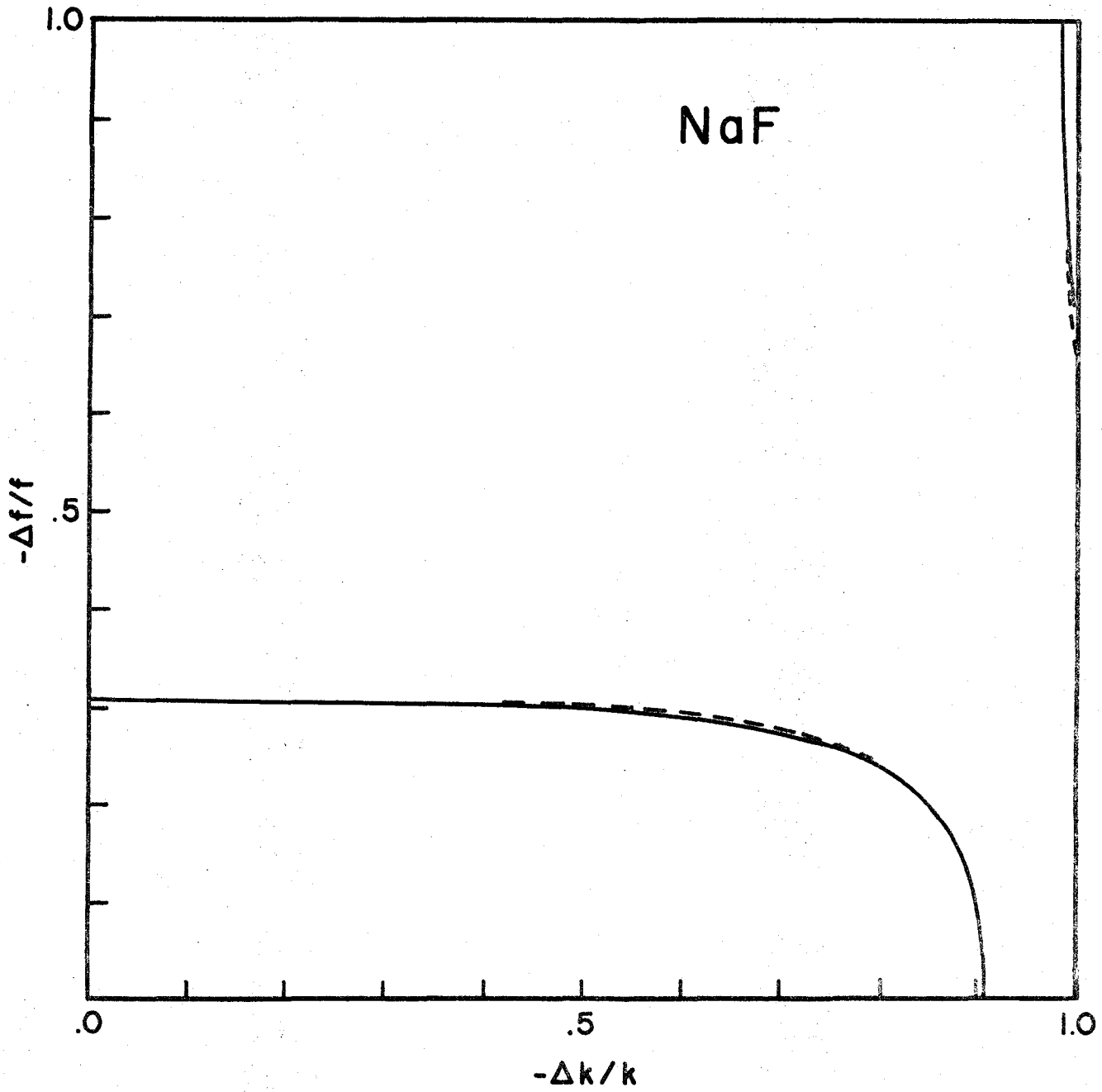

FIGURE 3. Plot of Δf vs. Δk for NaF. Local mode frequency Ω is 860 cm^{-1} and the unperturbed force constants are $f = 4.33 \times 10^4$ dynes/cm, $k = 1.13 \times 10^6$ dynes/cm. Solid curve includes motions of the nearest neighbours and the dashed curve is for motions confined to the H^- ion.

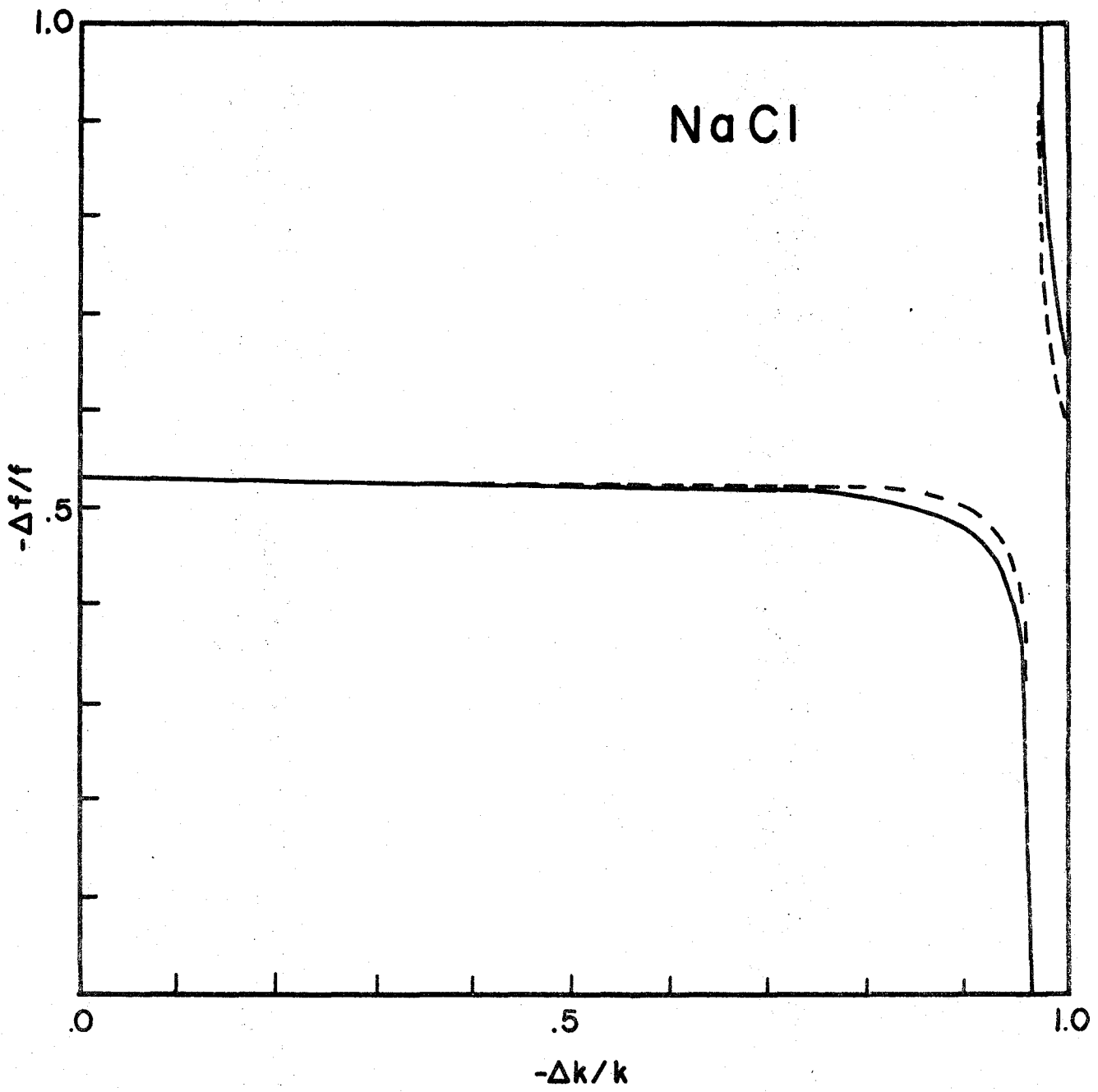

FIGURE 4. Plot of Δf vs. Δk for NaCl. Local mode frequency Ω is 562.6 cm^{-1} and the unperturbed force constants are $f = 2.50 \times 10^4$ dynes/cm, $k = 9.56 \times 10^5$ dynes/cm. Solid curve includes motions of the nearest neighbours and the dashed curve is for motions confined to the H^- ion.

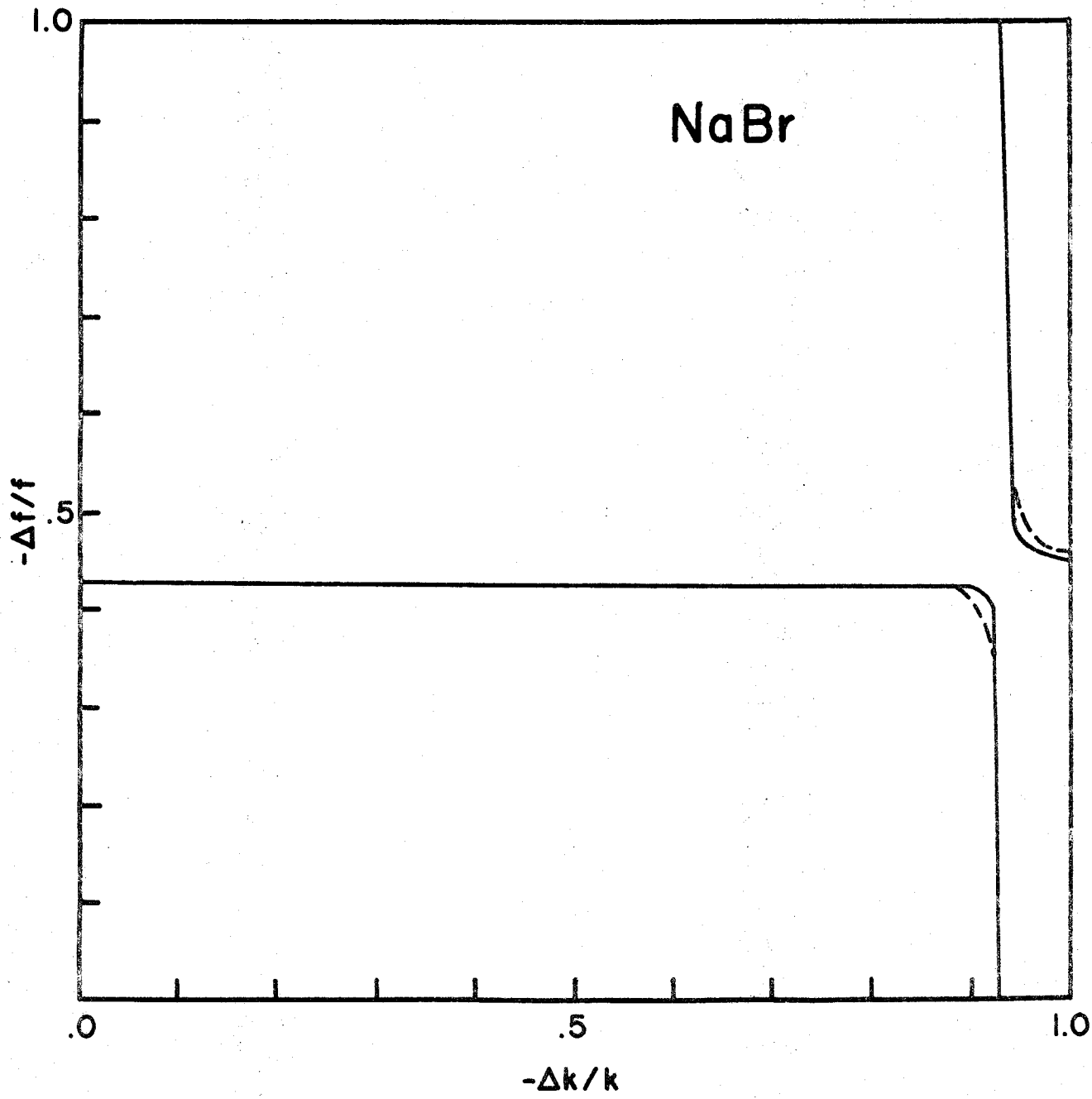

FIGURE 5. Plot of Δf vs Δk for NaBr. Local mode frequency Ω is 495.8 cm^{-1} and the unperturbed force constants are $f = 2.46 \times 10^5$ dynes/cm , $k = 7.29 \times 10^5$ dynes/cm. Solid curve includes motions of the nearest neighbours and the dashed curve is for motions confined to the H^- ion.

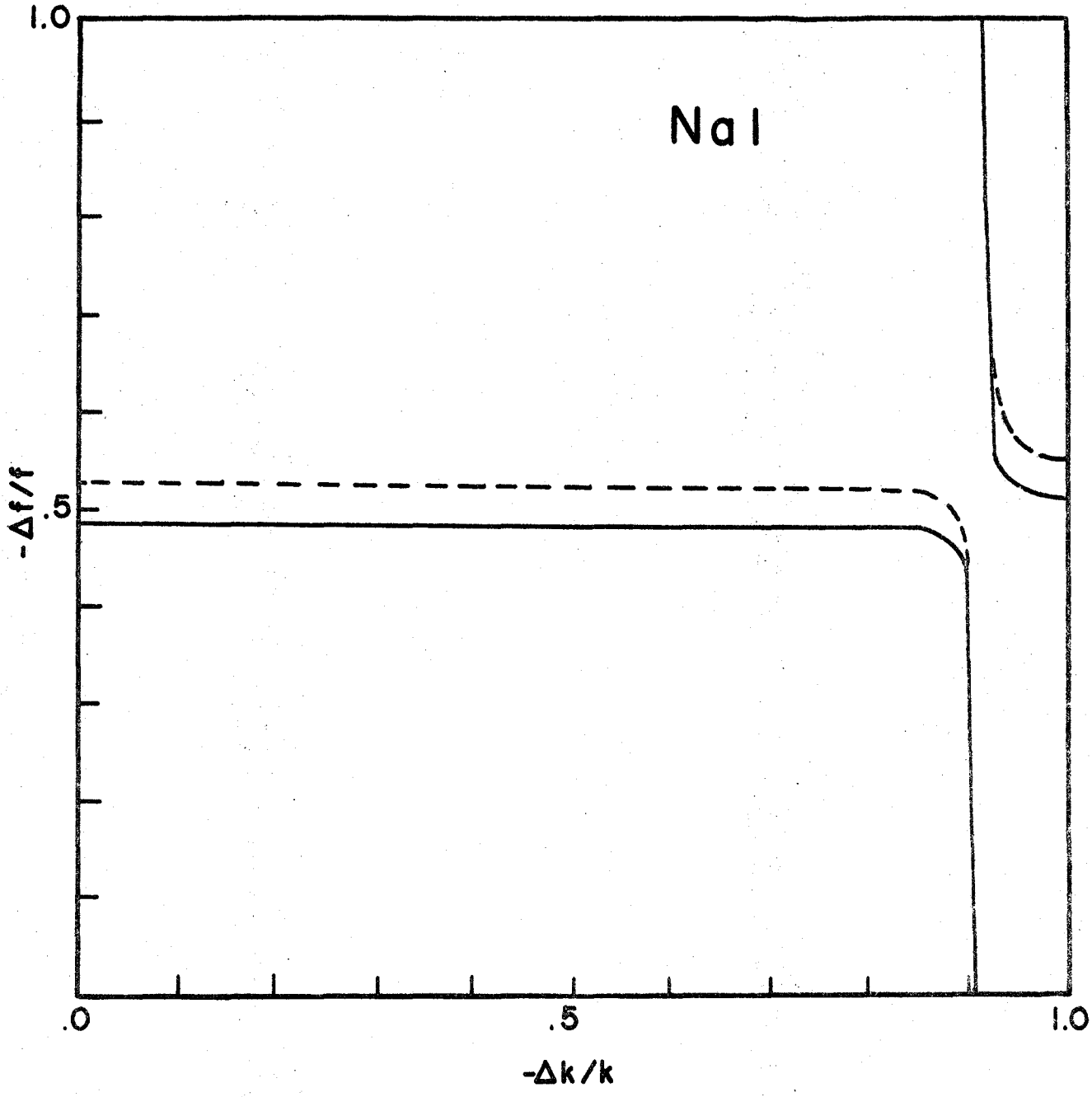

FIGURE 6. Plot of Δf vs Δk for NaI. Local mode frequency Ω is 426.8 cm^{-1} and the unperturbed force constants are $f = 1.73 \times 10^4$ dynes/cm , $k = 7.99 \times 10^5$ dynes/cm. Solid curve includes motions of the nearest neighbours and the dashed curve is for motions confined to the H^- ion.

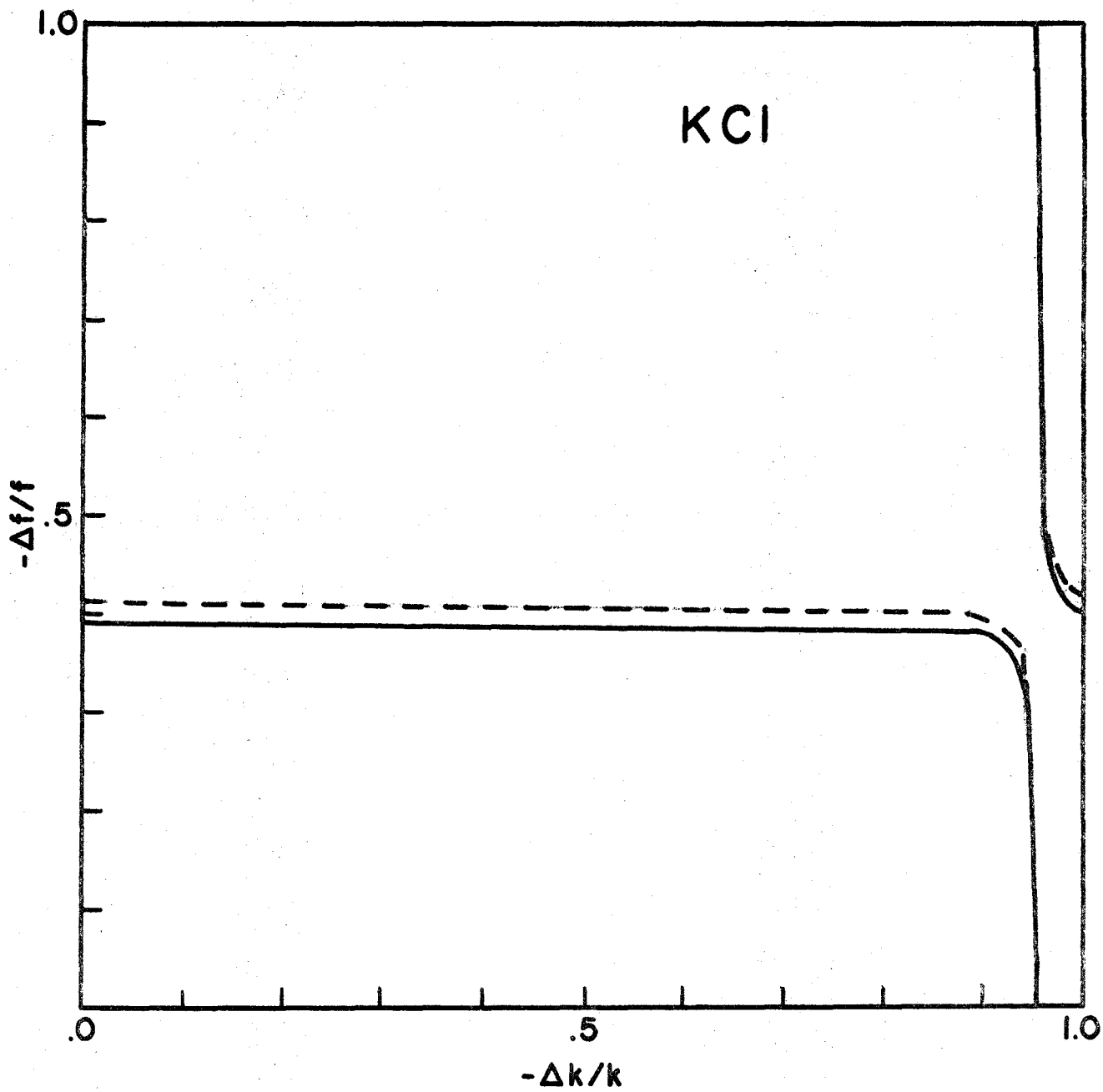

FIGURE 7. Plot of Δf vs Δk for KCl. Local mode frequency Ω is 501.6 cm^{-1} and the unperturbed force constants are $f = 2.30 \times 10^4$ dynes/cm, $k = 8.76 \times 10^5$ dynes/cm. Solid curve includes motions of the nearest neighbours and the dashed curve is for motions confined to the H^- ion.

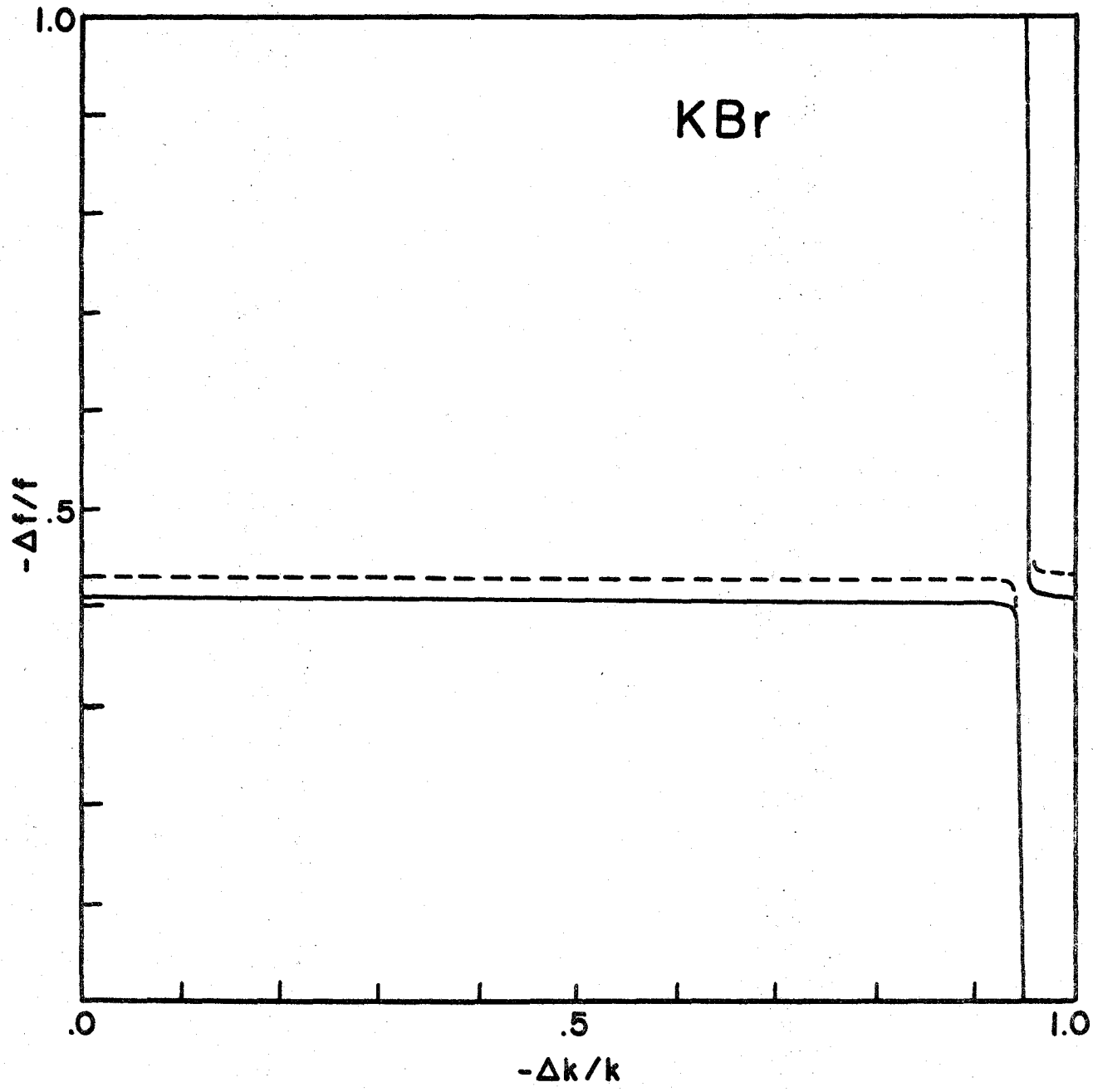

FIGURE 8. Plot of Δf vs Δk for KBr. Local mode frequency Ω is 444. cm^{-1} and the unperturbed force constants are $f = 2.15 \times 10^5$ dynes/cm, $k = 7.85 \times 10^5$ dynes/cm. Solid curve includes motions of the nearest neighbours and the dashed curve is for motions confined to the H^- ion.

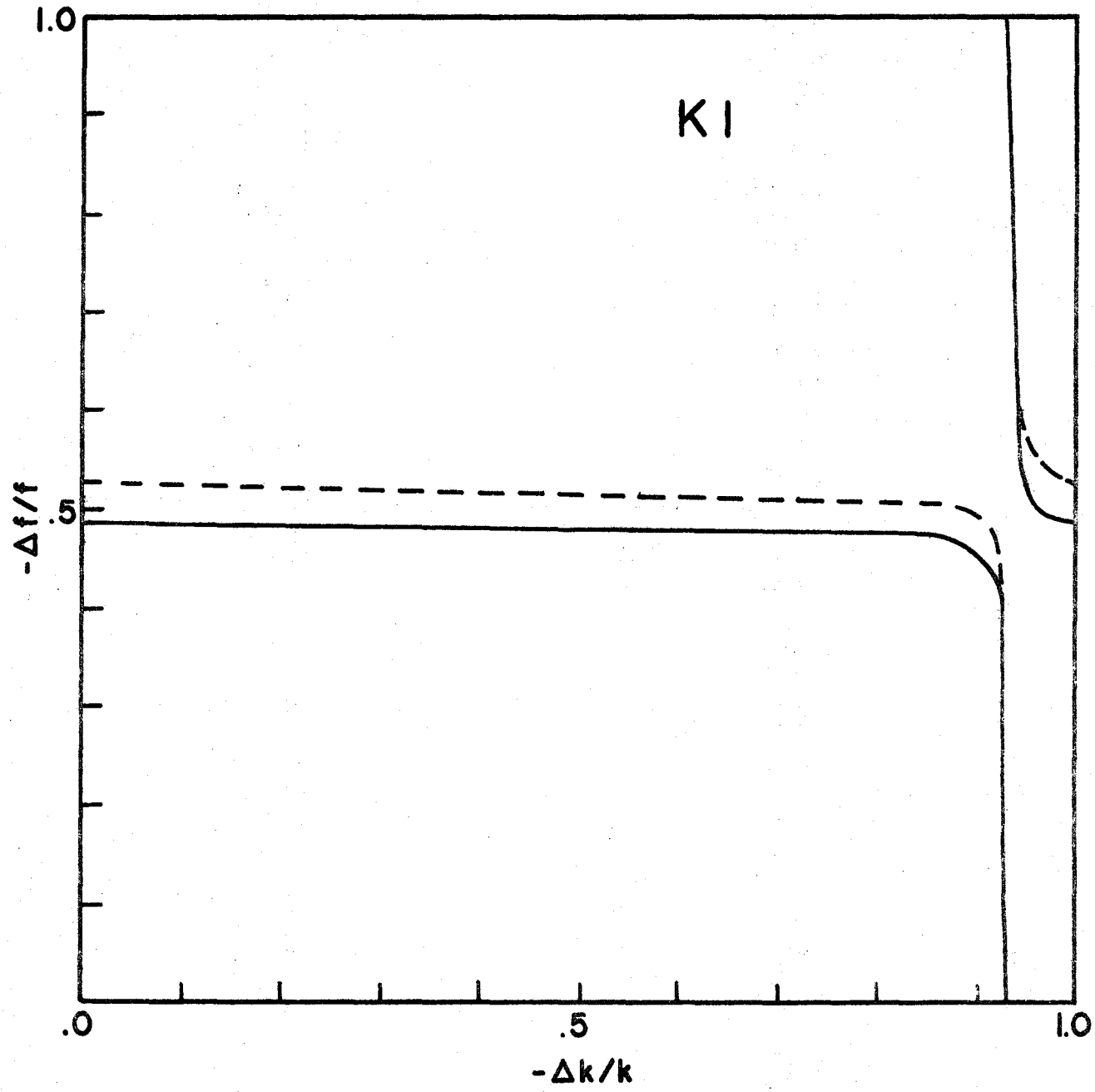

FIGURE 9. Plot of Δf vs Δk for KI. Local mode frequency Ω is 379.8 cm^{-1} and the unperturbed force constants are f = 1.81 × 10^4 dynes/cm, k = 1.02 × 10^6 dynes/cm. Solid curve includes motions of the nearest neighbours and the dashed curve is for motions confined to the H-ion.

Plots of Δf against Δk for the various alkali halides that were studied are given in Figures 3 to 9. Only those portions of the curves that correspond to a reduction in the core-shell isotropic force constant and in the shell-shell nearest neighbours force constant are shown since it is known that the H^- ion is associated with decreased forces (Jaswal and Montgomery, 1964, for example). The results are similar to the work of Page and Strauch (1967 and 1968) but with slight numerical differences due to the use of unperturbed phonons obtained from neutron scattering data rather than from the breathing shell model. Force constant changes along the upper branch of the curves were not used because they tend to produce unphysical results such as a reduction in the force constants of more than 100% and a very large or negative defect polarizability. The dashed curves are the result when only the coordinates referring to the defect are included in $\underset{\sim}{\gamma}(T_{1u})$. This approximation holds if the local mode vibration is very highly localised so, as can be seen from the plots, the assumption of local vibrations is a good one and that omitting the motions of the fourth nearest neighbours in (III-14) (i.e. by setting Δg zero) is justified.

Note that because the Δf versus Δk curves are nearly constant for $-\Delta k/k$ less than about 0.9, small errors in the determination Δf will result in widely differing values for Δk.

The situation for in-band resonances is not quite so clear (Takeno, 1967). The absorption coefficient for the side band and induced far infrared absorption has a factor

$$D(\omega^2) = \det|\underset{\sim}{I} + \underset{\sim\sim}{G\Gamma}| \qquad \text{(III-15)}$$

in the denominator which results from the inversion of $\underset{\sim}{I} + \underset{\sim\sim}{G\Gamma}$ required to evaluate $\underset{\sim}{\bar{G}}$. When the real and imaginary parts of $D(\omega^2)$ are denoted by $D_R(\omega^2)$ and $D_I(\omega^2)$ respectively the absorption is proportional to

$$\frac{D^*(\omega^2)}{D_R^2(\omega^2) + D_I^2(I)} \cdot$$

$D(\omega^2)$ is real for frequencies outside of the band of natural frequencies for the perfect lattice. If $D_R(\omega^2)$ is zero for any of these frequencies there will be poles in the calculated absorption as is the case for the local mode. For in-band frequencies $D(\omega^2)$ is complex and resonances may occur when

$$D_R(\omega^2) = 0 \cdot \qquad \text{(III-16)}$$

Near a resonant frequency, ω_o, the absorption may be approximated by the standard resonance form

$$\alpha(\omega) \propto \frac{D^*(\omega^2)}{\left|dD_R(\omega^2)/d\omega\right|^2_{\omega=\omega_o}} \quad \frac{1}{(\omega-\omega_o)^2 + (\Gamma_o/2)^2} \qquad \text{(III-17)}$$

where

$$\Gamma_o/2 = D_I(\omega^2)/[dD_R(\omega^2)/d\omega]_{\omega=\omega_o} \cdot$$

Not all solutions of (III-16) guarantee a sharp resonance. The width of $\Gamma_o/2$ of the resonance at ω_o must be small compared to the width of the lattice band. This occurs whenever $D_I(\omega^2)$ is small or when $|dD_R(\omega^2)/d\omega|_{\omega=\omega_o}$ is large or both. The incipient resonance occurs when $D_R(\omega^2)$ is very small but not zero and when the width is narrow. The best example of this last situation in the H^- ion spectra is in the E_g modes for the side bands. The incipent E_g resonances are the dominant side band features.

CHAPTER IV

CALCULATION OF THE ABSORPTION

A. SIDE BAND

The side band is attributed to third order anharmonic coupling of the local mode vibration to the perturbed vibrational modes of the nearest neighbour ions (Timusk and Klein, 1966). In this work the anharmonicities in the shell-shell force constants are assumed to be the most important ones. The independent anharmonic coefficients as determined by symmetry arguments are (Page and Strauch, 1968):

$$\begin{aligned} a &= \Phi^{S}_{xxx}(r_o\hat{x},0,0) \\ b &= \Phi^{S}_{yxy}(r_o\hat{x},0,0) \\ \text{and } c &= \Phi^{S}_{xyy}(r_o\hat{x},0,0) \end{aligned} \qquad \text{(IV-1)}$$

The superscript, S, signifies that the derivatives are taken with respect to the positions of the shells on the ions located at the positions indicated by the arguments of the coefficients. The derivatives are evaluated at the equilibrium positions. For a central potential c = b.

Symmetry considerations show that the local mode can couple to only the modes of the nearest neighbours which have A_{1g}, E_g, or T_{2g} symmetry (Kühner and Wagner, 1967). Gethins

(1968) has shown that the absorption constant for the upper frequency side band at low temperatures can be written in a form similar to

$$\alpha_{xx}(\omega) \propto \frac{(1+\frac{\omega}{\Omega})}{(1+\frac{\omega}{2\Omega})^2\omega^2} Im\{\frac{(1+2\xi)^2}{3} \underset{\sim}{G}_{SS}(\omega^2+i0^+;A_{1g}) + \frac{2(1-\xi)^2}{3} \underset{\sim}{G}_{SS}(\omega^2+i0^+;E_g) + 4\xi^2 \underset{\sim}{G}_{SS}(\omega^2+i0^+;T_{2g}) \qquad \text{(IV-2)}$$

where here shell cordinates have been substituted for the ion coordinates since only anharmonicity in the shell-shell forces is considered. The local mode frequency is Ω and ω is the frequency above Ω. The parameter ξ is the ratio c/a. The Green's function matrix elements correspond to the symmetrized coordinates of Equation (III-8) and to

$$S_{\alpha\beta}(T_{2g};r_o) = 1/\sqrt{2}\ (S_\alpha(g;r_o\hat{\beta}) - S_\beta(g;r_o\hat{\alpha})), \qquad \text{(IV-3)}$$
$$\alpha\beta = xy,yz,xz.$$

These elements refer to the shells of the nearest neighbour ions and were evaluated by the method described in Appendix A and from (III-4).

An estimate of ξ was made by looking at the forces in the alkali halide and alkali hydride crystals. It seems reasonable to assume that the forces between the hydrogen impurity and its nearest neighbours in the alkali halide host crystal are similar to those in the perfect alkali hydride crystal but evaluated at the nearest neighbour distance in

the perfect halide crystal. The interionic potential with an exponential respulsive part is approximately of the form

$$\Phi(r) = \lambda \exp(-r/\rho) - \frac{Z^2 e^2 \alpha_M}{r} \qquad \text{(IV-4)}$$

where r is the separation between ions, λ and ρ are repulsive force parameters, Ze is the ionic charge and α_M is the Madelung constant. The lattice energy of the crystal at equilibrium is

$$\Phi(r_o) = -\frac{Z^2 e^2 \alpha_M}{r_o} \left(1 - \rho/r_o\right) \qquad \text{(IV-5)}$$

and can be obtained from the enthalpy tables (Handbook of Chemistry and Physics, 1959 for example) by the use of Hess' Law. At room temperature the crystal energies obtained for sodium and potassium hydride crystals are

$$\text{NaH} : \Phi(r_o) = -191 \text{ kcal/mole}$$
$$\text{KH} : \Phi(r_o) = -169 \text{ kcal/mole.}$$

The corresponding values of ρ obtained with the approximation Z = 1 are

$$\rho_{NAH} = 0.48 \text{ Å}$$
$$\rho_{KH} = 0.50 \text{ Å}$$

where the lattice parameters (Gibb, 1962)

$$r_o(\text{NaH}) = 2.450 \text{ Å}$$
$$\text{and } r_o(\text{KH}) = 2.856 \text{ Å}$$

have been used. If the temperature dependence of the forces is assumed to be due only to changes in r_o with temperature,

TABLE I

Estimated anharmonic coupling parameters derived from a Born-Mayer potential and crystal energies calculated from Hess' Law. The uncertainty in ξ due to the accuracy of the data is about 10%. The generally small values obtained for ξ mean that the T_{2g} modes do not contribute very much to the side band absorption

Material	ξ
NaF	-0.17
NaCl	-0.14
NaBr	-0.13
KCl	-0.13
KBr	-0.12
KI	-0.11

then the room temperature values obtained above for ρ may be used to estimate the forces at low temperatures. The ratio of the anharmonic coefficients is

$$\xi = -\frac{\rho}{r_o}\left(\frac{1 - 2\rho/r_o}{1 - 6(\rho/r_o)^2}\right) \qquad \text{(IV-6)}$$

which was evaluated for each of the alkali halides using the appropriate ρ and lattice constants. The calculated estimates for ξ are given in Table I.

B. INDUCED FAR-INFRARED ABSORPTION

The absorption in the far-infrared of pure alkali halide crystals is normally restricted to the reststrahlen frequency. When impurities are present, translational symmetry is lost and the selection rule that restricted absorption to the reststrahlen no longer holds. For example, in addition to the high frequency local mode absorption of alkali halide crystals containing hydrogen, there is increased absorption in the region of frequencies near the top of the acoustic band. This absorption can be calculated from the model for the H^- ion used for the side bands by a method similar to that described by Woll et al. (1968).

An expression for the extra absorption due to an impurity in an alkali halide lattice is given by Klein (1968) as

$$\alpha(\omega) = \frac{4\pi(n_\infty^2+2)^2\omega}{Nv\ c9n(\omega)}\ Im(\underset{\sim}{Z}_x^\dagger \underset{\sim}{M}^{-\frac{1}{2}} \underset{\sim}{G}\underset{\sim}{T}\underset{\sim}{G}\underset{\sim}{M}^{-\frac{1}{2}} \underset{\sim}{Z}_x) \qquad \text{(IV-7)}$$

where n_∞ is the high frequency dielectric constant, $n(\omega)$ is the dielectric constant at the frequency ω and is assumed constant over the range of frequencies in the band of lattice modes, c is the velocity of light, $\underset{\sim}{G}$ is the unperturbed Green's function matrix, $\underset{\sim}{T}$ is the "scattering" matrix of Equation (III-6), and $\underset{\sim}{Z}_x$ is one of a set of three vectors $\underset{\sim}{Z}_x$, $\underset{\sim}{Z}_y$, and $\underset{\sim}{Z}_z$ with components

$$Z^{\alpha}_{\beta}(L\kappa) = Z_\kappa \delta_{\alpha\beta}. \qquad \text{(IV-8)}$$

The charge on the κ ion in the unit cell L is $Z_\kappa e$ and $\underset{\sim}{M}^{-\frac{1}{2}}$ is a diagonal matrix with elements $1/\sqrt{M_\kappa}\ \delta_{LL'}\delta_{\kappa\kappa}\delta_{\alpha\beta}$. In a rigid ion model of the alkali halides $Z_+ = -Z_- = Z$ and the vector $\underset{\sim}{M}^{-\frac{1}{2}}\underset{\sim}{Z}_x$ is proportional to the $\underset{\sim}{q}=0$ transverse optical phonon eigenvector polarized in the x-direction. However, in the case of the shell model both ion cores and shells have individual charges and the situation is somewhat more complicated. The Green's function matrix can be written in separated from as described in Appendix A. Then the vector $\underset{\sim}{R}_x(\omega)=\underset{\sim}{G}\underset{\sim}{M}^{-\frac{1}{2}}\underset{\sim}{Z}_x$ in Equation (IV-7) is somewhat modified and becomes

$$R_x(\omega) = \begin{pmatrix} \underset{\sim}{G}_{UU} & \underset{\sim}{G}_{US} \\ \underset{\sim}{G}_{SU} & \underset{\sim}{G}_{SS} \end{pmatrix} \begin{pmatrix} \underset{\sim}{M}^{-\frac{1}{2}} & 0 \\ 0 & \underset{\sim}{M}^{-\frac{1}{2}} \end{pmatrix} \begin{pmatrix} \underset{\sim}{X}_x \\ \underset{\sim}{Y}_x \end{pmatrix}. \qquad \text{(IV-9)}$$

The vectors $\underset{\sim}{X}_x$ and $\underset{\sim}{Y}_x$ are similar to $\underset{\sim}{Z}_x$ except that they refer to core and shell charges respectively.

In terms of the eigenvectors $\underset{\sim}{\varepsilon}$ and $\underset{\sim}{\eta}$ and eigenfrequencies $\omega_{\underset{\sim}{q}j}$ of Appendix A the components of $R_x(\omega)$ are

$$\{R_x(\omega)\}^U_{L\kappa\alpha} = \{\underset{\sim}{G}_{UU}\,\underset{\sim}{M}^{-\frac{1}{2}}\,\underset{\sim}{X}_x + \underset{\sim}{G}_{US}\,\underset{\sim}{M}^{-\frac{1}{2}}\,\underset{\sim}{Y}_n\}_{L'\kappa\alpha}$$

$$= \sum_{L'\kappa'\beta}\frac{1}{N}\sum_{\underset{\sim}{q}j}\frac{\varepsilon_\alpha(\kappa;\underset{\sim}{q}j)[\varepsilon^\dagger_\beta(\kappa,\underset{\sim}{q}j)X_{\kappa'}+\eta^\dagger_\beta(\kappa'\underset{\sim}{q}j)Y_{\kappa'}]\delta_{\beta x}\exp i\underset{\sim}{q}\cdot(R_{L\kappa}-R_{L'\kappa'})}{(\omega^2_{\underset{\sim}{q}j}-\omega^2)\sqrt{M_{\kappa'}}}$$

$$= \sum_{\kappa'j}\frac{\varepsilon_\alpha(\kappa;0j)}{\omega^2_{0j}-\omega^2}\,\frac{[\underset{\sim}{\varepsilon}^\dagger(\kappa';0j)\cdot\underset{\sim}{X}_x + \underset{\sim}{\eta}^\dagger(\kappa';0k)\,\underset{\sim}{Y}_x]}{\sqrt{M_{\kappa'}}} \qquad \text{(IV-10)}$$

and

$$\{R_x(\omega)\}^S_{L\kappa\alpha} = \sum_{\kappa'j}\frac{\eta_\alpha(\kappa;0j)}{\omega^2_{0j}-\omega^2}\,\frac{[\underset{\sim}{\varepsilon}^\dagger(\kappa';0j)\cdot\underset{\sim}{X}_x + \underset{\sim}{\eta}^\dagger(\kappa';0j)\cdot\underset{\sim}{Y}_x]}{\sqrt{M_{\kappa'}}}$$

$$+ \sum_{\kappa'}\phi^{-1}_{SS}\binom{\kappa\kappa'}{\alpha x}\frac{Y_{\kappa'}}{\sqrt{M_{\kappa'}}}\,.$$

The $\underset{\sim}{q} = 0$ vectors $\underset{\sim}{\varepsilon}(\kappa,0j)$ and $\underset{\sim}{\eta}(\kappa;0j)$ have non-zero x-components only for the transverse optic (TO) and transverse acoustic (TA) modes polarized in the x-direction. These components are

$$\eta_x(\pm;0,TA) = \varepsilon_x(\pm;0,TA) = [M_\pm/(M_+ + M_-)]^{\frac{1}{2}}$$

$$\varepsilon_x(\pm;0,TO) = \pm[M_\mp/(M_+ + M_-]^{\frac{1}{2}}$$

and $\eta_x(\pm;0,TO)$ which is obtained from $\varepsilon_x(\pm;0,TO)$ by means of Equation (A-17). The coefficients of the acoustic modes in Equation (IV-10) are zero so only the x-polarized transverse optic modes contribute to the sum over j.

The elements of $R_x(\omega)$ are independent of the unit cell L and so those components referring to the neighbours in the ± x-directions have the same sign. The vector is therefore "odd" in symmetry with respect to the H^- ion. This means if the same transformation is applied to $R_x(\omega)$ and to $\underset{\sim}{t}$, the non-zero block of $\underset{\sim}{T}$ in the defect space, as was applied to $\underset{\sim}{\gamma}$ and to $\underset{\sim}{G}$ to obtain the independent symmetrized blocks, then only the elements of T_{lux} symmetry appear in Equation (IV-7). The elements of $t(T_{lux})$ are obtained from

$$\underset{\sim}{t}(T_{lux}) = \underset{\sim}{\gamma}(T_{lux})[\underset{\sim}{I} + \underset{\sim}{g}(T_{lux})\underset{\sim}{\gamma}(T_{lux})]^{-1} \qquad \text{(IV-11)}$$

where $\underset{\sim}{g}(T_{lux})$ is the T_{lux} submatrix of $\underset{\sim}{G}$ within the defect space. The components for $R_x(\omega)$ in the same representation are

$$R_x(T_{lux};\omega) = \frac{p}{\omega_{TO}^2-\omega^2} \begin{vmatrix} \varepsilon_x(-,0,TO) \\ \eta_x(-,0,TO) \\ \sqrt{2}\eta_x(+,0,TO) \\ \sqrt{2}\eta_x(-,0,TO) \end{vmatrix} + \begin{vmatrix} 0 \\ R_x^-(0) \\ \sqrt{2}\ R_x^+(0) \\ \sqrt{2}\ R_x^-(0) \end{vmatrix}$$

where

$$p = \sum_{\kappa} \frac{\underset{\sim}{\varepsilon}^\dagger(\kappa,0,TO)\cdot\underset{\sim}{X}_\kappa + \underset{\sim}{\eta}^\dagger(\kappa,0,TO)\cdot\underset{\sim}{Y}_\kappa}{\sqrt{M_\kappa}}$$

and

$$R_x^\kappa(0) = \sum_{\kappa'} \phi_{SS}^{-1}\ (^{\kappa\kappa'}_{xx})Y_{\kappa'}/\sqrt{M_{\kappa'}}. \qquad \text{(IV-12)}$$

If the crystal is considered to contain a random distribution of non-interacting impurities with a concentration N per unit volume then the number of impurities is NNv so that the total induced absorption is

$$\alpha(\omega) = \frac{4\pi(n_\infty^2+2)^2\omega N}{9cn(\omega)} (R_x^\dagger(\omega) Imt(\omega^2-i0^+) R_x(\omega))_{T_{lux}} . \quad \text{(IV-14)}$$

This expression was used to calculate the line shape of the far-infrared absorption below the reststrahlen frequency.

CHAPTER V

RESULTS AND DISCUSSION

A. ANHARMONIC SIDE BANDS

Some of the features of the side bands of the H^- ion local modes are qualitatively common to all the materials studied. The most striking feature is the large broad peak in the acoustical region of the spectrum. This peak is attributed to an incipient resonance in the E_g modes of the nearest neighbours. Its position is mainly dependent on Δf and it is generally quite insensitive to Δg. A value of Δf was chosen within the relatively narrow range required by the local mode condition (III-14) to reproduce the observed positions of this peak. In principle, this choice of Δf then fixed Δk.

The gaps between the acoustic and optic modes in NaBr, KBr and KI appear in the side band spectra and there are strong narrow peaks near the top of the acoustic region and the bottom of the optic region in these materials. The positions of these latter features are primarily determined by Δg. In NaF, NaCl and KCl, which do not have gaps, no such peaks were seen in the measured side bands. Calculations of the side band for NaF and KCl show no evidence of fully developed resonances but an unobserved E_g resonance appears

at high frequencies in the calculations for NaCl when $-\Delta g$ is less than 2500 dynes/cm. (This point will be examined further in the discussion on NaCl.) Consequently, a definite value could not be assigned to Δg in these three materials. The values that were used were chosen to give the best overall fit to the side band shape.

A consequence of the relatively small motions of the shells against the cores is that the rigid ion defect model used by Gethins et al. (1967) is almost equivalent to the shell model defect with $\Delta k = 0$. In this case the local mode uniquely determines Δf and the same effective forces act for the side band modes as for the local mode. However, when this value of Δf is used in the side band calculations, the position of the incipient resonance is correctly predicted only in KCl, KBr, KI and NaBr. This indicates that in NaCl and NaI and especially NaF the effective force constant involved in the even parity motions of the nearest neighbours is different from the force constant for the odd parity motions.

The shell model defect attempts to account for different effective forces for motions of different parity by by allowing for a changed polarizability at the defect site. This is evident from the fact that Δk, which is related to the crystal polarizability of the H^- ion, appears only in the T_{1u} modes as shown in (III-8). The values of this polariza-

bility, which are tabulated in Table II, have been calculated from

$$\alpha_H = (Y\_e)^2/[k' + 2(f' + f_t)] \qquad (V\text{-}1)$$

where k' is the perturbed isotropic core-shell force constant at the defect site and f' and f_t are the perturbed longitudinal and unperturbed transverse force constants respectively, to the nearest neighbours. The polarizability of the H^- ion depends strongly on the host lattice in qualitative agreement with the results of Wood and Gilbert (1967) who found quantum mechanically that no definite value can be assigned which is valid for all alkali halide crystals. However, in the potassium halides changes in k are required to obtain quantitative agreement with their polarizabilities. These changes (in units of $-\Delta k/k$) are 0.70, 0.62 and 0.57 for KCl, KBr and KI respectively; all of which lie on the very flat portion of the Δf vs Δk curves (Figures 7 to 9) where Δk cannot be accurately determined from sideband spectra and local mode position. Therefore, the experimentally derived force constants are not inconsistent with the values needed to give Wood and Gilbert's results.

The results of the calculations indicate that it is generally not possible to associate certain Van Hove singularities (Van Hove, 1953) in the phonon density of states with the observed peaks in the side band spectra.

TABLE II

Effective crystal polarizabilities of H^- ions in the potassium and sodium halides. Values in column A were calculated from (V-1) using the parameters fitted to the side band spectra and the local mode position (Table III). Column B contains the values calculated by Wood and Gilbert (1967). The host lattice anion polarizabilities, α_-, are from the shell model parameters in Table V.

Crystal	$\alpha_H(\mathring{A}^3)$		$\alpha_-(\mathring{A}^3)$
	A	B	
NaF	3.63	-	0.70
NaCl	18.87	-	2.16
NaBr	4.32	-	3.97
KCl	2.18	6.95	2.12
KBr	3.11	8.00	3.05
KI	4.59	10.04	4.51

The principal observed peaks can be associated with nearest neighbour resonances which are a consequence of the perturbed environment of the defect site. A definite feature of the unperturbed density of states that appears in the side bands is the gap between the acoustic and optic modes. There is also an indication that some of the high frequency peaks seen in NaCl are due to remnants of Van Hove singularities.

The values of the parameters which were fitted to the side band spectra for the rigid ion and shell model defect models are compared in Table III and the calculated positions of the peaks are compared with the observed positions in Table IV. The force constant changes for KBr and KI differ slightly from those of Gethins et al. (1967) because some minor terms which were neglected in the paper have been included in the results here. The nearest neighbour force constant changes in the potassium halides are the same for the rigid ion and shell defect models in agreement with the earlier remark that these models are nearly equivalent when $\Delta k = 0$. The absorption specific to each material will be discussed in greater detail after the next section.

B. INDUCED FAR-INFRARED ABSORPTION

In addition to the local mode and side band absorption the presence of H^- ions in the crystals increased the

TABLE III

Force constant changes fitted to the side band and local mode frequency of the H^- ion in the alkali halides. The rigid ion defect model is that described by Gethins et al. (1967) with new calculations for KCl, NaF, NaCl and NaBr.

HOST CRYSTAL	DEFECT MODEL				
	RIGID ION		SHELL		
	$-\Delta f$	$-\Delta g$	$-\Delta f$	$-\Delta g$	$-\Delta k$
NaF	12,200	0	6,500	0	960,000
NaCl	12,300	4750	11,700	4700	860,000
NaBr	10,060	4000	10,800	5500	45,000
KCl	9,095	0	9,095	0	0
KBr	8,855	4400	8,855	4100	0
KI	8,945	5150	8,945	5150	0

Note: All quantities are in dynes/cm.
In several cases the number of significant figures exceeds the accuracy to which the force constant changes have been determined.

TABLE IV

Calculated and observed positions of the local mode and side band peaks of the substitutional H^- ion in the potassium and sodium halides.

HOST CRYSTAL	DEFECT MODEL: RIGID ION	DEFECT MODEL: SHELL	OBSERVED	LOCAL MODE
NaF:				
Incip.Res.	146	168	168	860 ± 1
NaCl:				
Incip.Res.	78	81	81	562.6 ± 0.5
E_g res.	89	94	(unobserved)	
NaBr:				
Incip.Res.	56	56.5	56	495.8 ± 0.5
E_g res.	86	84.5	83.5	
A_{1g} res.	134	137	140	
KCl:				
Incip.Res.	64	64	64	501.6 ± 0.5
KBr:				
Incip. res.	43	44	44	444[a]
E_g res.	80	80	80	
A_{1g} res.	108	110	111	
KI:				
Incip.res.	29	30.5	31	379.8 ± 0.5
E_g res.	67	66.8	65	
A_{1g} res.	89.5	92	93.5	

NOTE: All quantities are in cm^{-1}.

Side band positions are the frequencies above the local mode frequencies. Experimental accuracy of the side band peaks is ± 1 cm^{-1} except for NaF in which it is ± 5 cm^{-1}. Temperatures were 7 ± 2 °K.

[a] Timusk and Klein (1966).

absorption in the far-infrared region. These absorption spectra are shown in the next section where they will be discussed individually in more detail.

Generally the H^- ion induced absorption spectrum consists of a relatively narrow band below the reststrahlen and corresponds to frequencies in the upper portion of the acoustic phonon spectrum. As in the absorption induced by other impurities in the alkali halides (Klein and Macdonald, 1968 and Timusk and Ward, 1967, for example) the H^- ion induced absorption bands contain features which can in several instances be associated with Van Hove singularities in the unperturbed phonon density of states. These singularities are due to saddle points and local extrema in the frequency surfaces of the branches in the Brillouin zone. Some of these critical points occur at $\underset{\sim}{q}$ points which have high symmetry and their frequencies have been determined fairly accurately by neutron scattering measurements. These frequencies agree quite well with the infrared observations. Other frequencies at critical points of lower symmetry have not been determined as well by neutron spectroscopy or have not been measured at all and are found only by interpolation from the shell model for that particular alkali halide. These latter features are not in such good agreement with the experimental infrared results. This is especially true for critical points in off symmetry positions where similar effects

have been noted in the vibronic side band of Sm^{++} electronic transitions in KBr by Timusk and Buchanan (1967). The positions of the "pure" lattice singularities may be shifted because of the presence of the impurities (Timusk and Ward, 1969), but the amount of displacement at the concentrations of hydrogen used in this work is much smaller than can normally be detected by the neutron scattering measurements which have been used to identify the singularities.

The critical point frequencies are distinct features in the calculated and observed spectra of the absorption in the materials studied here except for KBr and KI in which resonances due to the perturbation of the lattice tend to obscure the singularities and make them difficult to identify.

The far-infrared spectral calculations used the model parameters previously determined by fitting to the side band spectra and local mode positions. Calculations were also made with different values of the parameters to investigate the sensitivity of the results to parameter changes. In several cases the solutions produced spurious resonances when the force constant changes were different from the side band fitted values. These resonances appeared as very strong peaks in the low frequency regions of the calculated spectra and had no counterparts in the observed absorption. Therefore, the fitted force constants appear to represent the correct physical situation. Variations

of the parameters over ranges where the solutions do not have spurious resonances affects the strength of the absorption but has only a slight effect on the positions of the calculated peaks except for those in KBr and KI. This indicates that the peaks are related to Van Hove singularities in the unperturbed density of states. The peaks in KBr and KI, however, are due to relatively high frequency resonances which are only placed near the observed positions when Δf and Δg are close to the values obtained from fits to the side band spectra. Figures 10 and 11 show, for example, the effect of changing Δf and Δg on the resonance in KBr. The general shape and positions of the odd mode resonances responsible for the far-infrared absorption in KBr and KI are reproduced by the model whose parameters were fixed by fitting to the even mode side band resonances . This is another indication the models are a good representation of the defect.

The effect of varying Δk is to diminish the absorption as the core-shell force constant is weakened. The absorption at low frequency regions of the spectrum is reduced more rapidly than at the high frequencies and the spurious resonances that appear for some values of Δf and Δg are sometimes eliminated.

FIGURE 10

Effect of Δf on the calculated far-infrared absorption in KBr. The six plots are for Δf -5855, -6855, -7855, -8855, -9855, and -10,855 dynes/cm and Δg = 4100 dynes/cm. The effect is to move the two peaks to lower frequencies as Δf becomes more negative. The peak heights and widths are also greatly affected. The heavy curve is for Δf = -8855 dynes/cm which is the value obtained from fitting to the side band spectrum.

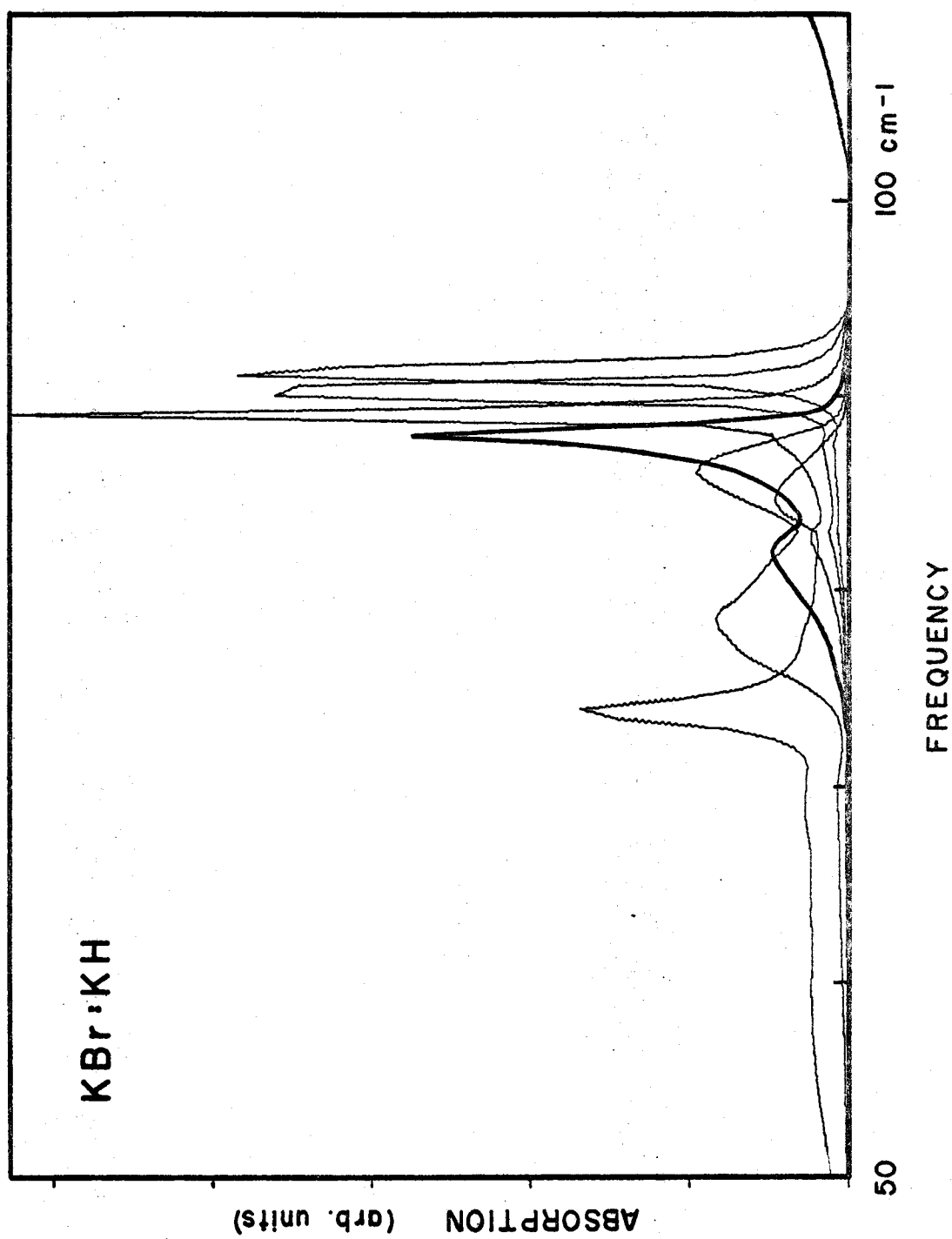
KBr:KH
ABSORPTION (arb. units)
50
100 cm-1
FREQUENCY

FIGURE 11

Effect of Δg on the calculated far-infrared absorption in KBr. The six plots are for variations in Δg from -3600 dynes/cm to -6100 dynes/cm in steps of -500 dynes/cm and with Δf = 8855 dynes/cm. As Δg becomes more negative, the effect is a shift to lower frequencies of the two peaks. The high frequency peak is also reduced in amplitude and broadened and the lower frequency peak increases in strength.

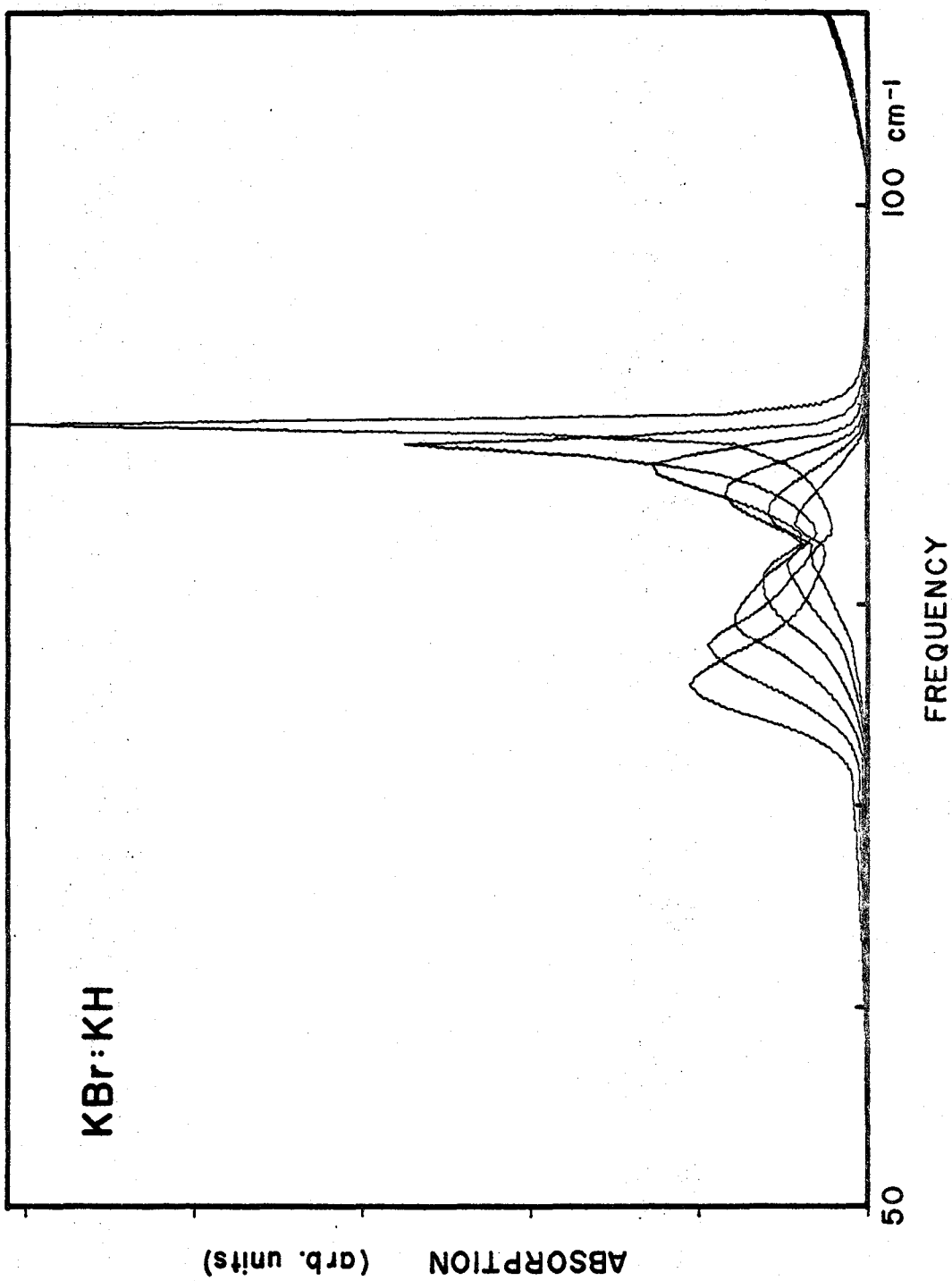
KBr:KH
ABSORPTION (arb. units)
50
100 cm-1
FREQUENCY

C. SPECIFIC ABSORPTION SPECTRA

1. NaF

The side band spectrum for NaF is shown in Figure 12. The remarkable result in this material is that a small value of Δf is required to fit to the incipient resonance, which suggests that the forces binding the H^- ion to the NaF lattice are similar to those binding the F^- ions. This seems reasonable since the ionic radii of the H^- (1.40 Å) and F^- (1.36 Å) ions in sodium chloride structure crystals are nearly the same so the overlap and consequently the repulsive forces are expected to be similar. Therefore, relaxation of the surrounding sodium ions is also expected to be slight so that the force constant change Δg should be small. This is in agreement with the good fit obtained for the side band with $\Delta g = 0$. No resonances are predicted in either of the perturbed E_g or A_{1g} modes of the calculations nor are there any unexplained peaks in the observed side band. The rather large change, Δk, required to satisfy the local mode condition is in agreement with the dissimilar polarizabilities of the fluorine and H^- ions.

The observed and calculated absorption spectra for the far-infrared are shown in Figure 13. The relatively small perturbation due to the H^- ion in NaF results in a calculated far-infrared absorption that is weak and has no resonance. This is in agreement with the experiment. The

FIGURE 12

Observed and calculated side band absorption of the H^- ion local mode in NaF. Relative scales have been chosen for the same peak heights at 168 cm^{-1}. The calculated curve is for $\Delta f = -6500$ dynes/cm and $\Delta g = 0$ dynes/cm. The large absorption below 50 cm^{-1} in the experimental curve is due to the edge of the local mode.

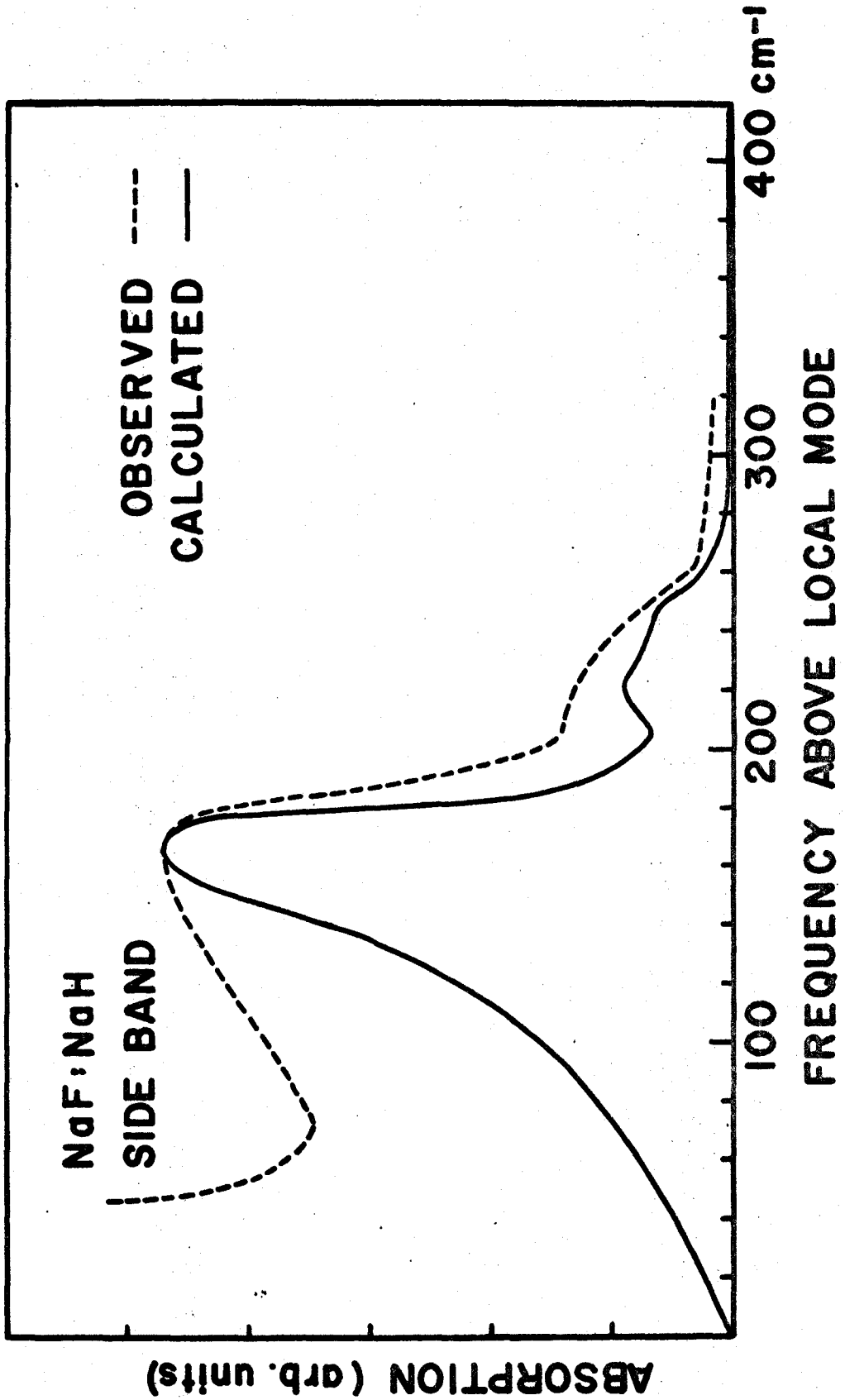
NaF:NaH
SIDE BAND
OBSERVED
CALCULATED
100
200
300
400 cm⁻¹
FREQUENCY ABOVE LOCAL MODE
ABSORPTION (arb. units)

FIGURE 13

Induced far infrared absorption due to H^- ions in NaF. The observed absorption is very weak and there is no evidence of resonances. The calculated curve is based on the shell model for the defect with the force constant changes $\Delta f = -6500$ dynes/cm, $\Delta g = 0$ dynes/cm and $\Delta k = -096000$ dynes/cm obtained by fitting to the local mode and anharmonic side band spectrum.

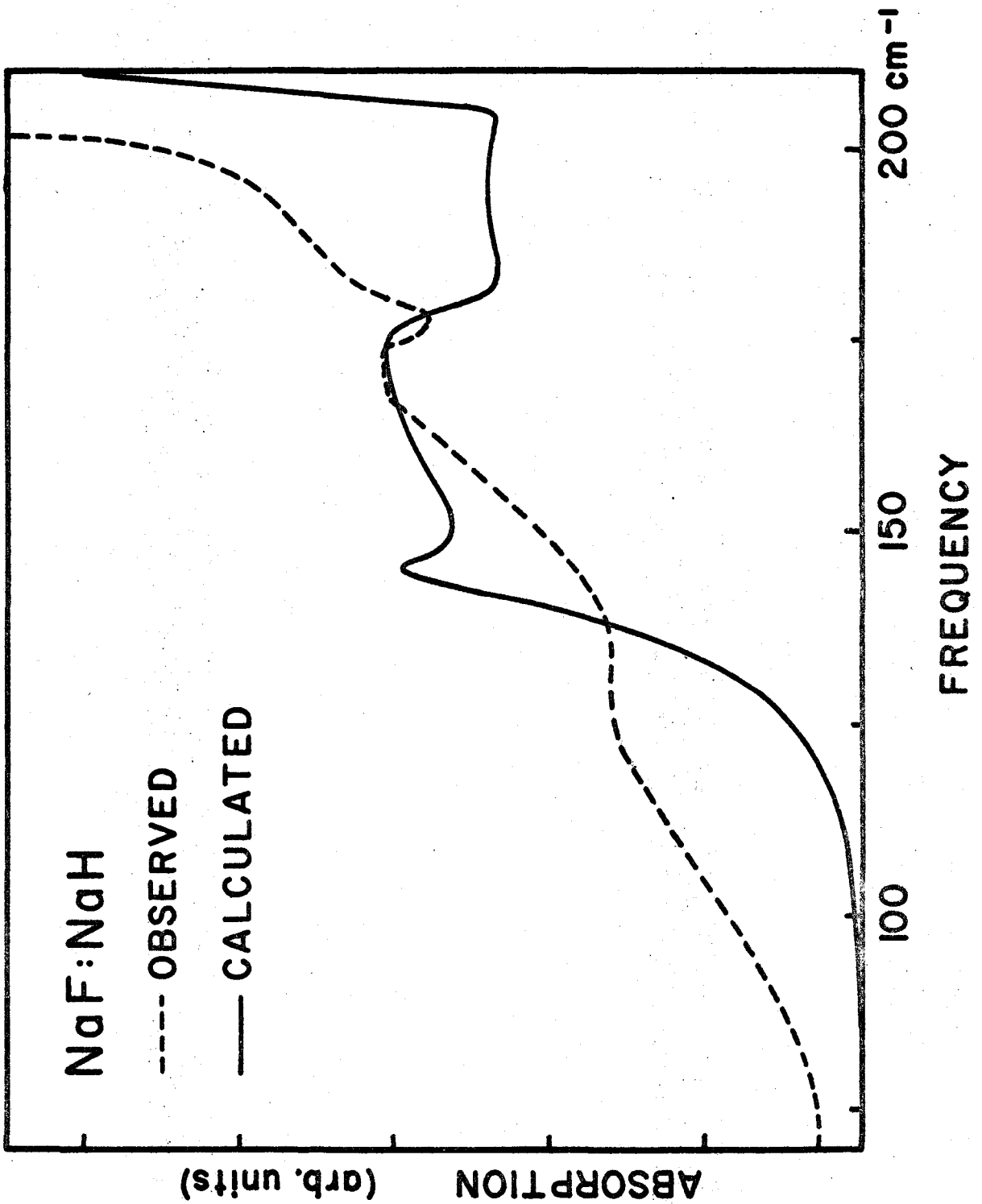
NaF:NaH
OBSERVED
CALCULATED
ABSORPTION
(arb. units)
100
150
200 cm⁻¹
FREQUENCY

FIGURE 14

Unperturbed phonon density of states for NaF. The upper curves are the individual frequency distributions for the six phonon polarization branches and the lower curve is the total density of states. The curves have been normalized so that $\int \rho_{total}(\omega) d\omega = 1$ and were produced by sorting frequencies at 62500 wave vectors into 0.5 cm^{-1} wide bins by the method developed by Gilat and Raubenheimer (1966).

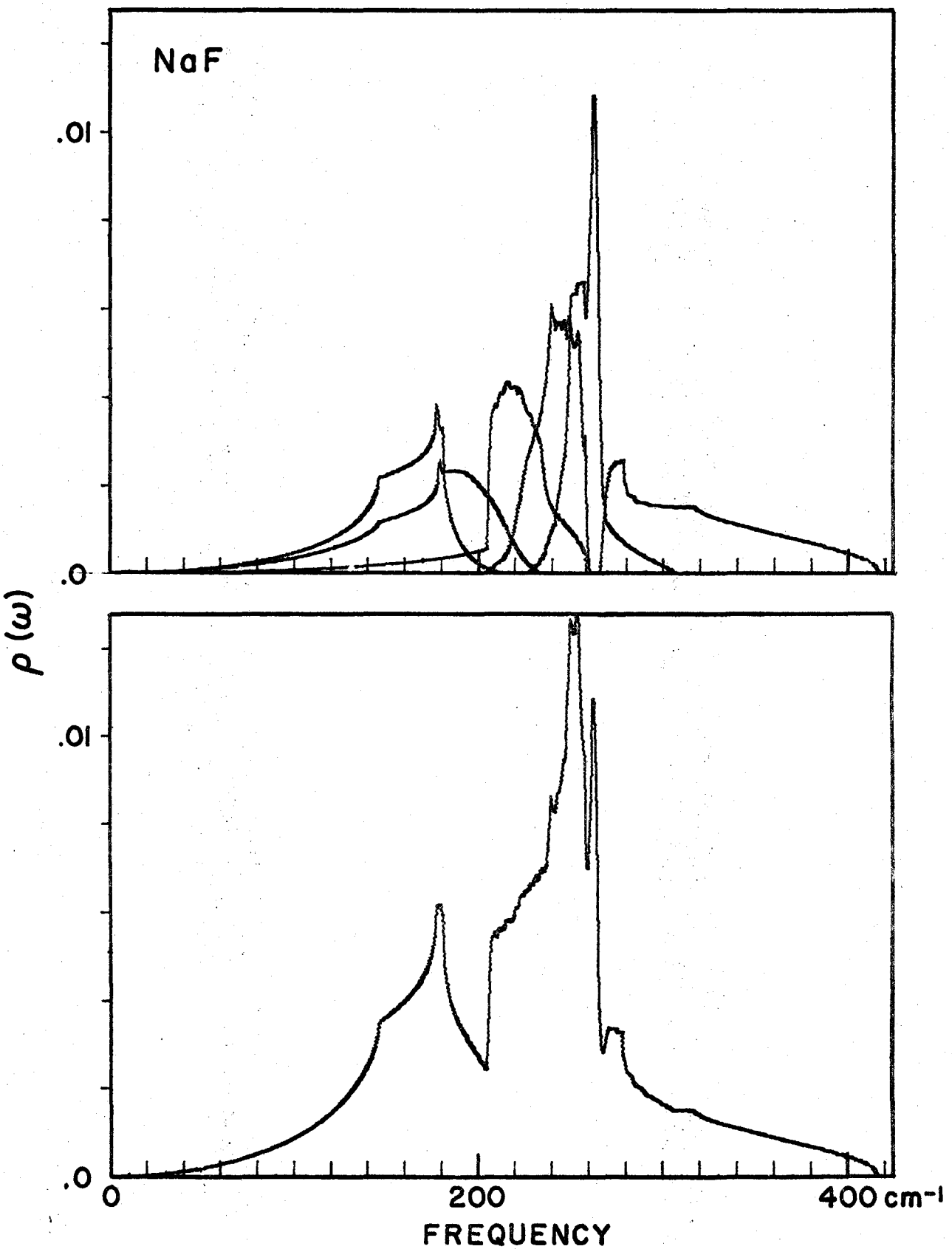
NaF
.01
.0
ρ(ω)
.01
.0
0
200
400 cm⁻¹
FREQUENCY

absorption shown between 50 cm^{-1} and 200 cm^{-1} is weak and possibly is not entirely due to H^- ions. The shoulder at 177.8 cm^{-1} in the calculation is associated with a critical point in the first phonon branch at the L point and is a prominent feature in the phonon density of states (Figure 14). The corner at 174 cm^{-1} in the observed spectrum may be related to this singularity. However, this feature may also be caused by absorption induced by other impurities.

There is a dramatic increase in absorption in both the theoretical and experimental curves beyond 205 cm^{-1} coinciding with the start of the fourth phonon branch which is the first optical branch and has its minimum frequency at the L point.

2. NaCl

The side band spectra for NaCl are shown in Figure 15. The calculations show than an E_g resonance occurs in the acoustic region where the density of E_g states is large so that it is very broad and hidden under the incipient resonance at 81 cm^{-1}. A definite value cannot be assigned to Δg by using the position of the E_g resonance since no corresponding peak appears in the observed spectra. However, a peak does appear in the calculated spectrum if Δg is not sufficiently negative. Lack of an observed resonance restricts Δg to values more negative than -2500 dynes/cm.

FIGURE 15

Observed and calculated side band in NaCl with perturbed lattice parameters $\Delta f = -11{,}700$ dynes/cm and $\Delta g = -4700$ dynes/cm. The curves were normalized for equal areas. The small peaks at 118, 124, 135, 158, 173 cm^{-1} which appear in the calculated and measured spectrum are probably due to remnants of Van Hove singularities in the density of states for NaCl. The sharp peaks below 20 cm^{-1} are most likely due to perturbed H^- ions. Similar peaks appear in the other side band spectra and have previously been reported in KBr (Timusk and Klein, 1966).

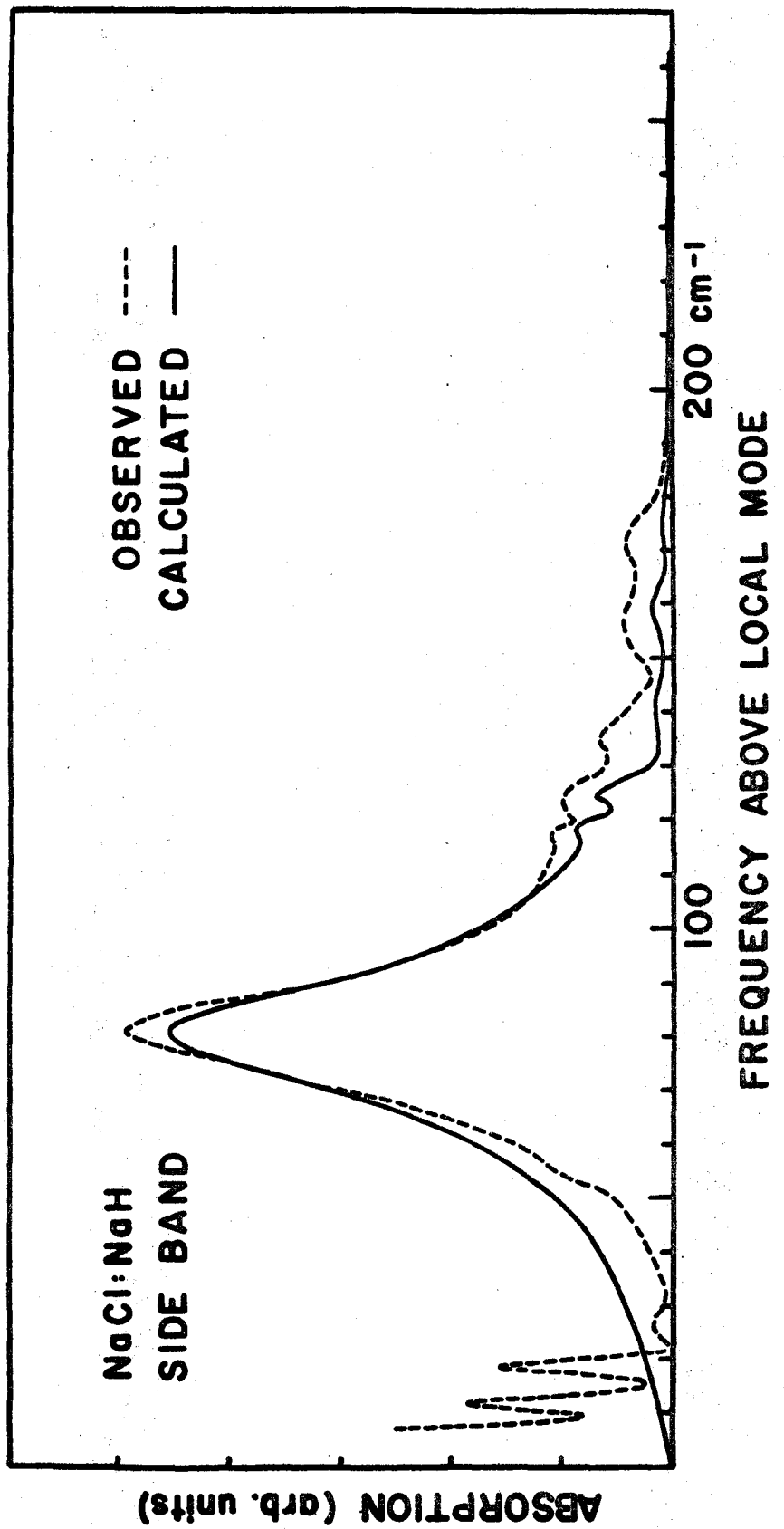
NaCl:NaH
SIDE BAND
OBSERVED ----
CALCULATED ——
ABSORPTION (arb. units)
100
200 cm⁻¹
FREQUENCY ABOVE LOCAL MODE

FIGURE 16

Unperturbed phonon density of states for NaCl. Upper curves are the branch frequency distributions and the lower curve is the total density of states. The Van Hove singularities at 87.3 cm^{-1} and 116.8 cm^{-1} in the first branch and at 122.3 cm^{-1} in the second branch lead to similar features in the far-infrared absorption spectrum.

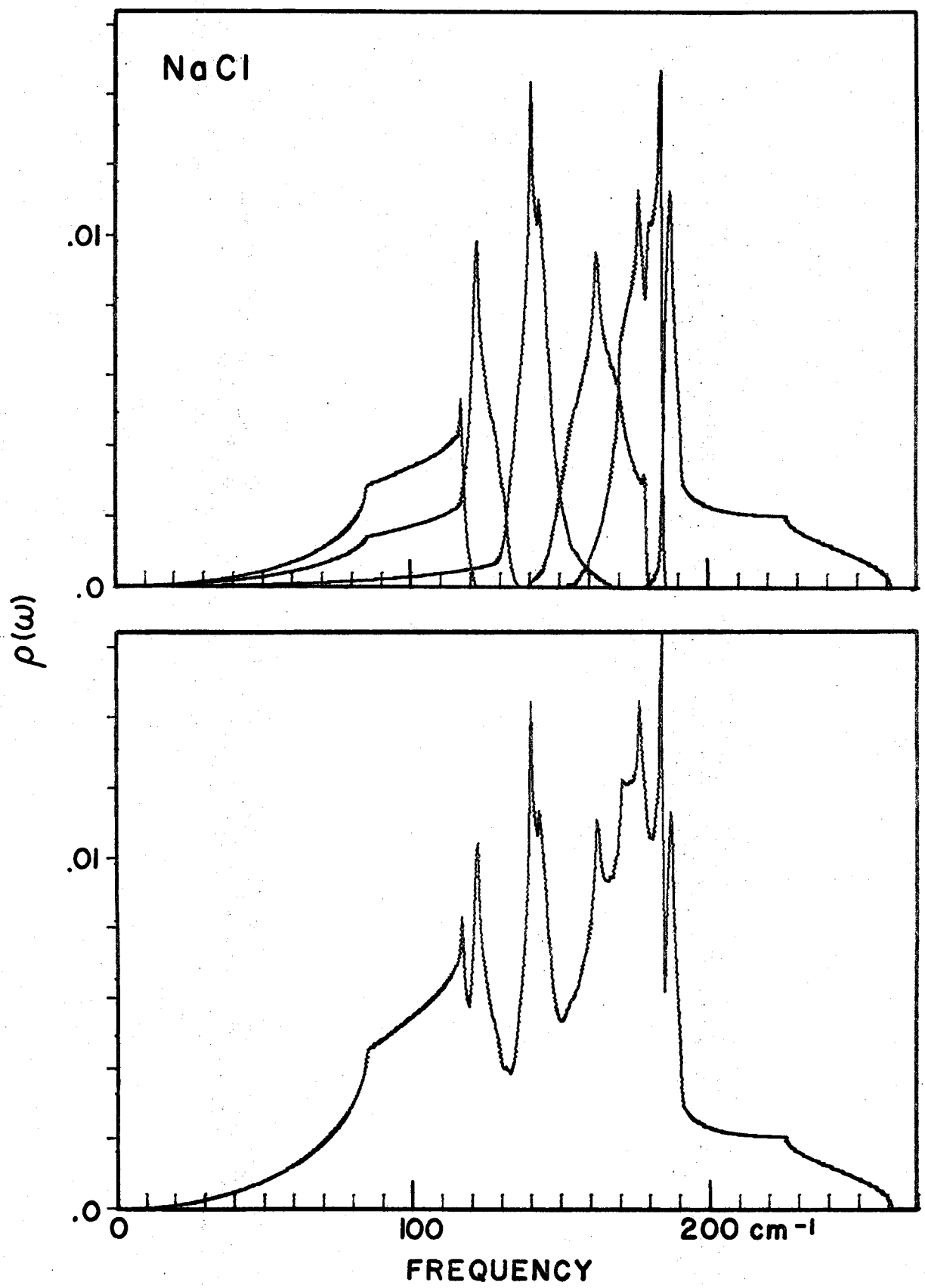
NaCl
.01
.0
ρ(ω)
.01
.0
0
100
200 cm⁻¹
FREQUENCY

FIGURE 17

Induced far-infrared absorption due to H^- ions in NaCl. The calculated absorption is based on the shell model defect with the force constant changes Δf = -11,700 dynes/cm, Δg = -4700 dynes/cm and Δk = -860,000 dynes/cm obtained by fitting to the local mode and anharmonic side band absorption. Van Hove singularities appear at 87.3 cm^{-1}, 117 cm^{-1} and 124 cm^{-1} in the experiment.

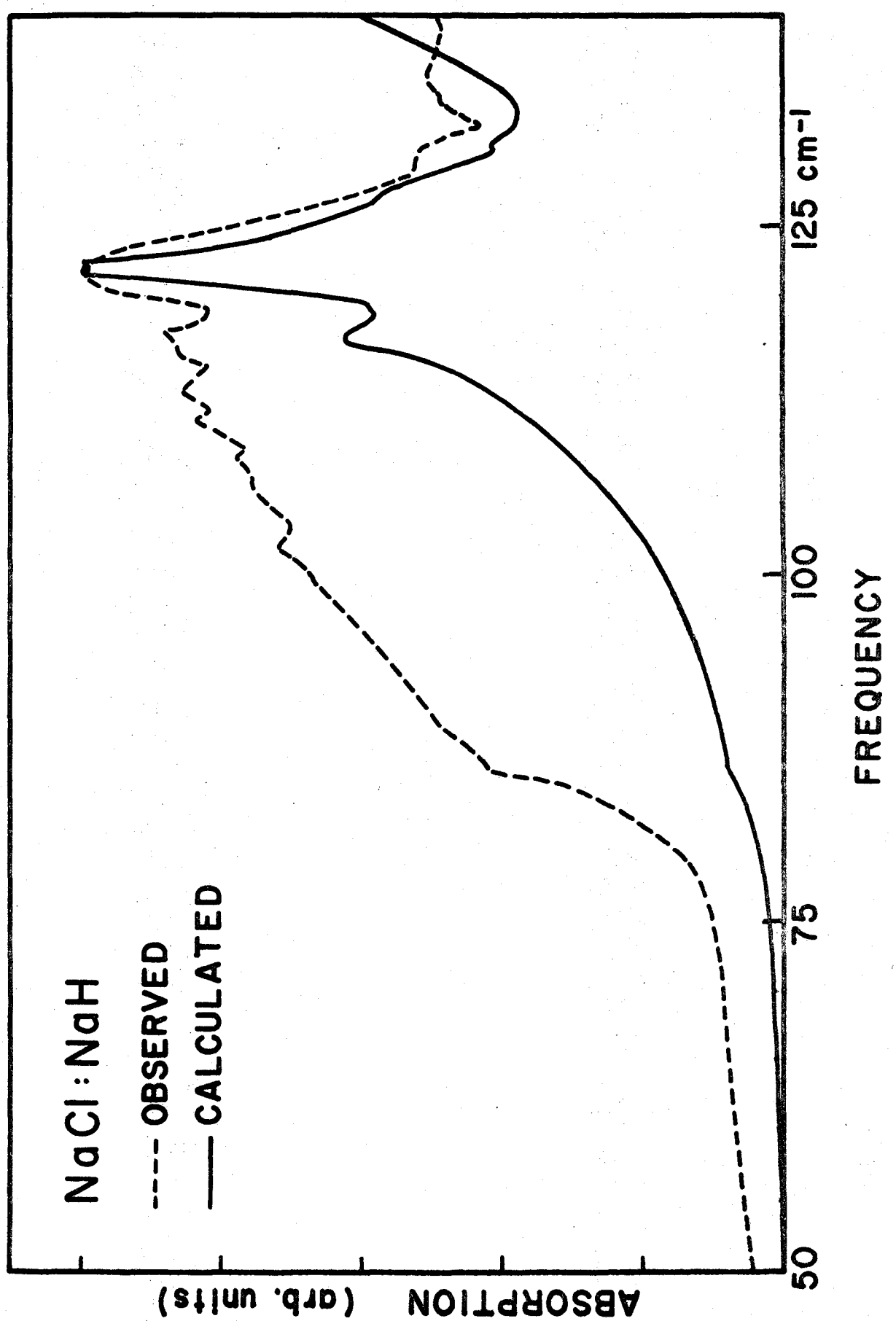
NaCl:NaH
OBSERVED
CALCULATED
ABSORPTION (arb. units)
50
75
100
125 cm⁻¹
FREQUENCY

A change in g of -4700 dyne/cm was chosen because the overall shape of the side band and the far-infrared absorption are reproduced best with this value.

The value of Δf required to fit to the incipient resonance is -11700 dyne/cm. With this value the local mode condition requires a fairly large value for Δk. The effective crystal polarizability of the H^- ion with Δk =-860000 dyne/cm might be unphysically large which indicates that the change in k may be too great.

There are several small peaks in the observed sideband appearing at 118, 124, 135, 158 and 173 cm^{-1} which correspond to similar peaks in the calculated sideband. These peaks are attributed to remnants of critical points in the density of states (Figure 16) and can be identified with phonon frequencies at certain points in the Brillouin zone. For example the 118 cm^{-1} observed peak seems to be related to the saddle point frequency of 116.8 cm^{-1} in the first phonon branch at $q = \frac{\pi}{r_0}$ (0.62,0.62,0.0).

Peaks at 122.3 cm^{-1} and 140 cm^{-1} in the calculations arise from phonons at $\frac{\pi}{r_0}$ (0.54,0.54,0) and at W in the second and third branches respectively. The assignment of such phonons to the observed peaks is only approximate since the latter are not so well defined and are shifted by a few wave numbers.

The H^- ion induced far-infrared absorption is stronger

in NaCl than in NaF. The observed and calculated spectra are shown in Figure 17. A Van Hove singularity is clearly evident at 87.3 cm^{-1} and is associated with the saddle points in the first and second phonon branches at the X point in the Brillouin zone. This is perhaps one of the best observations of this particular critical point in the alkali halides. The frequency agrees well with the 87.0 cm^{-1} value obtained from neutron scattering measurements at 80°K (Almqvist et al. 1968). The observed peaks at 117 cm^{-1} and 124 cm^{-1} appear to correspond to the singularity at 116.8 cm^{-1} in the first phonon branch and to the one at 122.3 cm^{-1} in the second branch respectively. The absorption increases rapidly above 140 cm^{-1} where the first optical branch begins.

In the calculated spectrum the X point singularity becomes more clearly defined and the absorption around 90 cm^{-1} increases relative to the rest of the spectrum at smaller values of $-\Delta k$. As this is in better agreement with the shape of the observed absorption it is another indication that the value of $-\Delta k$ obtained from fitting the side band and local mode condition is too large.

3. NaBr

The experimental side band results differ from those of Fritz et al. (1965). They observed a peak near 83 cm^{-1} from the local mode frequency and attributed it to a

FIGURE 18

Side band of the H^- ion absorption in NaBr. Dotted peaks in the observed spectrum at 43, 129 and 177 cm^{-1} are due to H^- ions perturbed by impurities. The 129 cm^{-1} peak has been identified as being due to OH^-. Force constant changes were $\Delta f = -10{,}800$ dynes/cm and $\Delta g = -5500$ dynes/cm. The peak at 83.6 cm^{-1} is attributed to an E_g resonant mode of the nearest neighbour ions.

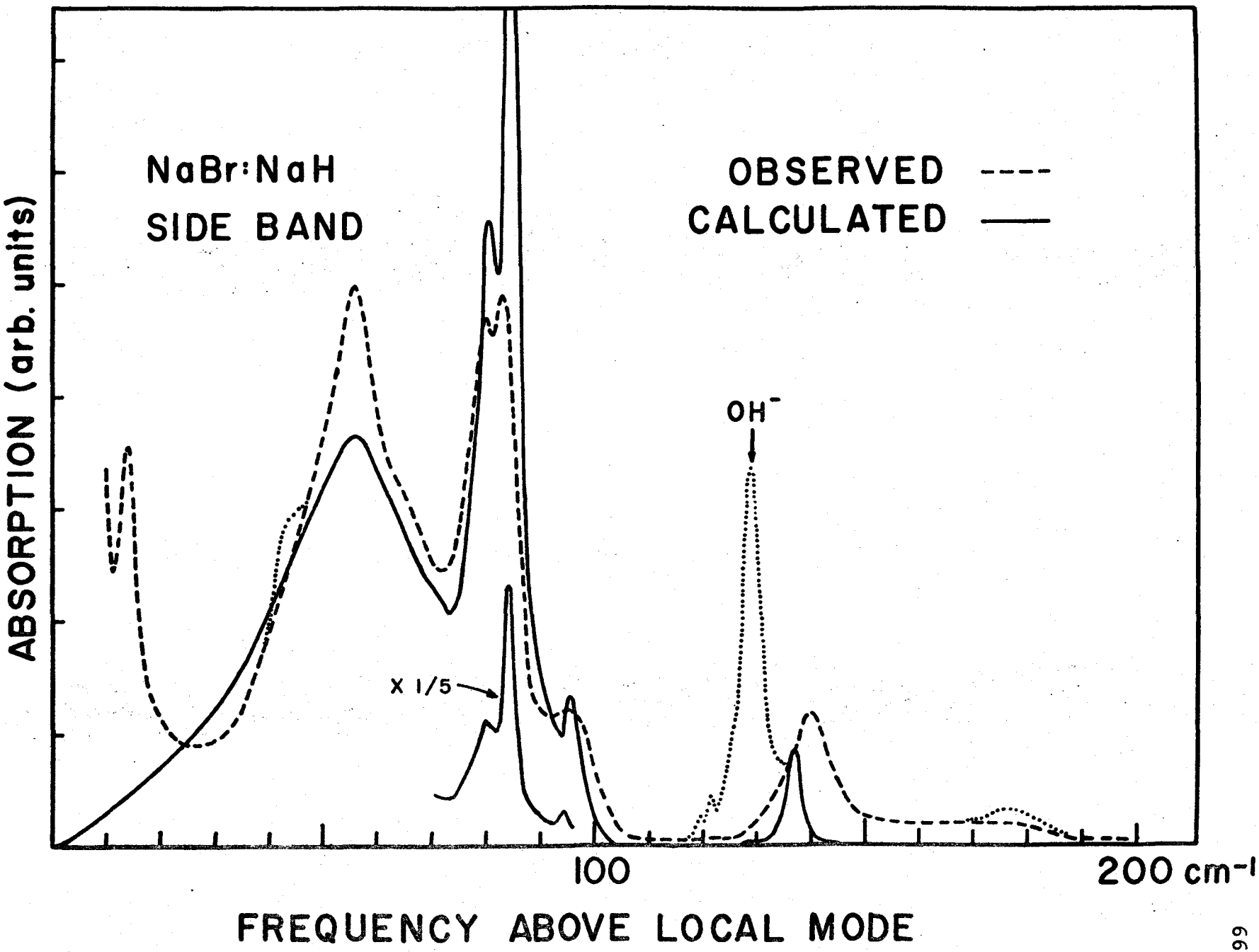
NaBr:NaH
SIDE BAND
OBSERVED
CALCULATED
OH⁻
X 1/5
ABSORPTION (arb. units)
100
200 cm⁻¹
FREQUENCY ABOVE LOCAL MODE

local mode displaced by a nearby impurity which they thought was most likely chlorine. However, the double peak which appears at 79 cm^{-1} and 83.5 cm^{-1} as shown in Figure 18 was found to be independent of chlorine concentrations up to about 5%. Furthermore these peaks are unaffected in crystals containing up to 0.1% I^-, F^-, Ca^{++}, K^+, Li^+ and OH^- impurities in the melt materials from which they are grown. The shape and strength of these peaks in crystals from several different sources are constant to within experimental error (10%) in relation to the other features of the side band. Also an E_g resonance appears in the calculated spectrum which describes the double 83 cm^{-1} peak very well. The force constant changes required to fit the side band are reasonable and there are no unexplained features in the observed spectrum nor are there any unobserved resonances in the calculations. Therefore, it is concluded that the 83 cm^{-1} peaks are part of the side band. A partial test of this conclusion would be to study the shifting and splitting of the 83.5 cm^{-1} resonance under stress.

A strong peak at 129 cm^{-1} was also observed. This peak varied in strength between samples and increased considerably in crystals grown from melts with up to 0.1% OH^- impurity added. This feature was greatly reduced in a crystal prepared from optical grade NaBr in which the OH^- concentration was

expected to be low. The peak strength also varied with H^- ion concentration and was not present in untreated crystals. Therefore it is attributed to a local mode displaced by the presence of a nearby OH^- impurity. The position of the gap observed in the experiment coincides with the gap in the density of states calculated from the neutron scattering derived shell model phonons. There is no evidence of any significant shift. The side band absorption is very weak in the optic region so the exact end point is difficult to determine. There is no discernable absorption beyond the maximum host lattice frequency at 201 cm^{-1} in crystals with up to 10^{18} H^- ions/cm^3.

The far-infrared spectra are shown in Figure 19. The pointed feature in the experiment at 57 cm^{-1} coincides with the 56.5 cm^{-1} saddle points frequency of the first and second phonon branches which occur (Figure 20) at the X point in the Brillouin zone. The observed peak at 77.5 cm^{-1} appears to correspond to the theoretical peak at 71.8 cm^{-1} which is due to a critical point at L in the frequency surface of the first phonon branch. The frequency determined by the neutron scattering measurements (Reid et al. 1970) is 71 ± 1 cm^{-1}. The 6 cm^{-1} discrepancy with the infrared absorption peak is larger that might be expected for the uncertainty in the L point phonon even though the neutron scattering measurements tend to be less accurate for phonons in this

FIGURE 19

Induced far-infrared absorption due to H^- ions in NaBr. The calculated absorption is from the shell model for the defect with the force constant changes $\Delta f = -10800$ dynes/cm, $\Delta g = -5500$ dynes/cm and $\Delta k = -45{,}000$ dynes/cm. The experimental peaks which appear at 57 cm^{-1}, 77.5 cm^{-1} and 98.9 cm^{-1} are attributed to Van Hove singularities.

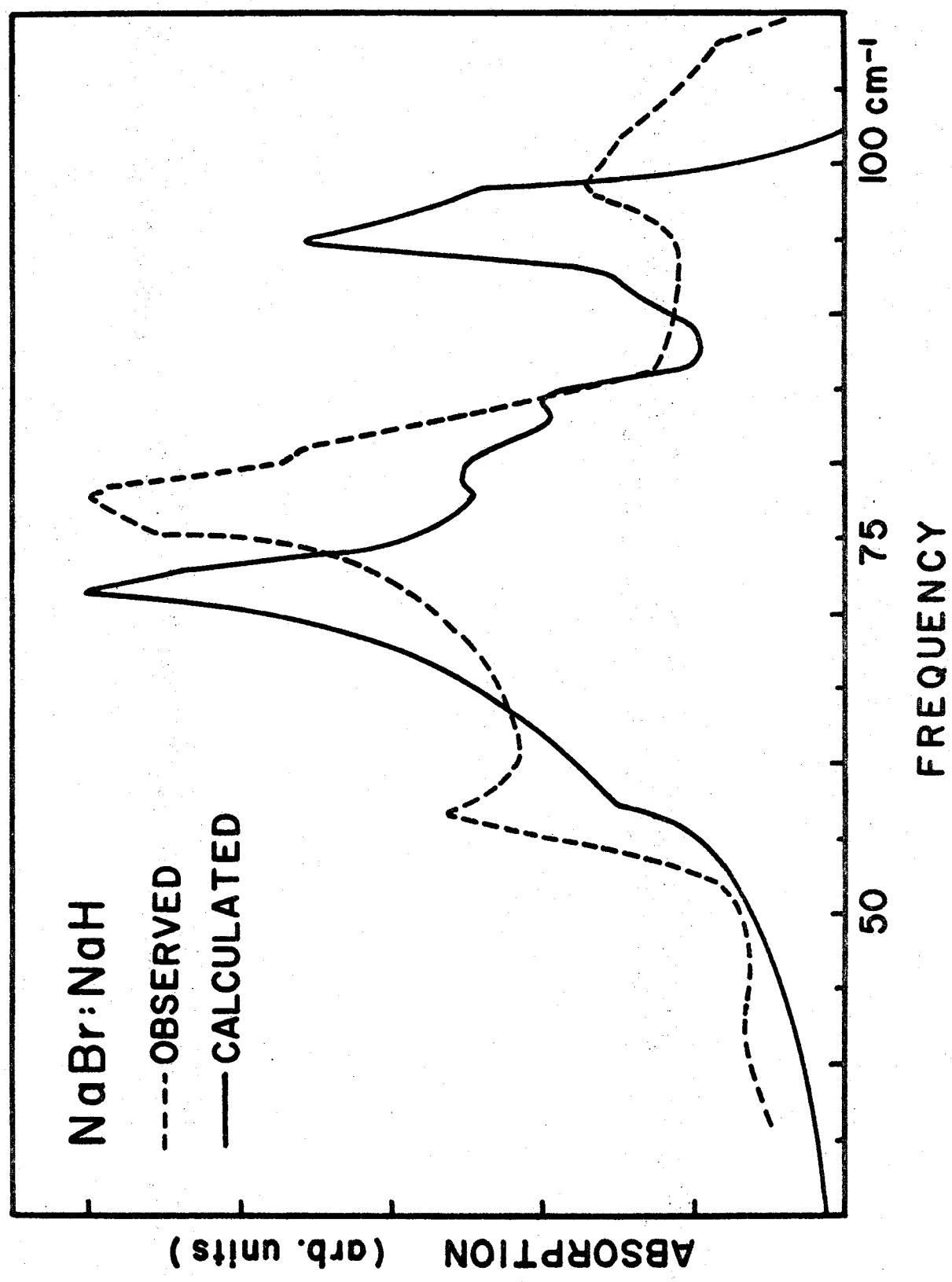
NaBr:NaH
---OBSERVED
—CALCULATED
ABSORPTION (arb. units)
50
75
100 cm⁻¹
FREQUENCY

FIGURE 20

Unperturbed phonon density of states for NaBr. Upper curves are branch frequency distributions and the lower curve is the total density of states. The Van Hove singularities at 56.5 cm^{-1}, 71 cm^{-1}, 94.3 cm^{-1} appear in the induced far-infrared absorption spectrum.

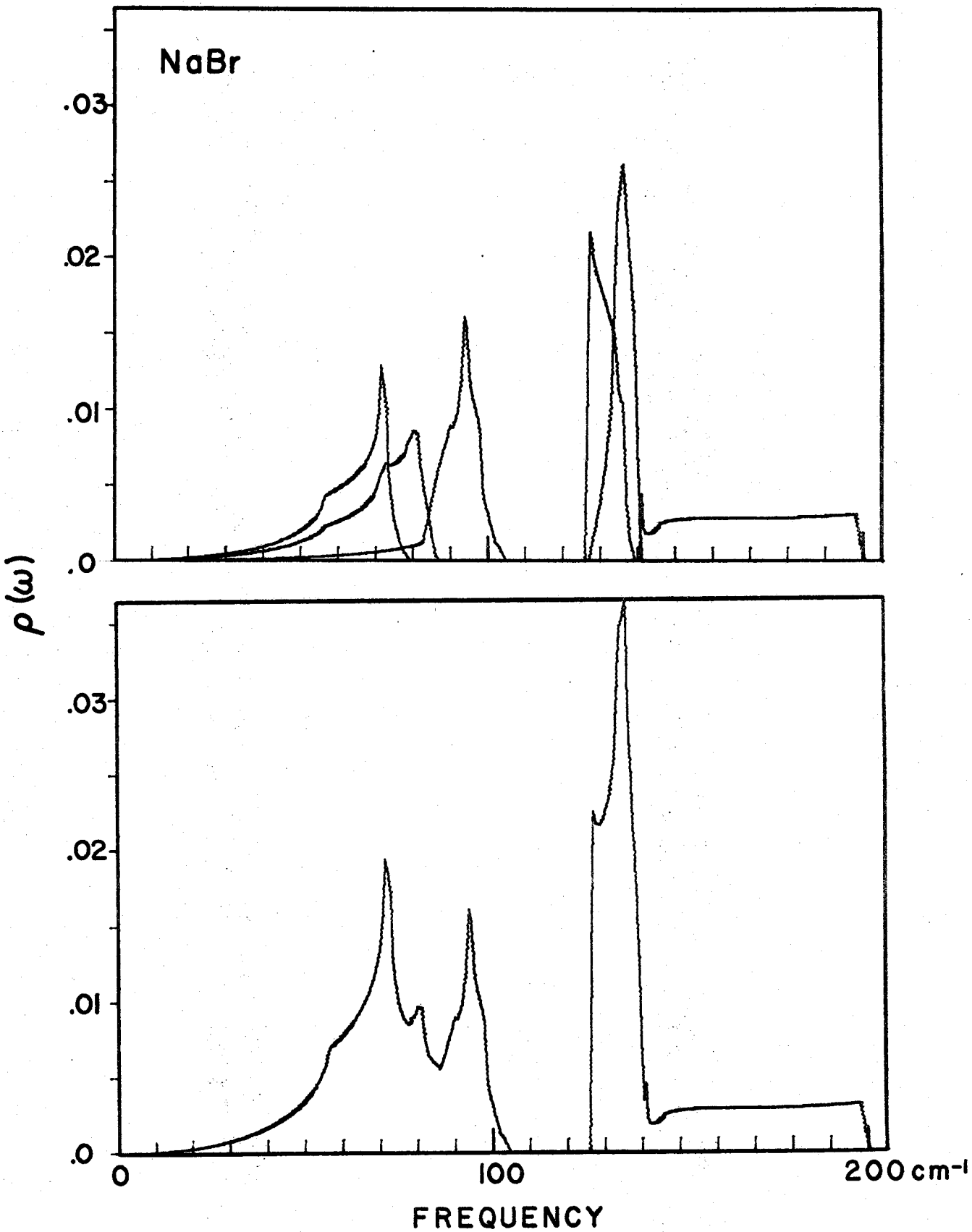
NaBr
.03
.02
.01
.0
ρ(ω)
.03
.02
.01
.0
0
100
200 cm-1
FREQUENCY

region of the zone. Temperature differences between the neutron scattering and infrared measurements may account for some of the discrepancy. Also, the assignment of the infrared peak to the L point phonon may be fortuitous since the calculated and observed peaks differ in the detailed shapes near their maximum intensities.

The shoulder at 81.4 cm^{-1} in the experimental curve seems to correspond to the peak at 80.5 cm^{-1} in the calculations where the density of phonons in the second branch is maximum. The calculated peak at 84.3 cm^{-1} is not visible in the experimental spectrum. A small decrease in k (about 6%) was required in the calculations to eliminate a spurious resonance which appeared at 20 cm^{-1} when $\Delta k = 0$. The rest of the spectrum is not affected by this change.

The location of the critical point associated with the strong 95.0 cm^{-1} peak has not been determined but it does not lie along any of the symmetry directions. This feature would seem to be related to the observed 98.9 cm^{-1} peak. The discrepancy could be due to the same considerations discussed for the 77.5 cm^{-1} peak.

4. NaI

The only published spectrum of the side band in NaI is that of Bäurele and Fritz (1967). It was obtained with some difficulty due to the presence of strongly perturbed

local modes. Attempts to reproduce their results failed. However, some of the spectra that were measured had a small peak at 426 cm^{-1} where Baürele and Fritz observed the local mode. In each case the remainder of the spectrum had a very broad and strong absorption centred around 480 cm^{-1} which completely hid any other features which might have been correlated with their results. Calculations were performed to obtain predictions for the published spectrum but no negative value of Δf exists which could reproduce the position of the reported acoustic band peak at 47 cm^{-1} and satisfy the local mode condition. The calculated peak moves up to 46 cm^{-1} if $\Delta f = 0$ but a zero change in f seems unreasonable since the ionic radius of the H^- ion is much smaller than that of the I^- ion so that different repulsive forces are expected. It is possible that the peaks assigned to the side band are incorrect. However, the other nearest peak which was reported at 32 cm^{-1} and rejected by Baürele and Fritz, cannot be fitted with any values of Δf either. Another possibility is that some other force constants are important in the case of NaI. These may include the transverse force constant to the nearest neighbours or force constants to second neighbours. The defect centre responsible for the observed absorption may also have a different structure from the substitutional H^- ion centre of the other alkali halides. No far-infrared measurements were made for NaI since a suitable sample could not be obtained.

5. KCl

The KCl:KH side band spectra are shown in Figure 21. A reversal of curvature in the shape of high frequency side of the incipient resonance is evident in both the experimental and calculated curves. The small peak at 117 cm^{-1} has been observed by Fritz (1965) and was thought possibly to be due to other impurities. It now seems more likely to be part of the side band since it is the same relative size from sample to sample and it also appears in the calculates spectrum which used neutron based phonon data. No resonances appear in the calculations and there are no unexplained major peaks in the side band. As in NaF the spectrum is described well with $\Delta g = 0$. The small peaks near the local mode are most likely due to perturbed local modes. Similar peaks appear in some of the other side band spectra and have been observed by Timusk and Klein in KBr (1966) and by Elliott et al. (1966) in CaF_2 crystals containing H^- ions. The absorption in the high frequency tail is greater in the experiment than predicted by the calculations and is probably due to contributions from dipole moment interactions and two phonon side band processes.

The induced far-infrared absorption is compared with the calculated spectrum in Figure 22. The step discontinuity in the experiment is between 99 cm^{-1} and 107 cm^{-1} and resembles a similar feature induced in KBr by other impurities (Timusk

FIGURE 21

Side band of the H^- ion local mode in KCl with $\Delta f = -9095$ dynes/cm and $\Delta g = 0$ dynes/cm.

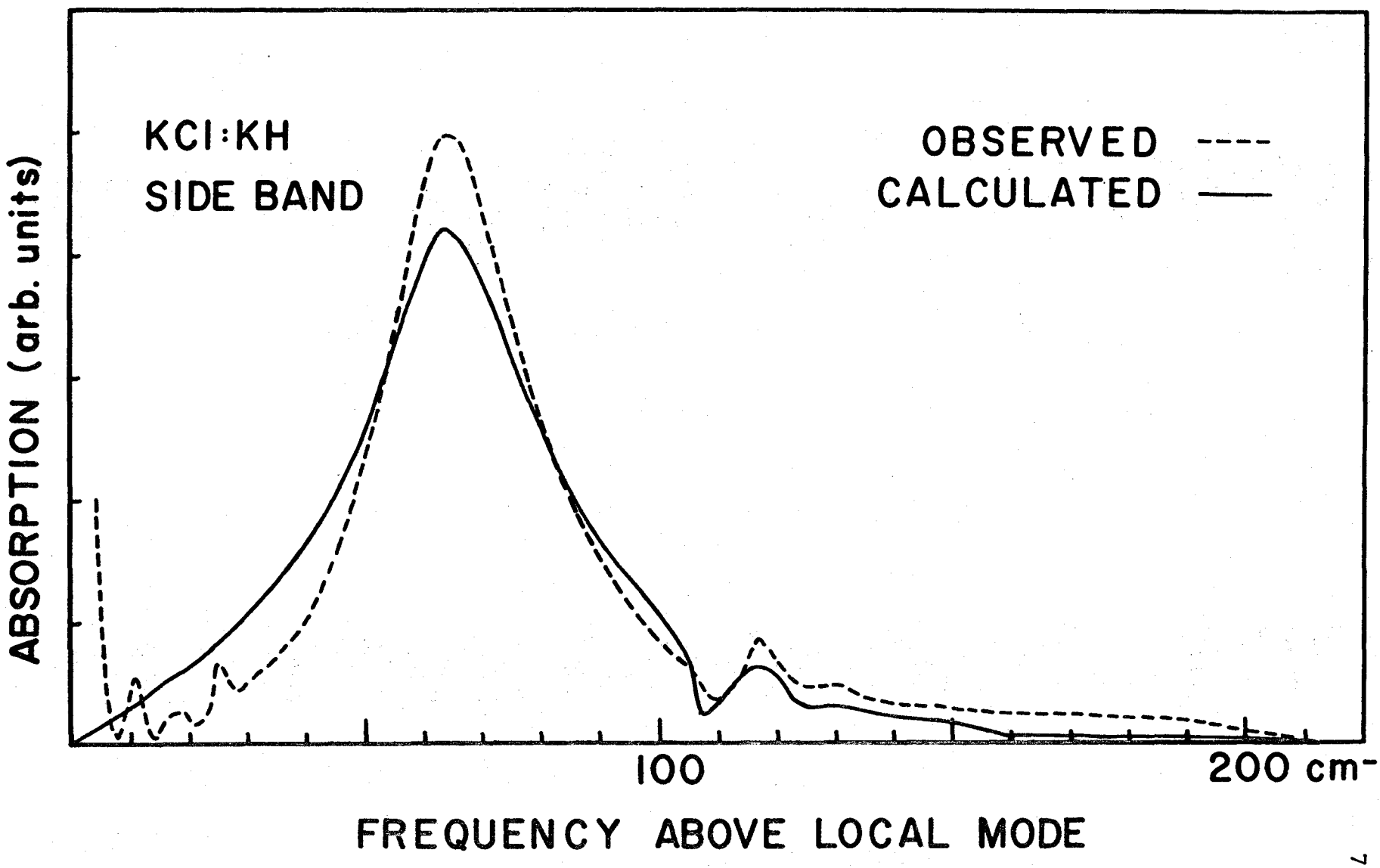
KCl:KH
SIDE BAND
OBSERVED
CALCULATED
ABSORPTION (arb. units)
100
200 cm⁻¹
FREQUENCY ABOVE LOCAL MODE

and Ward, 1969). The peak at 109 cm^{-1} is possibly due to a resonance induced by unknown impurities which may have been introduced into the crystal during the hydrogenating processes. The absorption shows a marked increase beyond 115 cm^{-1} where the optical branches begin (Figure 23).

In the calculated spectrum the step is formed by discontinuities in the slope of the curve at 106 cm^{-1} and 108 cm^{-1}. The first feature arises from a saddle point and the second from the nearly degenerate maximum in the dispersion surface of the second acoustical phonon branch. The maximum occurs at an off symmetry point in the zone and its frequency is in good agreement with the absorption measurements. The saddle point is located at approximately $\frac{\pi}{r_0}$ (0.52,0.52,0.0) in the Brillouin zone. The frequencies along the (111) direction which were measured by neutron spectroscopy (Copley et al., 1969) tend toward a somewhat lower value than predicted by the shell model at L and are in better agreement with the absorption experiments. This singularity also appears at 100 cm^{-1} in the vibronic side band of Sm^{++} in KCl (Buchanan and Woll, 1969) which is further evidence that this critical point is closer to 99 cm^{-1}. It is interesting to note that the similar features in KBr occur in the same region of q-space (Timusk and Ward, 1969).

FIGURE 22

Induced far-infrared absorption due to H^- ions in KCl. The calculated curve is from the shell model defect with the force constant changes $\Delta f = -9095$ dynes/cm and $\Delta g = \Delta k = 0$ dynes/cm. The step discontinuity between 99 cm^{-1} and 107 cm^{-1} is attributed to a saddle point at $\frac{\pi}{r_0}$ (0.52,0.52,0.0) and the maximum in the second acoustical phonon branch.

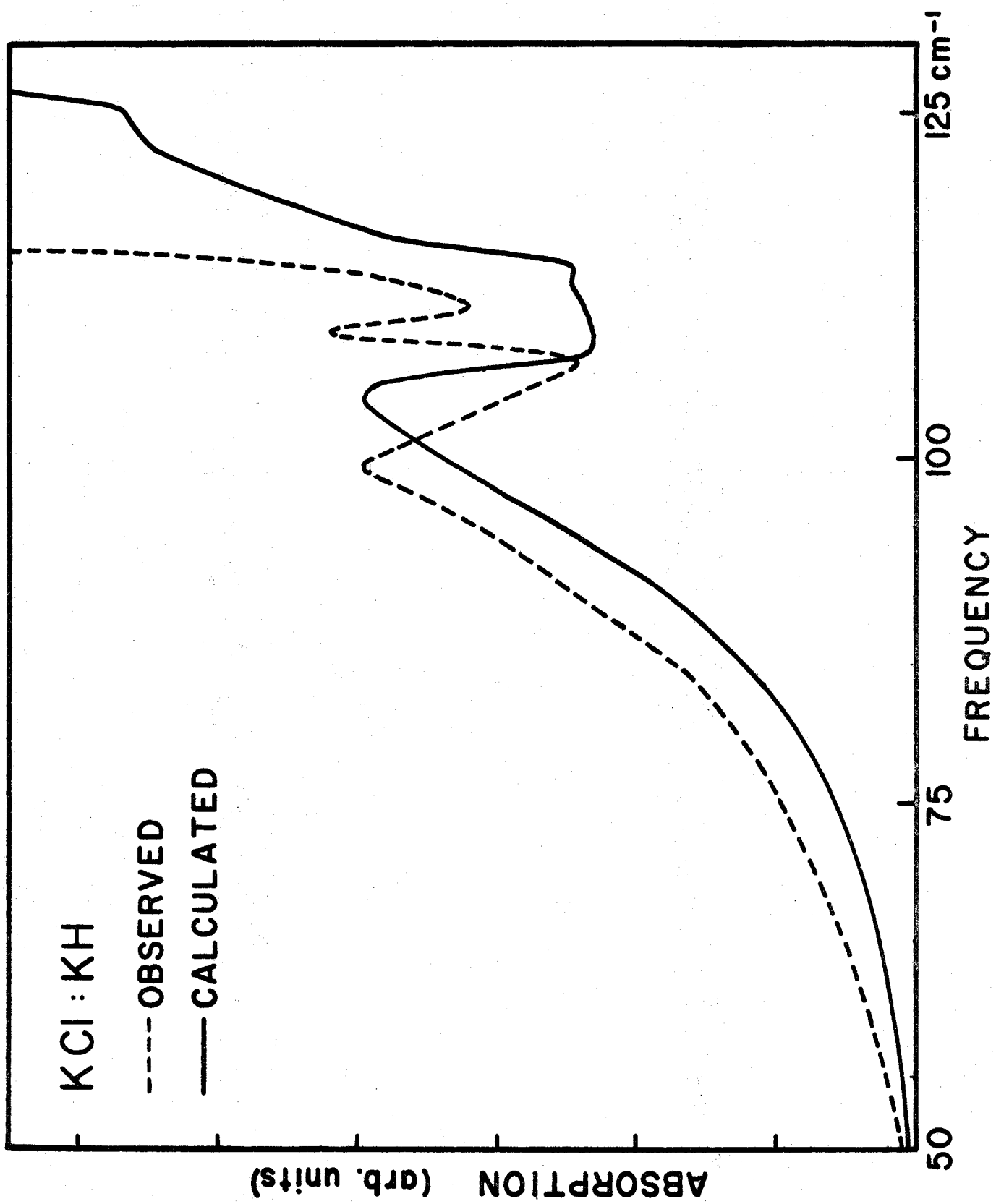
KCl : KH
OBSERVED
CALCULATED
ABSORPTION (arb. units)
50
75
100
125 cm⁻¹
FREQUENCY

FIGURE 23

Unperturbed phonon density of states for KCl. Upper curves are branch frequency distributions and the lower curve is the total density of states. The Van Hove singularity at 106 cm^{-1} appears to be incorrectly positioned by the shell model for KCl. Experimental evidence places it at 99 cm^{-1}.

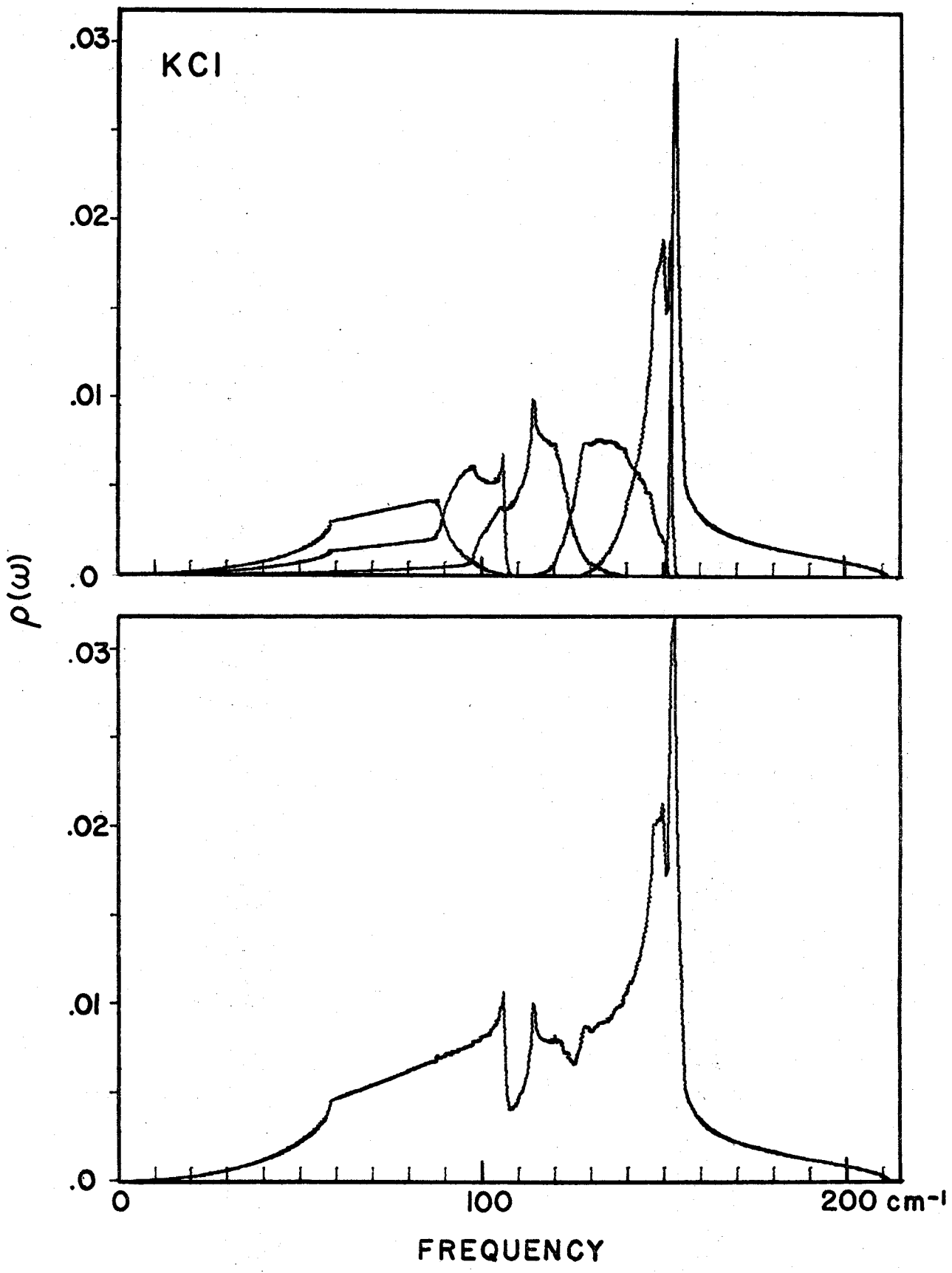
KCl
.03
.02
.01
.0
ρ(ω)
.03
.02
.01
.0
0
100
200 cm-1
FREQUENCY

6. KBr

The H^- ion side band in this material has been studied extensively by Gethins et al. (1967) and their rigid ion defect model calculations require careful comparison with the shell model defect results. Qualitatively the spectrum in Figure 24 is very similar to the rigid ion defect spectrum. Quantitatively the shell model results are an improvement over the simpler model. The E_g and A_{1g} resonances are now fitted to well within the experimental uncertainties. The splitting of the peaks near 80 cm^{-1} in the present calculation is not related to the model of the defect but is a result of the improved resolution provided by the modified Gilat-Raubenheimer method of obtaining the histograms. Gethins et al. used a simpler technique.

The far-infrared absorption spectra in KBr are shown in Figure 25. The experimental curve has a broad band between 75 cm^{-1} and 92 cm^{-1} and its main feature is a strong peak at 88.8 cm^{-1}. This peak is attributed to the incipient T_{1u} resonance that appears at 88.5 cm^{-1} in the calculations. The experimental absorption also exhibits some changes in slope that can be associated with Van Hove singularities. The singularities at 77.2 cm^{-1} and 82.7 cm^{-1} can be related to the 77.8 cm^{-1} and 83.3 cm^{-1} saddle points of the shell model spectrum (Figure 26) in the highest acoustical branch at the W point and at an off symmetry point in the (001) plane of the zone, respectively. The singularity at 88 cm^{-1} in

FIGURE 24

Calculated and observed side band in KBr with $\Delta f = 8855$ dynes/cm and $\Delta g = -4100$ dynes/cm. The experimental curve is from Timusk and Klein (1966).

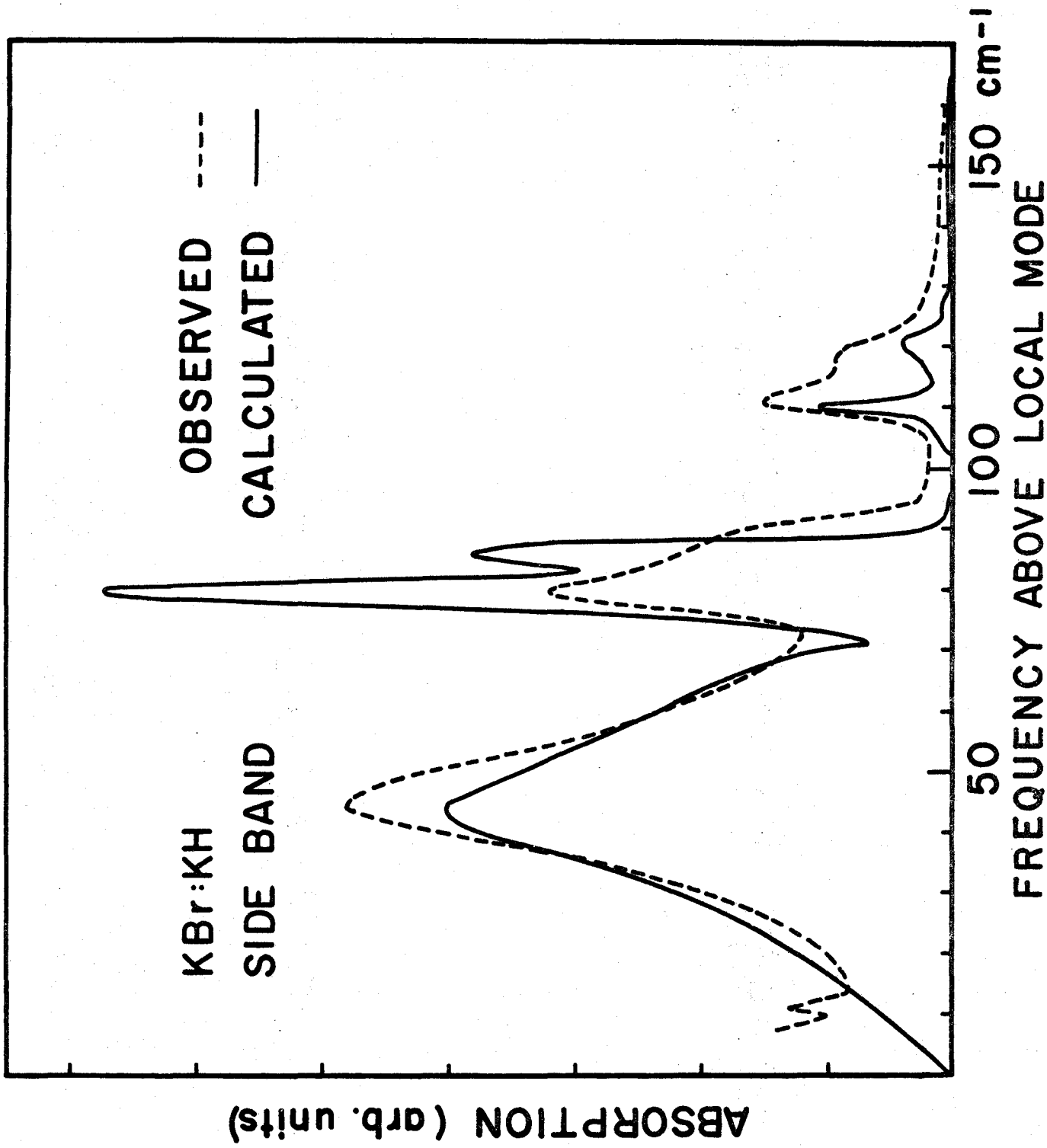
KBr:KH
SIDE BAND
OBSERVED
CALCULATED
ABSORPTION (arb. units)
50
100
150 cm-1
FREQUENCY ABOVE LOCAL MODE

FIGURE 25

Induced far-infrared absorption due to H^- ions in KBr. The calculated curve is from the shell model defect with force constant changes $\Delta f = -8855$ dynes/cm, $\Delta g = -4100$ dynes/cm and $\Delta k = 0$ dynes/cm. The main feature is the strong peak at 88.5 cm^{-1} which is attributed to a resonance of the perturbed T_{1u} modes of the lattice.

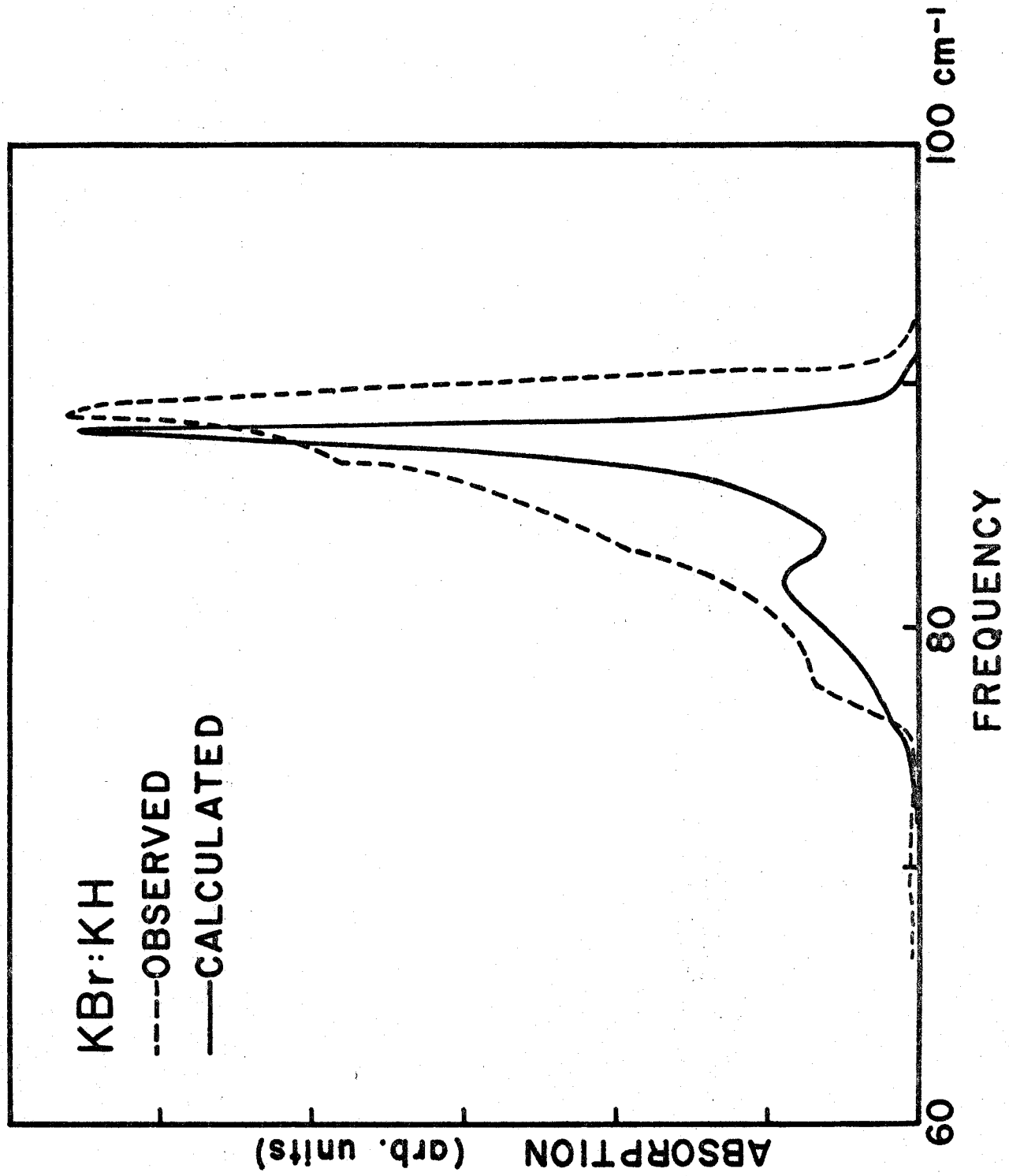
KBr:KH
----OBSERVED
——CALCULATED
ABSORPTION (arb. units)
60
80
100 cm-1
FREQUENCY

density of states is due to a saddle point at $\frac{\pi}{r_0}$ (.65, 0., 0.) and coincides with the resonance. The other singularities do not appear in the theoretical curve. This suggests that the features appearing experimentally may arise from other mechanisms than the absorption induced by H^- ions. The peak at 82 cm^{-1} in the calculations is not a Van Hove singularity since its position is sensitive to force constant changes.

The calculated width of the incipient resonance peak is much narrower than observed experimentally. The width of the observed peak is probably partly due to anharmonic broadening effects which are not given correctly by the harmonic theory. However, it is interesting to look at the effect of changes in the core-shell force constant, k. Figure 27 shows the result of varying Δk from 0 to -500000 dyne/cm. A change of Δk = -490000 dyne/cm is necessary to obtain Wood and Gilbert's value for the hydrogen polarizability but then, as can be seen from the figure, the calculated absorption no longer resembles the experiment. If $\Delta k \approx$ -200000 dyne/cm the resonance is broadened and qualitatively appears more like the observed absorption. However, it is also shifted down in frequency. The actual situation probably involves some reduction in k but not as much as apparently required by the polarizability estimate.

FIGURE 26

Unperturbed phonon density of states for KBr. The upper curves are branch frequency distributions and the lower curve is the total density of states.

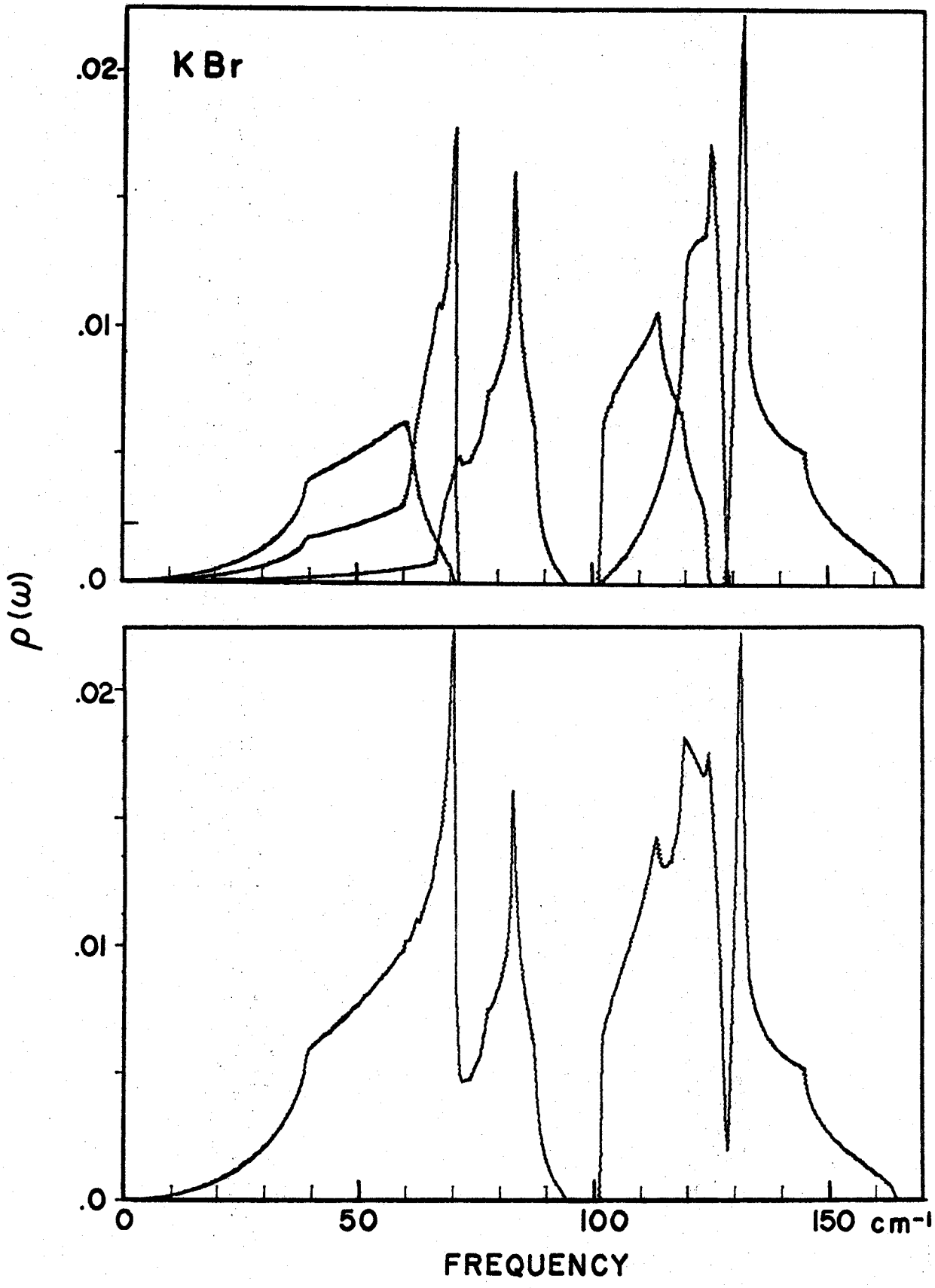
KBr
.02
.01
.0
ρ(ω)
.02
.01
.0
0
50
100
150 cm⁻¹
FREQUENCY

FIGURE 27

Effect of Δk on the calculated far-infrared absorption in KBr. The plots are for $\Delta k = 0, \ldots, -500{,}000$ dynes/cm in increments of -100,000 dynes/cm. As Δk becomes more negative the peaks are shifted down in frequency, the high frequency peak becomes weaker and the low frequency peak becomes stronger. The heavy curve is for $\Delta k = -200{,}000$ dynes/cm which qualitatively appears more like the observed absorption.

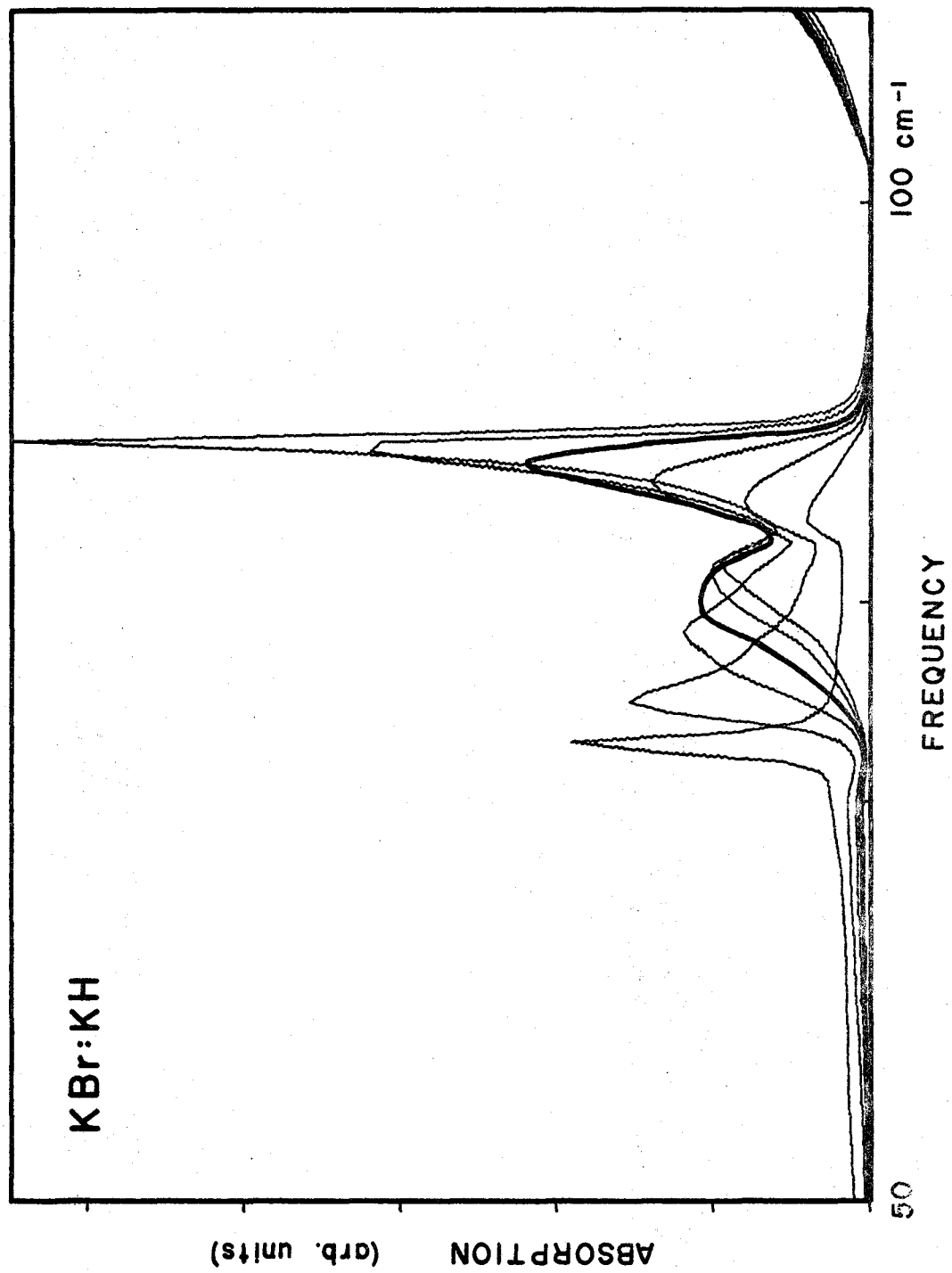
KBr:KH
ABSORPTION (arb. units)
50
100 cm⁻¹
FREQUENCY

7. KI

The side band absorption spectra for KI are shown in Figure 28. As in KCl, both the observed and calculated curves have a reversal of curvature on the high frequency side of the incipient E_g resonance. The theoretical results which used the shell model for the defect are an improvement over those based on the rigid ion defect. The A_{1g} and E_g resonances in the shell model calculation are simultaneously fitted to within experimental error by $\Delta g = -5150$ dynes/cm whereas only one or the other of the resonances can be fitted exactly by the rigid ion defect calculation. The induced far-infrared absorption spectra are given in Figure 29. The observed spectrum due to H^- ions consists of a relatively narrow band between about 50 cm^{-1} and 70 cm^{-1} with three distinct peaks at 58.0 cm^{-1}, 60.7 cm^{-1} and 64.1 cm^{-1}. The calculated absorption is also confined to the same narrow band and has a peak at 59.5 cm^{-1}, and an incipient T_{1u} resonance at 65.6 cm^{-1}.

A clear interpretation of the spectra is difficult to make. The positions of both the resonance and the 59.5 cm^{-1} peak in the calculations are sensitive to force constant changes so they are not related to Van Hove singularities. However, for sufficiently large variations of the parameters the peaks move sufficiently to reveal a Van Hove singularity at 62.8 cm^{-1}

FIGURE 28

Observed and calculated side band in KI with $\Delta f = -8945$ dynes/cm and $\Delta g = -5150$ dynes/cm.

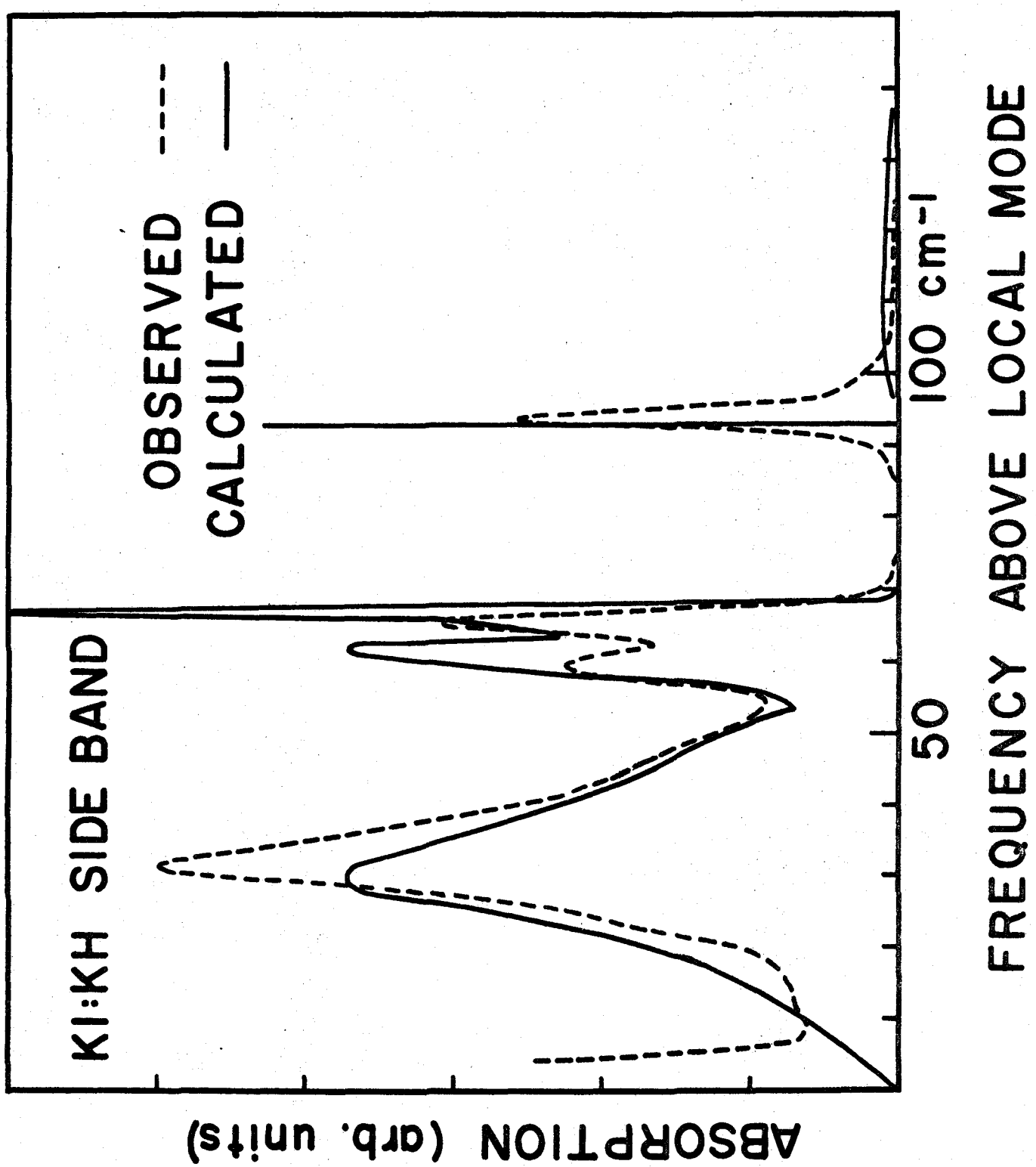
KI:KH SIDE BAND
OBSERVED
CALCULATED
50
100 cm⁻¹
FREQUENCY ABOVE LOCAL MODE
ABSORPTION (arb. units)

due to an off symmetry saddle point in the highest acoustical branch. The 60.7 cm^{-1} peak is known to be shifted slightly to lower frequencies in crystals containing deuterium impurity (Timusk et al. 1968). The shift may be interpreted as the result of different anharmonic zero point energy effects for the two isotopes and does not occur in the harmonic theory. This favours assigning the resonance to the 60.7 cm^{-1} peak which is in better agreement with the present model than in the rigid ion defect model since the resonance now appears at 65.5 cm^{-1} instead of 67.5 cm^{-1}. The 58 cm^{-1} experimental peak could then be assigned to the peak at 59.5 cm^{-1} in the theoretical curve leaving the remaining peak at 64 cm^{-1} to be associated with the 62.8 cm^{-1} saddle point singularity.

The observed width of the peak associated with the incipient resonance is greater than the theoretical width. As in the case of KBr, a similar broadening occurs as the k force constant is reduced. Figure 28 shows the effect as Δk varies from 0 to -600,000 dynes/cm. The resonance is broadened and reduced in intensity as k is decreased and it also shifts slightly to lower frequencies. A value of $\Delta k \approx -150000$ dynes/cm improves the overall appearance of the calculated spectrum but this is still much smaller than the -580,000 dyne/cm change in the force constant required to get Wood and Gilbert's hydrogen polarizability. In this respect the result is similar to the situation in KBr.

FIGURE 29

Induced far-infrared absorption due to H^- ions in KI. The calculated spectrum is from the shell model for the defect with force constant changes $\Delta f = -8945$ dynes/cm, $\Delta g = -5150$ dynes/cm and $\Delta k = 0$ dynes/cm. The model apparently predicts the position of the resonance too high by about 5 cm^{-1}.

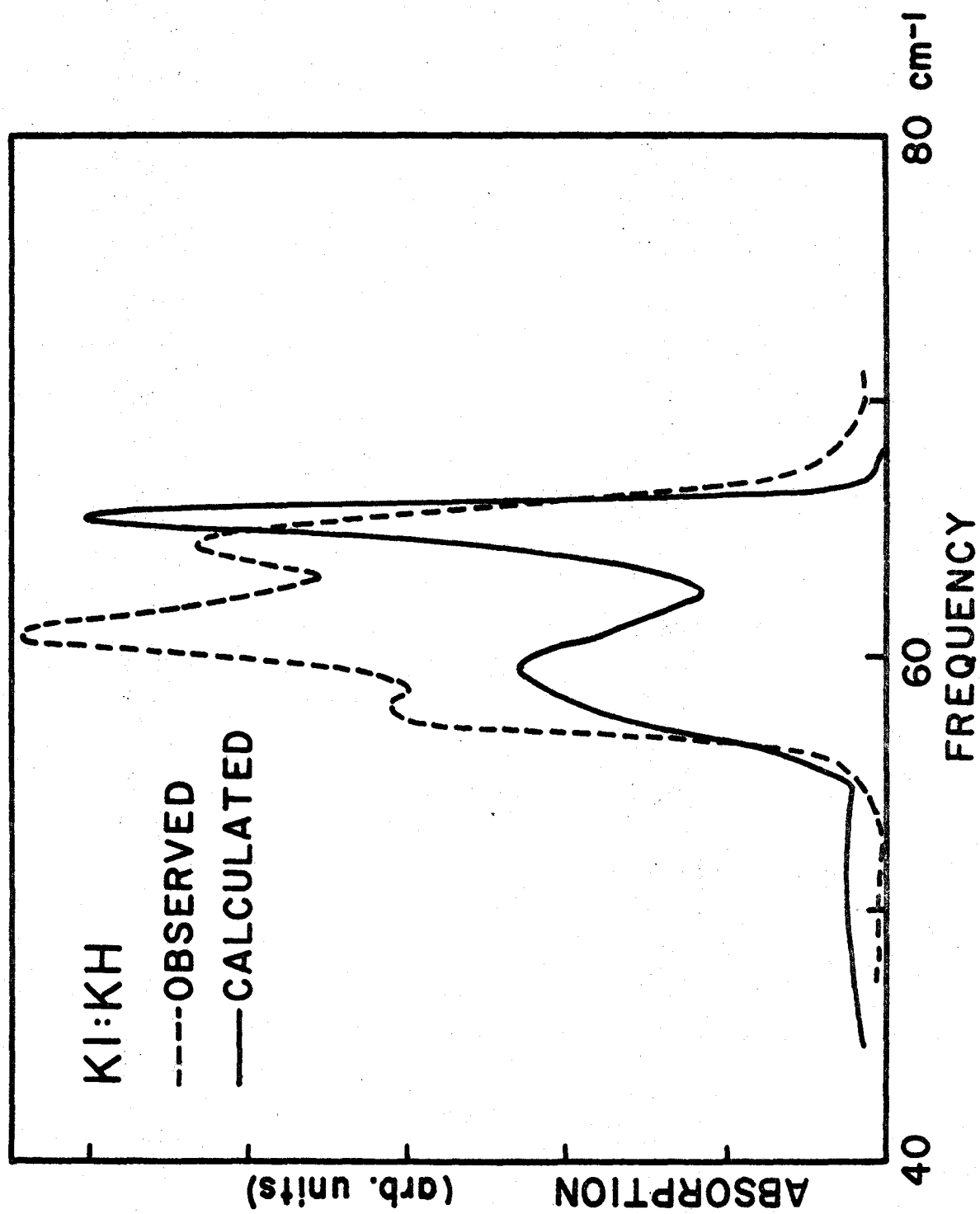
KI:KH
----OBSERVED
——CALCULATED
ABSORPTION
(arb. units)
40
60
80 cm⁻¹
FREQUENCY

FIGURE 30

Unperturbed phonon density of states for KI. The upper curves are branch frequency distributions and the lower curve is the total density of states.

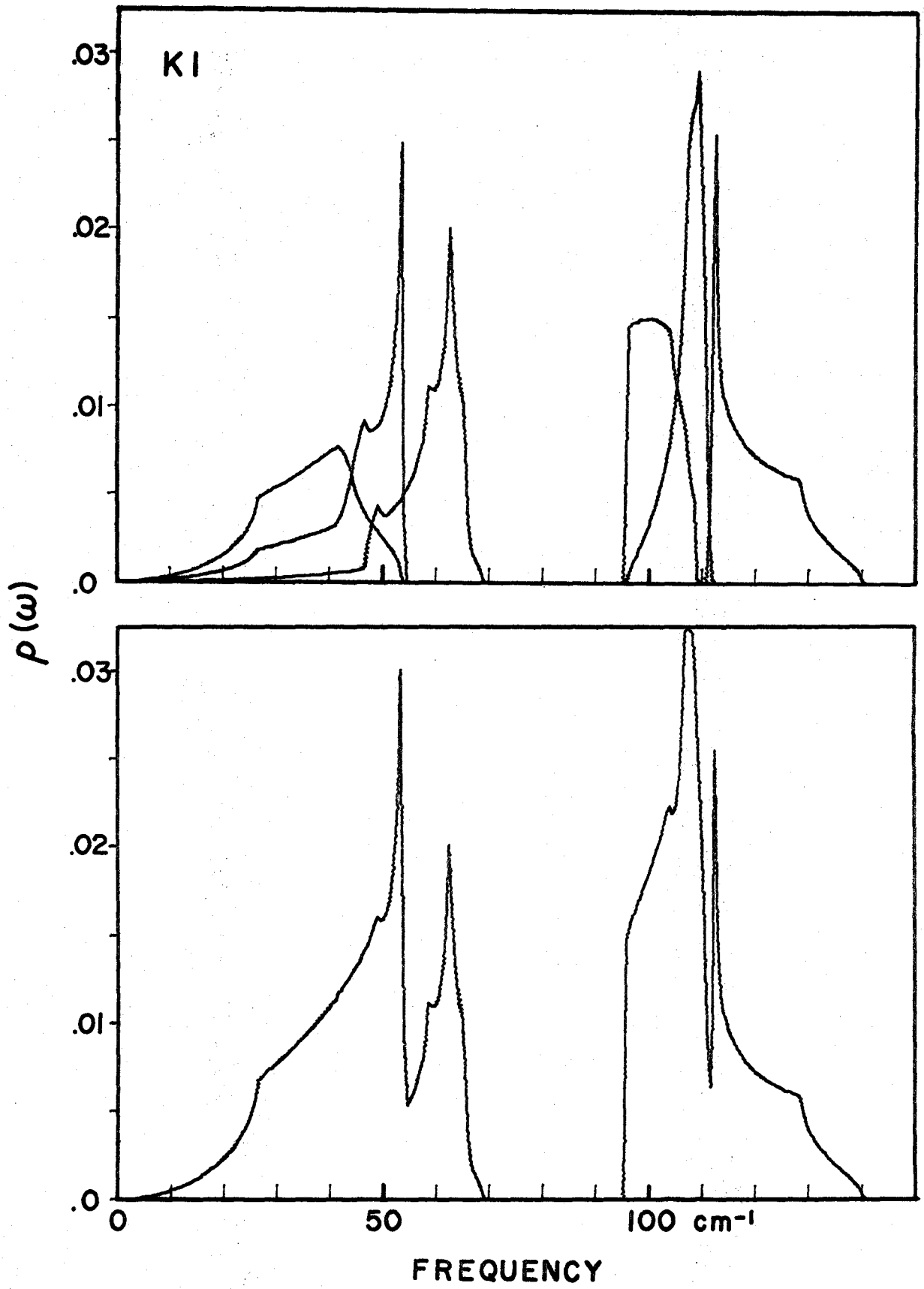
KI
.03
.02
.01
.0
ρ(ω)
.03
.02
.01
.0
0
50
100 cm⁻¹
FREQUENCY

FIGURE 31

Effect of Δk on the calculated far-infrared absorption in KI. The plots are for Δk = 0, -200,000, -400,000, -600,000 dynes/cm. As Δk is made more negative the high frequency peak is considerably reduced in strength and the low frequency peak narrows and increases in strength except for Δk -600,000 dynes/cm when both peaks are considerably weakened. There is also some shifting of the peaks to lower frequencies.

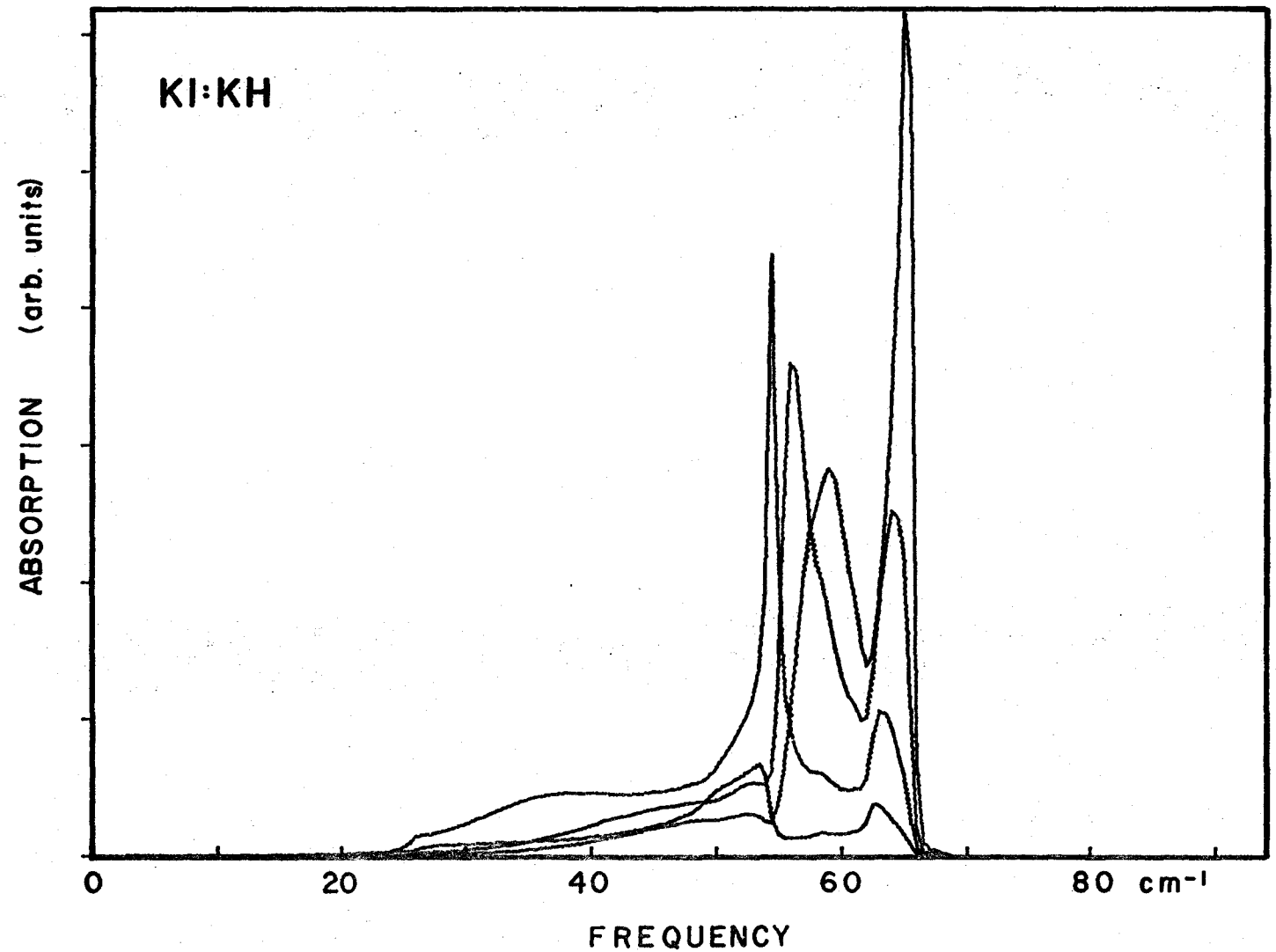
KI:KH
ABSORPTION (arb. units)
0
20
40
60
80 cm⁻¹
FREQUENCY

CHAPTER VI

CONCLUSION

A detailed experimental examination and extensive numerical calculations of the infrared absorption due to H^- ions in the sodium and potassium halides has shown that the salient features of the spectra can be understood in terms of a relatively simple model. The shell model description of the defect centre has not substantially changed the conclusions of earlier work which used a rigid ion model. The side band is due almost entirely to coupling of the local mode to the perturbed modes of the nearest neighbours. The location of the incipient E_g resonance of the anharmonic side band is determined by Δf and the A_{1g} and E_g resonances around the gap between the acoustic and optic modes by Δg. The Δk force constant change is required only in the sodium halides as a correction to obtain the observed position of the local mode. The shell model improves the agreement for the side band spectrum in the potassium halides without requiring any change in k, but at the expense of some additional complexity. Also many smaller details of the side bands are reproduced with greater accuracy by the use of neutron scattering derived phonon data with the shell model.

Although the model contains three parameters, these are determined by the positions of only a few features of the absorption. The remaining structure such as the number and shapes of the peaks and the positions of other peaks are reproduced by the calculations in very good agreement with experiment. Furthermore the model with the same values for the parameters is very successful in describing the additional induced far-infrared absorption.

Several features which are visible in the far infrared spectra are interpreted as Van Hove singularities. The positions of some of these agree very well with those predicted by the alkali halide shell model phonons while others differ by up to 8%. The discrepancies may be attributed to temperature differences between the infrared and neutron scattering experiments, shell model errors, uncertainties in the neutron measurements, or fortuitous identification of the features.

In addition to the small discrepancies in the positions of some features of the absorption spectra certain other difficulties remain. The widths and relative strengths of the calculated peaks are not yet consistent with experiment. The discrepancies in widths is most likely due to neglecting anharmonic broadening. Bilz et al. (1967) has pointed out that approximations leading to the expression for the sideband absorption are not justified when strong impurity

effects are present and that neglect of certain terms in the derivation can have a large effect on the intensities of the peaks and that some shifting may occur. However, Gethins (1968) calculated a "corrected" side band spectrum for KI and found that although there was a slight overall improvement the effects were not as large as estimated by Bilz et al.

The model also neglects other changes in the lattice due to the presence of the hydrogen. Principally these changes include alterations in the transverse force constants to nearest neighbours and in force constants to second neighbours, Coulomb effects due to relaxation, changes in core and shell charges, and changes in the ionic charge at the defect site. Therefore, while the force constant changes were determined for the simple model used here to within 3% or 4% these changes are by no means absolute. However, in view of the success of the model in describing the anharmonic side bands and the far infrared absorption it would appear that it accounts for the most significant aspects of the perturbed lattice. Including the other force constant changes, charge changes and anharmonic corrections will, of course, be expected to further improve the results but only at the expense of introducing many more adjustable parameters and of greatly increasing the complexity of the interpretation.

Since the experiments and simple analysis have revealed the most important features, a consistent and thorough quantum mechanical treatment such as started by Wood and Öpik (1967) and Wood and Gilbert (1967) is needed to justify the use of more complicated mechanisms for the absorption due to H^- ions in the alkali halides.

APPENDIX A

DYNAMICS OF THE UNPERTURBED LATTICE

1. Diagonalization of the Equation of Motion

In the harmonic approximation the vibrational Hamiltonian may be written

$$H_o = \frac{1}{2}\dot{\underset{\sim}{\chi}}^{\dagger}\dot{\underset{\sim}{\chi}} + \frac{1}{2}\underset{\sim}{\chi}^{\dagger}\underset{\sim}{\phi}\underset{\sim}{\chi} \qquad \text{(A-1)}$$

The vector $\underset{\sim}{\chi}$ contains the mass reduced displacements from equilibrium of the particles in the lattice. The κth particle in the Lth unit cell is located at $R(L\kappa)$ and its displacement in the $\hat{\alpha}$ direction is $\chi_\alpha(L\kappa)/\sqrt{M_\kappa}$ where M_κ is the mass of the ion. The matrix $\underset{\sim}{\phi}$ contains the mass reduced force constants defined by

$$\phi_{\alpha\beta}(L\kappa,L'\kappa') = (1/\sqrt{M_\kappa M_\kappa}) \left.\frac{\partial^2\Phi}{\partial\chi_\alpha(L\kappa)\partial\chi_\beta(L'\kappa')}\right|_{\chi=0} \qquad \text{(A-2)}$$

where Φ is the potential energy of the crystal and $\chi=0$ denotes that the derivative is evaluated at the equilibrium positions of the particles. The equation of motion for a crystal with N unit cells, n particles per unit cell and an assumed time dependence $\exp(-i\omega t)$ is the 3nN dimensional matrix equation

$$(\underset{\sim}{\phi} - \omega^2\underset{\sim}{I}) = 0. \qquad \text{(A-3)}$$

This matrix equation is formally diagonalized by the unitary transformation matrix $\underset{\sim}{D}$ whose elements are

$$D_{\underset{\sim}{q}j,L\kappa\alpha} = (1/\sqrt{N})\varepsilon_\alpha(\kappa\underset{\sim}{q}j)\ \exp(i\underset{\sim}{q}\cdot\underset{\sim}{R}(L\kappa)). \qquad \text{(A-4)}$$

The transformation is to a representation of plane waves denoted by the wave vector $\underset{\sim}{q}$ and the polarization index j. Each of these normal modes of the lattice has a characteristic frequency $\omega_{\underset{\sim}{q}j}$. The eigenvectors $\underset{\sim}{\varepsilon}(\kappa\underset{\sim}{q}j)$ give the relative vibrational directions and amplitudes of the ions for the $\underset{\sim}{q}j$ mode and satisfy the orthonormality and completeness conditions

$$\sum_{\kappa\alpha} \varepsilon^*_\alpha(\kappa\underset{\sim}{q}j)\varepsilon_\alpha(\kappa\underset{\sim}{q}j') = \delta_{jj'} \text{ and } \sum_j \varepsilon^*_\beta(\kappa',\underset{\sim}{q}j)\varepsilon_\alpha(\kappa\underset{\sim}{q}j) = \delta_{\alpha\beta}\delta_{\kappa\kappa'}. \qquad \text{(A-5)}$$

The elements of the inverse transformation matrix $\underset{\sim}{D}^{-1}$ are

$$D^{-1}_{L\kappa\alpha,\underset{\sim}{q}j} = (1/\sqrt{N})\varepsilon^*_\alpha(\kappa\underset{\sim}{q}j)\ \exp(-i\underset{\sim}{q}\cdot\underset{\sim}{R}(L\kappa)). \qquad \text{(A-6)}$$

For the alkali halides $\underset{\sim}{\varepsilon}(\kappa\underset{\sim}{q}j)$ is real so $\varepsilon_\alpha(\kappa\underset{\sim}{q}j) = \varepsilon^*_\alpha(\kappa\underset{\sim}{q}j)$.

The Green's function matrix for the perfect lattice is defined by the equation

$$(\underset{\sim}{\phi} - \omega^2\underset{\sim}{I})\underset{\sim}{G}(\omega^2) = \underset{\sim}{I}. \qquad \text{(A-7)}$$

In the $\{\underset{\sim}{q}j\}$ representation $\underset{\sim}{\phi}$ is diagonal with elements $\omega^2_{\underset{\sim}{q}j}\delta_{\underset{\sim}{q}\underset{\sim}{q}'}\delta_{jj'}$, so the elements of $\underset{\sim}{G}$ are

$$G(\omega^2;\underset{\sim}{q}j,\underset{\sim}{q}'j') = \delta_{\underset{\sim}{q}\underset{\sim}{q}'}\delta_{jj'}/(\omega^2_{\underset{\sim}{q}j} - \omega^2). \qquad \text{(A-8)}$$

The transformation back to the $\{L\kappa\alpha\}$ representation by means of $\underset{\sim}{D}^{-1}$ gives

$$G(\omega^2;L\kappa\alpha,L'\kappa'\beta) = (1/N)\sum_{\underset{\sim}{q}j} \frac{\varepsilon_\beta(\kappa\underset{\sim}{q}j)\varepsilon^*_\alpha(\kappa\underset{\sim}{q}j)\exp\{i\underset{\sim}{q}\cdot(\underset{\sim}{R}(L\kappa)-\underset{\sim}{R}(L'\kappa'))\}}{\omega^2_{\underset{\sim}{q}j} - \omega^2}$$

In practice, the transformation D may be done in two steps,

$$\underset{\sim}{D} = \underset{\sim}{D}(2)\cdot\underset{\sim}{D}(1)$$

$$\text{where } D(1)_{\underset{\sim}{q}\alpha\kappa',L\beta\kappa} = (1/N)\exp(i\underset{\sim}{q}\cdot\underset{\sim}{R}(L\kappa))\ \delta_{\alpha\beta}\delta_{\kappa\kappa'} \qquad \text{(A-10)}$$

$$\text{and} \quad D(2)_{\underset{\sim}{q}j,\underset{\sim}{q}'\kappa\alpha} = \varepsilon_{\alpha}(\kappa\underset{\sim}{q}j)\delta_{\underset{\sim}{q}\underset{\sim}{q}'}.$$

Transformation $\underset{\sim}{D}(1)$ takes advantage of the translational symmetry of the lattice and periodic boundary conditions. Under this transformation the equation of motion becomes block diagonal in $\underset{\sim}{q}$ with each block being 3n dimensional where n is the number of particles in the unit cell. This partially diagonalized space is called the $\{\underset{\sim}{q}\kappa\alpha\}$ representation.

2. The Shell Model

The shell model description of the alkali halides was originally introduced by Dick and Overhauser (1958) to explain the dielectric properties of these materials. The representation of the alkali halide lattice vibrations in terms of this model was introduced by Woods et al. (1960) and extended by Cowley (1963). The model assumes that each ion consists of a heavy central core containing the nucleus and inner shell electrons surrounded by a rigid shell of valence electrons whose mass is negligible in the adiabatic approximation. The core and shell are connected by an isotropic force constant G_{κ}. In the dynamical model used here, short range repulsive over-lap forces are assumed to act only between shells and extend

out to second neighbours. Long range coulomb forces are taken into account by Ewald summations over the lattice (Kellerman, 1940).

In the $\{q\kappa\alpha\}$-representation the eigenvalue problem is equivalent to solving the 12-dimensional matrix equation

$$\begin{pmatrix} \underset{\sim}{G} + \underset{\sim\sim\sim}{XCX} - \omega^2 \underset{\sim}{I} & \underset{\sim\sim\sim}{XCY} - \underset{\sim}{G} \\ \underset{\sim\sim\sim}{XCX} - \underset{\sim}{G} & \underset{\sim}{R} + \underset{\sim}{G} + \underset{\sim\sim\sim}{YCY} \end{pmatrix} \begin{pmatrix} \underset{\sim}{U} \\ \underset{\sim}{S} \end{pmatrix} = 0 \qquad \text{(A-11)}$$

which can be reduced to the formal form of (A-3) with

$$\underset{\sim}{\phi} = \underset{\sim}{G} + \underset{\sim\sim\sim}{XCX} - (\underset{\sim\sim\sim}{XCY} - \underset{\sim}{G})(\underset{\sim}{R} + \underset{\sim}{G} + \underset{\sim\sim\sim}{YCY})^{-1}(\underset{\sim\sim\sim}{YCX} - \underset{\sim}{G})$$

The 6 component vector $\underset{\sim}{U}$ contains the mass reduced coordinates for the ion cores and $\underset{\sim}{S}$ contains the corresponding coordinates for the shells. The elements of the 6 dimensional mass reduced force constant matrices are

$$\underset{\sim}{G} = \begin{pmatrix} \underset{\sim 1}{G} & 0 \\ 0 & \underset{\sim 2}{G} \end{pmatrix}, \quad \{\underset{\sim\kappa}{G}\}_{\alpha\beta} = (e^2/v) G_\kappa / M_\kappa \, \delta_{\alpha\beta}$$

$$\underset{\sim}{X} = \begin{pmatrix} \underset{\sim 1}{X} & 0 \\ 0 & \underset{\sim 2}{X} \end{pmatrix}, \quad \{\underset{\sim\kappa}{X}\}_{\alpha\beta} = \underset{\sim\kappa}{X} \, \delta_{\alpha\beta} \qquad \text{(A-12)}$$

$$\underset{\sim}{Y} = \begin{pmatrix} \underset{\sim +}{Y} & 0 \\ 0 & \underset{\sim -}{Y} \end{pmatrix}, \quad \{\underset{\sim\kappa}{Y}\}_{\alpha\beta} = \underset{\sim\kappa}{Y} \, \delta_{\alpha\beta}$$

$$\underset{\sim}{R} = \begin{pmatrix} \underset{\sim ++}{R} & \underset{\sim +-}{R} \\ \underset{\sim -+}{R} & \underset{\sim --}{R} \end{pmatrix}$$

$$\{\underset{\sim}{R}_{\kappa\kappa'}\}_{\alpha\beta} = (e^2/v\sqrt{M_\kappa M_{\kappa'}})\{[A + 2(B+B'') + 2A_{\kappa\kappa} + 4B_{\kappa\kappa}$$

$$-(A_{\kappa\kappa}+B_{\kappa\kappa})\cos q_\alpha r_o(\cos q_x r_o+\cos q_y r_o+\cos q_z r_o-\cos q_\alpha r_o)$$

$$-2B_{\kappa\kappa}(\cos q_x r_o \cos q_y r_o \delta_{\alpha z}+\cos q_y r_o \cos q_z r_o \delta_{\alpha x}$$

$$+\cos q_z r_o \cos q_x r_o \delta_{\alpha y})]\delta_{\alpha\beta}\delta_{\kappa\kappa'}$$

$$+[(A_{\kappa\kappa}-B_{\kappa\kappa})\sin q_\alpha r_o \sin q_\beta r_o(1-\delta_{\alpha\beta})]\delta_{\kappa\kappa'}$$

$$-[A\cos q_\alpha r_o+(B+B'')(\cos q_x r_o+\cos q_y r_o+\cos q_z r_o-\cos q_\alpha r_o)]$$

$$\cdot\delta_{\alpha\beta}(1-\delta_{\kappa\kappa'})\}$$

and

$$\{\underset{\sim}{C}_{\kappa\kappa'}\}_{\alpha\beta}=(e^2/v\sqrt{M_\kappa M_{\kappa'}}) \sum_{L-L'} \frac{\partial^2}{\partial\chi_\alpha(L\kappa)\,\partial\chi_\beta(L'\kappa')} \frac{1}{|R(L\kappa)-R(L'\kappa')|}\Bigg|_{\chi=0}$$

$$\exp\{iq\cdot(R(L\kappa)-R(L'\kappa'))\}$$

where $\kappa = \pm$ for the positive and negative ions. The summation in the coefficients for $\underset{\sim}{C}$ were evaluated by Kellerman (1940) using the Ewald method. The force constants $G_\pm$ and shell charges $Y_\pm e$ are usually expressed in terms of the somewhat more physical electrical and mechanical polarizabilities

$$\alpha_\pm = Y_\pm^2\, e^2/(G_\pm+A+2(B+B'')) \qquad \text{(A-13)}$$

and

$$d_\pm = -(A+2(B+B''))Y_\pm/(G_\pm+A+2(B+B''))$$

respectively. The core charges are $X_\pm e$ and the total ionic charges are $Z_\pm e$ with $Z_\pm = X_\pm + Y_\pm$. Crystal neutrality requires $Z_+ = -Z_- = Z$. The repulsive force constants are defined in

in terms of parallel and perpendicular second derivatives of the repulsive potentials $V_{\kappa\kappa'}(r)$ which act between the nearest and second nearest neighbours.

$$(e^2/2v)\ A_{\kappa\kappa'} = (d^2V_{\kappa\kappa'}(r)/dr^2)_{\parallel}$$
$$(e^2/2v)\ B_{\kappa\kappa'} = \frac{1}{r}\ (d\ V_{\kappa\kappa'}(r)/dr)_{\parallel} \qquad \text{(A-14)}$$
$$(e^2/2v)\ (B_{\kappa\kappa'}+B''_{\kappa\kappa'}) = (d^2V_{\kappa\kappa'}(r)/dr^2)_{\perp}$$

where $v = 2r_o^3$ is the unit cell volume and r_o is the equilibrium distance between nearest neighbours. To avoid unnecessary complexity in Equation (A-12) the double subscripts have been omitted from the constants when $\kappa \neq \kappa'$. Non-central forces are accounted for between nearest neighbours by the constant B". The forces between second neighbours are assumed to be central. The parameter B can be expressed in terms of B_{++} and B_{--} by the equilibrium condition

$$B + 2B_{++} + 2B_{--} + (2/3)\alpha_M\ Z^2 = 0 \qquad \text{(A-15)}$$

where $\alpha_M = 1.74756$ is the Madelung constant. The values of the eleven parameters for the shell model (namely A, B", A_{++}, B_{++}, A_{--}, B_{--}, Z, α_+, α_-, d_+, d_-) have been determined for most of the common alkali halides by least squares fitting to the results of inelastic neutron scattering experiments completed within the last few years. The values used in this work are listed in Table VI. A computer program which was originally obtained from Chalk River by Dr. Timusk was used to diagonalize (A-3). Solutions were calculated for 1505 $\underset{\sim}{q}$-points in the

TABLE V

SHELL MODEL PARAMETERS

Parameters	Units	NaF[a] (295°K)	NaCl[b] (80°K)	NaBr[c] (295°K)	NaI[d] (100°K)	KCl[e] (115°K)	KBr[d] (90°K)	KI[f] (90°K)
A		9.26	9.459	11.39	9.937	12.12	13.15	13.4
B		- .918	- .879	-1.165	-.841	-1.10	-1.19	-1.09
B''		.188	.0438	.125	.0264	.075	.0341	- .066
A_{++}	$e^2/2v$	.0	.0	.0	.0	.0	.0	- .16
B_{++}		.0	.0	.0	.0	.0	.0	- .01
A_{--}		.34	.6272	.0	.6182	-.101	- .399	- .29
B_{--}		-.02	.0084	.0	-.041	.0581	.0540	.05
Z	e	.907	.8601	1.00	.8899	.9179	.9657	.92
α_+	v	.0109	.0035	.017	.0301	.0282	.0302	.0268
d_+	e	.01	.0056	-.160	-.112	-.025	-.101	-.11
α_-	v	.0284	.0495	.074	.0657	.0350	.0433	.0530
d_-	e	.116	.1262	.19	.1365	.1215	.1406	.13
r_o	Å	2.310	2.794	2.987	3.21	3.122	3.278	3.492
v	$Å^3$	24.6	43.6	53.6	66.0	60.57	80.4	85.16
M_+	u.	22.99	22.99	22.99	22.99	39.10	39.10	39.10
M_-	u.	19.00	35.45	79.91	126.9	35.45	79.91	126.9

References:

[a]Buyers, 1967 .

[b]from a least squares fit to the data of Almqvist et al. 1968.

[c]Reid et al. 1970.

[d]Cowley et al. 1963.

[e]Copley et al. 1969.

[f]Dolling et al. 1966.

FIGURE 32

Irreducible 1/48 of the face centred cubic Brillouin zone as defined by Kellerman (1940). Certain symmetry points and directions in the notation of Bouckaert et al. (1936) are labelled. The arrangement of the 1505 cubes used in the Gilat and Raubenheimer calculation of the histogram is also shown. Frequencies and eigenvectors were evaluated at $\underset{\sim}{q}$ points in the centre of each of the cubes.

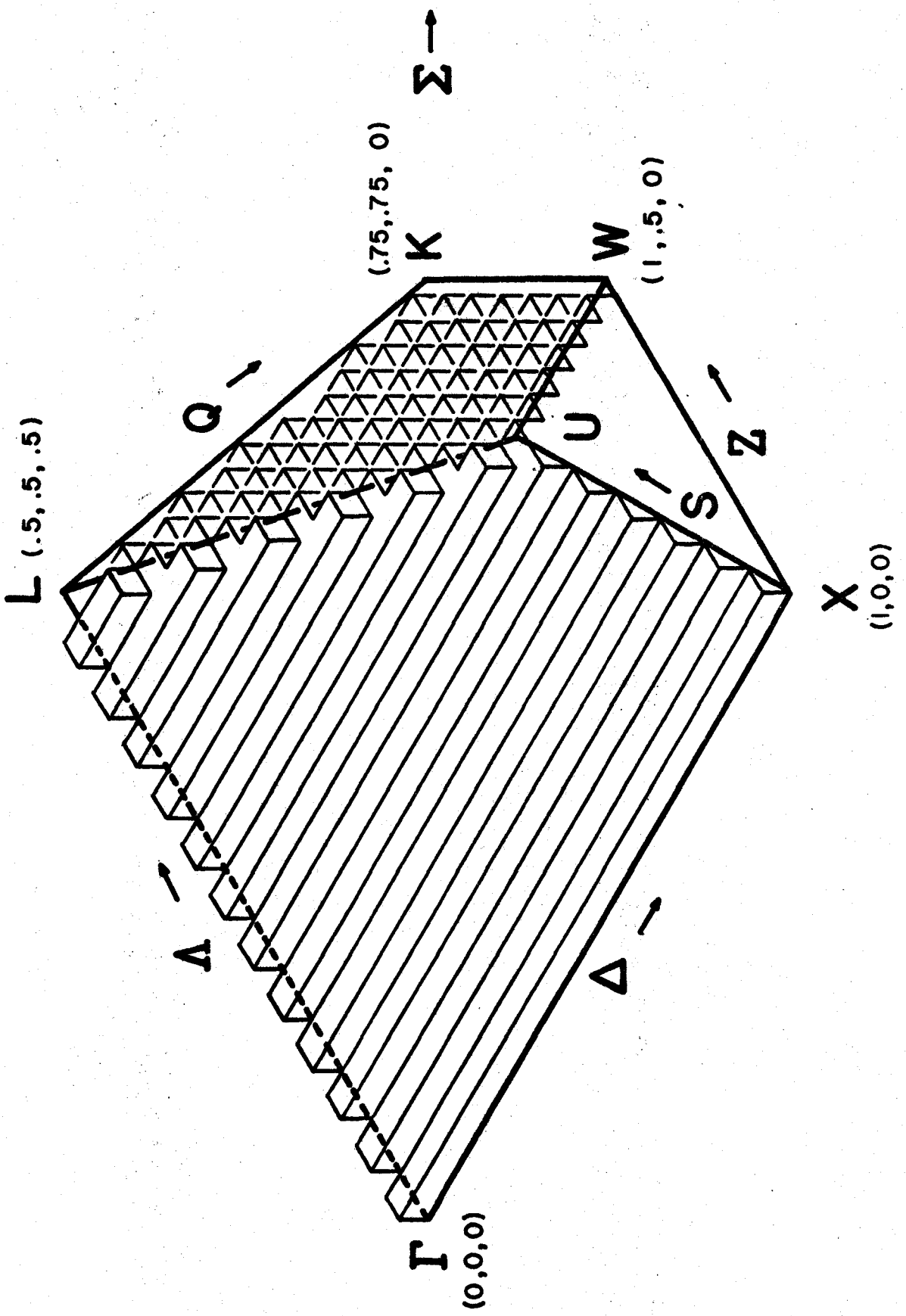
Σ
K
(.75,.75, 0)
W
(1,.5, 0)
Q
U
Z
S
L (.5,.5,.5)
X
(1,0,0)
Λ
Δ
Γ
(0,0,0)

irreducible 1/48th of the Brillouin zone defined by Kellerman (1940) and shown in Figure 32 . Application of the symmetry operations for the O_h group to this subzone generates information at 62500 points in the full zone. Values of $\underset{\sim}{q},\omega(\underset{\sim}{q}j)$ and $\underset{\sim}{\varepsilon}(\kappa\underset{\sim}{q}j)$ for NaF, NaCl, NaBr, NaI, KCl, KBr and KI were calculated and stored on magnetic computer tape.

3. Calculation of the Unperturbed Green's Function Matrices

The separated form of the definition of the Green's function matrix for the shell model in the $\{q\kappa\alpha\}$ representation is

$$\begin{pmatrix} \underset{\sim}{G}+\underset{\sim}{X}\underset{\sim}{C}\underset{\sim}{X}-{}^{2}\underset{\sim}{I} & \underset{\sim}{Y}\underset{\sim}{C}\underset{\sim}{Y}-\underset{\sim}{G} \\ \underset{\sim}{Y}\underset{\sim}{C}\underset{\sim}{X}-\underset{\sim}{G} & \underset{\sim}{R}+\underset{\sim}{G}+\underset{\sim}{Y}\underset{\sim}{C}\underset{\sim}{Y} \end{pmatrix} \begin{pmatrix} \underset{\sim}{G}_{UU} & \underset{\sim}{G}_{US} \\ \underset{\sim}{G}_{SU} & \underset{\sim}{G}_{SS} \end{pmatrix} = I \qquad \text{(A-16)}$$

where

$$\{\underset{\sim}{G}_{UU}\}^{\kappa\kappa'}_{\alpha\beta} = \sum_j \frac{\varepsilon_\beta(\kappa,\underset{\sim}{q}j)\ \varepsilon^*_\alpha(\kappa,\underset{\sim}{q}j)}{\omega^2_{\underset{\sim}{q}j}-\omega^2}$$

$$\{\underset{\sim}{G}_{US}\}^{\kappa\kappa'}_{\alpha\beta} = \sum_j \frac{\varepsilon_\beta(\kappa,\underset{\sim}{q}j)\ \eta^*_\alpha(\kappa,\underset{\sim}{q}j)}{\omega^2_{\underset{\sim}{q}j}-\omega^2}$$

$$\{\underset{\sim}{G}_{SU}\}^{\kappa\kappa'}_{\alpha\beta} = \sum_j \frac{\eta_\beta(\kappa,\underset{\sim}{q}j)\,\varepsilon^*_\alpha(\kappa,\underset{\sim}{q}j)}{\omega^2_{\underset{\sim}{q}j}-\omega^2}$$

$$\{\underset{\sim}{G}_{SS}\}^{\kappa\kappa'}_{\alpha\beta} = \sum_j \frac{\eta_\beta(\kappa,\underset{\sim}{q}j)\ \eta^*_\alpha(\kappa,\underset{\sim}{q}j)}{\omega^2_{\underset{\sim}{q}j}-\omega^2} + \phi^{-1}_{SS}(^{\kappa\kappa'}_{\alpha\beta});$$

with

$$\underset{\sim}{\phi}_{SS} = \underset{\sim}{R} + \underset{\sim}{G} + \underset{\sim}{Y}\underset{\sim}{C}\underset{\sim}{Y}$$

and where the shell "eigenvectors" are given by

$$\begin{bmatrix} \underset{\sim}{\eta}(+;\underset{\sim}{q}j) \\ \\ \underset{\sim}{\eta}(-;\underset{\sim}{q}j) \end{bmatrix} = -(\underset{\sim}{R}+\underset{\sim}{G}+\underset{\sim\sim\sim}{YCY})^{-1}(\underset{\sim\sim\sim}{YCX}-\underset{\sim}{G}) \begin{bmatrix} \underset{\sim}{\varepsilon}(+;\underset{\sim}{q}j) \\ \\ \underset{\sim}{\varepsilon}(-;\underset{\sim}{q}j) \end{bmatrix} \qquad \text{(A-17)}$$

which comes from (A-9). The matrix elements can be transformed to the $\{L\kappa\alpha\}$-representation by the inverse of $\underset{\sim}{D}(1)$ in (A-10) and then to the symmetrized coordinate space by the transformation in (III-8) and (IV-3).

In practice one writes

$$G_{PQ}(\omega^2;\Gamma_i) = \sum_{\underset{\sim}{q}j} \frac{P(\Gamma_i;r)\ Q^{\dagger}(\Gamma_i;r')}{\omega^2_{\underset{\sim}{q}j} - \omega^2} \qquad \text{(A-18)}$$

where P and Q depend on qj and represent U or S and $\Gamma_i = A_{1g}, E_g, T_{2g}$ and T_{1u}. Only the matrix elements referring to the H^- ion and its first and fourth neighbours are needed for the calculations. The quantities $U(\Gamma_i)$ and $S(\Gamma_i)$ required are

$$\begin{aligned}
U_\alpha(T_{1u};0) &= (1/\sqrt{N})\ \varepsilon_\alpha(-,\underset{\sim}{q}j) \\
S_\alpha(T_{1u};0) &= (1/\sqrt{N})\ \eta_\alpha(-,\underset{\sim}{q}j) \\
S_\alpha(T_{1u};r) &= \sqrt{2/N}\ \ \eta_\alpha(\kappa;\underset{\sim}{q}j)\cos q_\alpha r \\
S(A_{1g};r) &= -i\sqrt{2/3N}\ \sum_\alpha \eta_\alpha\ (\kappa;\underset{\sim}{q}j)\sin q_\alpha r \\
S(E_g;r) &= -i\sqrt{1/N}\ (\eta_x(\kappa;\underset{\sim}{q}j)\sin q_x r - \eta_y(\kappa;\underset{\sim}{q}j)\sin q_y r) \\
S_{\alpha\beta}(T_{2g};r_o) &= -i\sqrt{1/N}_\alpha(\eta_\alpha(\kappa;\underset{\sim}{q}j)\sin q_\beta r_o - \eta_\beta(\kappa;\underset{\sim}{q}j)\sin q_\alpha r_o)
\end{aligned} \qquad \text{(A-19)}$$

where $r = r_o$ for nearest neighbours and $r = 2r_o$ for fourth neighbours. Only one of the two E_g configurations and one of

the three T_{2g} and T_{1u} configurations is needed since the others are generated by the symmetry operations of the cubic group. The sum in (A-18) is done by first forming the products PQ^+ and summing over the $\underset{\sim}{q}$'s which are related to each other by the 48 symmetry operations and have the same frequency and second by summing over the $\underset{\sim}{q}$'s in the irreducible 1/48th of the Brillouin zone. This latter sum was accomplished by evaluating the imaginary parts of $G(\omega^2+0^+)$ using the identity

$$Im\ \frac{1}{\omega_{\underset{\sim}{q}j}^2-\omega^2} = \frac{2\pi}{\omega}\ \delta(\omega_{\underset{\sim}{q}j}-\omega) \qquad \text{(A-20)}$$

and "sorting" the contributions $\sum_{R\epsilon O_h} R\ PQ^+$ into histograms by the method developed by Gilat and Raubenheimer (1966). The real parts of G were found by numerical integration as described by Timusk and Klein (1966) using the relation

$$Re\ G(\omega^2) = \frac{2}{\pi}\int_0^{\omega_{max}} \frac{G(s^2+i0)-G(0)}{s^2-\omega^2}\ sds + \frac{1}{\pi}\ ImG(0)\ln\left|\frac{\omega_{max}-\omega}{\omega_{max}+\omega}\right| \qquad \text{(A-21)}$$

which is in a form convenient for numerical calculations. The contribution of $\underset{\sim}{\phi}_{SS}^{-1}$ to $\underset{\sim}{G}_{SS}$ is real and independent of frequency and so must be added to the results for $\underset{\sim}{G}_{SS}$ from (A-21).

APPENDIX B

BREATHING SHELL MODELS

The possibility of spherical deformations of the eletronic shells of the ions in the alkali halides was considered by Nüsslein and Schröder (1967) and Schröder (1966). Their motive was to improve the agreement between the shell model parameters determined from the bulk properties of the crystals and the parameters obtained by least squares fitting to the phonon data from inelastic neutron scattering. They showed how to introduce the extra degree of freedom (the "breathing" motion of the shells) without introducing any new parameters. However, the breathing shell model lacked any quantum mechanical justification. Bilz et al. (1969) treated the problem quantum mechanically and showed that Schröder's assumptions were justified but that there were some missing terms in the off diagonal elements of the dynamical matrix. Even without these terms the breathing shell model provided a slightly better fit to the neutron scattering data,especially at the zone boundary. The overall fit does not appear to give a significant improvement over the ordinary shell model (Dolling et al. 1968). The breathing shell model should be reconsidered in the light of the results of Bilz et al. before it is used extensively.

Page and Strauch (1967) incorporated the breathing shell model into their calculations on the local mode. Their results were quite insensitive to whether or not the breathing motion was included. Some calculations were made which account for breathing effects and these support their results. Furthermore, calculations of the side band are largely unaffected by including breathing coordinates. These results are not surprising since the amplitudes of the breathing motions are of the order of 1% of the amplitudes of the ions themselves. In view of this and the fact that the correct form of the breathing shell model is unclear, this model was not used in the calculations presented in Chapter V.

BIBLIOGRAPHY

Almqvist, L., Raunio, G., and Stedman, R. 1968. Neutron Inelastic Scattering (International Atomic Energy Agency, Vienna), Vol. I, 295.

Bäurele, D. and Fritz, B. 1967. phys. stat. sol. 24, 207.

Bilz, H., Strauch, D., and Fritz, B. 1966. J. de. Phys. 27, Suppl. C2-3.

Bilz, H., Zeyher, R., and Wehner, R.K. 1967. phys. stat. sol. 20, K167.

Bilz, H., Schröder, U. and Gliss, Bernd 1969. Bull. Am. Phys. Soc. Series II, Vol. 14, No. 3, 302.

Bouckhaert, L.P., Smoluchowski, R. and Wigner, E. 1936. Phys. Rev. 50, 58.

Buchanan, M. and Woll, E.J., Jr. 1969. Can. J. Phys. 47, 1757.

Buyers, W.J.L. 1967. Phys. Rev. 153, 923.

Copley, J.R.D., MacPherson, R.W. and Timusk, T. 1969. Phys. Rev. 182, 965.

Cowley, R. A., Cochran, W., Brockhouse, B.N. and Woods, A.D.B. 1963. Phys. Rev. 131, 1030.

Dick, B.J. and Overhauser, A.W. 1958. Phys. Rev. 112, 90.

Dolling, G., Cowley, R.A., Schittenhelm, C., and Thorson, I.M. 1966. Phys. Rev. 147, 577.

Dolling, G., Smith, H.G., Nicklow, R.M., Vijayaraghavan, and Wilkinson, M.K. 1968. Phys. Rev. 168, 970.

Dötsch, H., Gebhardt, W., and Martius, C.H. 1965. Solid State Commun. 3, 297.

Dötsch, H. 1969. phys. stat. sol. 31, 649.

Elliott, R.J., Hayes, W., Jones, G.D., MacDonald, H.F. and Sennet, C.T. 1965. Proc. Roy. Soc. (London) A289, 1.

Fieschi, R., Nardelli, G.F. and Terzi, N. 1965. Phys. Rev. 138, A203.

Fritz, B. 1965. Lattice Dynamics, Edited by R. F. Wallis (Pergamon Press Inc., Oxford).

Fritz, B., Gross, U., and Bäurle, D. 1965. phys. stat. sol. 11, 231.

Gethins, T., Timusk, T. and Woll, E.J. Jr., 1967. Phys. Rev. 157, 744.

Gethins, T. 1968. Ph.D. Thesis, McMaster University.

Gibb, Thomas R. P., Jr. 1962. Progress in Inorganic Chemistry, Vol. 3, edited by F. Albert Cotton (John Wiley and Sons, Inc., New York) p. 315.

Handbook of Chemistry and Physics, 1959. Forty-First Edition, Charles D. Hodgman, Editor, Chemical Rubber Publishing Co., Cleveland, Ohio.

Hilsch, R. and Pohl, R.W. 1938. Trans. Faraday Soc. 34, 883.

Jaswal, S.S. and Montgomery, D.J. 1964, Phys. Rev. 135, A1257.

Kellerman, E.W. 1940. Phil. Trans. Roy. Soc. (London) 238, 513.

Klein, Miles V. 1968. Physics of Color Centers edited by W. Beall Fowler (Academic Press Inc., New York) Chapt. 7.

Klein, M.V. and Macdonald, H.F. 1968. Phys. Rev. Letters 20, 1031.

Kühner, D. and Wagner, M. 1967. Zeits. für Phys. 207, 111.

Lifshits, I.M. 1956. Nuovo Cimento, Suppl. 3, 716.

Mitra, S.S. and Brada, Y. 1965. Physics Letters 17, 19.

Nüsslein, V. and Schröder, U. 1967. phys. stat. sol. 21, 309.

Page, John B., Jr. and Dick, B.G. 1967. Phys. Rev. 163, 910.

Page, J.B., Jr. and Strauch, D. 1967. phys. stat. sol. 24, 469.

Page, John B., Jr. and Strauch, Dieter. 1968. Proceedings of the First International Conference on Localized Excitations in Solids, edited by R. F. Wallis (Plenum Press, New York), 559.

Raunio, G., Almqvist, L. and Stedman, R. 1969. Phys. Rev. 178, 1496.

Raunio, G., and Almqvist, L. 1969. phys. stat. sol. 33, 209.

Raunio, G. and Rolandson, S. 1970 (to be published).

Reid, J.S., Smith, T. and Buyers, W.J.L. 1970. Phys. Rev. B. (to be published).

Rosenstock, H. and Klick, C. 1960, Phys. Rev. 119, 1198.

Schäfer, G. 1960. J. Phys. Chem. Solids 12, 233.

Schröder, U. 1966. Solid State Commun. 4, 347.

Sievers, A.J. 1965. Low Temperature Physics, Vol. LT9, Pt. B, edited by J. G. Daunt et al. (Plenum Press Inc., New York).

Strauch, D. 1968. phys. stat. sol. 30, 495.

Takeno, Shazo. 1967. Prog. Theoret. Phys. 38, 995.

Timusk, T. and Buchanan, M. 1967. Phys. Rev. 164, 345.

Timusk, Thomas and Klein, Miles V. 1966. Phys. Rev. 141, 664.

Timusk, T. and Ward, R.W. 1969. Phys. Rev. Letters 22, 396.

Timusk, T., Woll, E.J., Jr., and Gethins, T. 1968. Proceedings of the First International Conference on Localized Excitations in Solids, edited by R. F. Wallis (Plenum Press Inc.. New York).

Tumber, A.J. 1968. M.Sc. thesis, McMaster University.

Van Hove, L. 1953. Phys. Rev. 89, 1189.

Wallis, R. and Maradudin, A. 1960. Progr. Theoret. Phys. (Kyoto) 24, 1055.

Wood, R.F. and Öpik, U. 1967. Phys. Rev. 162, 736.

Wood, R. F. and Gilbert, R.L. 1967. Phys. Rev. 162, 746.

Woll, E.J., Jr., Gethins, T. and Timusk, T. 1968. Can. J. Phys. 46, 2263.

Woods, A.D.B., Brockhouse, B.N., Cowley, R.A. and Cochran, W. 1963. Phys. Rev. 131, 1025.

Xinh, Nguyen Xuan. 1966. Solid State Commun. 4, 9.

Xinh, Nguyen X. 1967. Phys. Rev. 163 896.